

# For Reference

---

**NOT TO BE TAKEN FROM THIS ROOM**

For Reference

---

NOT TO BE TAKEN FROM THIS ROOM

Ex libris  
UNIVERSITATIS  
ALBERTAENSIS













THE UNIVERSITY OF ALBERTA

Mass Spectrometric Studies using 40 to 100 kev Protons:

(a) Primary Ionization and Fragmentation of Some Molecules, (b) Ion-Molecule Reactions with some Hydrocarbons and Polar Molecules.

by

Jon Gerald Collins

A THESIS

SUBMITTED TO THE FACULTY OF GRADUATE STUDIES  
IN PARTIAL FULFILMENT OF THE REQUIREMENTS FOR THE DEGREE  
OF DOCTOR OF PHILOSOPHY

DEPARTMENT OF CHEMISTRY

EDMONTON, ALBERTA

DECEMBER, 1966



UNIVERSITY OF ALBERTA

FACULTY OF GRADUATE STUDIES

The undersigned certify that they have read,  
and recommend to the Faculty of Graduate Studies for  
acceptance, a thesis entitled Mass Spectrometric  
Studies using 40 to 100 kev Protons: (a) Primary  
Ionization and Fragmentation of Some Molecules, (b) Ion-  
Molecule Reactions with some Hydrocarbons and Polar  
Molecules submitted by JON GERALD COLLINS in partial  
fulfilment of the requirements for the degree of  
Doctor of Philosophy.



## ABSTRACT

Ionization phenomena in gases were studied mass spectrometrically using a 40 to 100 kev proton beam as the ionizing medium. The research involved two separate areas in the field of ionization phenomena. The first dealt with ionization cross sections and fragmentations of molecules induced by the high energy protons. The second area of research was studies of ion-molecule reactions at high ion source pressures.

Ionization and charge transfer cross sections for Kr, Ne,  $N_2$ ,  $CH_4$ ,  $C_2H_4$  and  $n-C_4H_{10}$  were measured with 40 to 100 kev protons. The simple ionization cross sections are almost constant in this energy range, while the charge transfer cross sections are roughly 40% of the total ionization at 40 kev and decrease to about 10% at 100 kev. The ionization cross sections of a variety of molecules, including some alkanes, alkenes, alkynes, chloroalkanes and benzene, were measured with 100 kev protons and could be linearly related to the molecular polarizabilities.

The mass spectra of a number of hydrocarbons were measured with 50 and 100 kev protons. The mass





spectra are qualitatively very similar to spectra obtained with electrons of the same velocity (55 ev for 100 kev protons). This is to be expected from a qualitative extension of the Bethe-Born equation to ionization of molecular electrons. Since the mass spectra change little with velocity, the fragmentation patterns with 50-75 ev electrons are a good guide to ionization by any (singly) charged particle with velocity higher than  $3 \times 10^8$  cm/sec.

Fragments of high appearance potentials and doubly charged ions are considerably more abundant in 50-100 kev proton spectra than at higher proton energies or in the electron impact spectra. Conclusions can be made as to the charge exchange mass spectra produced by particles with velocities in the range  $10^8$  cm/sec. These mass spectra are very different from charge transfer spectra obtained at low primary ion energies. Thus there is little dependence on the recombination energy of the primary ion. The charge transfer spectra seem not very different from the spectra produced by simple ionization. This means that the distribution of internal energies imparted to the new ion cannot be very different from that in pure ionization.



Ion-molecule reactions in methane were studied at ion source pressures up to 2.2 torr. Since use of 100 kev protons as the ionizing medium for mass spectral studies at elevated ion source pressures is a new method, comparisons with previous studies to test the technique were thought to be desirable. Good agreement was found with previous studies of ionic reactions in methane using electron impact indicating that this new ionizing medium can be useful in ion-molecule reaction studies in the gas phase. The main secondary product ions  $\text{CH}_5^+$  and  $\text{C}_2\text{H}_5^+$ , were found to be essentially inert in methane. The product ions  $\text{C}_2\text{H}_4^+$  and  $\text{C}_3\text{H}_5^+$ , which are of lesser intensities, also appear to be unreactive. No product ions of higher mass than  $\text{C}_3\text{H}_7^+$  are found which could be unequivocally ascribed to ion-molecule reactions. Reaction cross sections for the primary and secondary ions in methane were measured.

At varying ion source pressures up to 1.25 torr, extensive ionic polymerization, due to ion-molecule reactions, was found in ethylene. Ions up to mass 140 were found in mass spectrum at 1 torr. One principal series of ions found is of general formula  $\text{C}_k\text{H}_{2k-1}^+$ , where k is odd. Reaction cross sections for the primary and some secondary ions in ethylene were





measured.

Ion-molecule reactions in nitric oxide-ethylene mixtures were studied at varied nitric oxide concentrations at total ion source pressures up to 1 torr.

The primary  $\text{NO}^+$  formed by both ionization (by the proton beam) and by charge transfer from some ions of ethylene reacts rapidly with ethylene to yield mainly  $\text{C}_4\text{H}_8\text{NO}^+$ . Other NO-containing hydrocarbon ions such as  $\text{C}_2\text{H}_5(\text{NO})_2^+$  and  $\text{C}_6\text{H}_{12}\text{NO}^+$  were also observed in the spectra. From studies with low NO concentrations it was shown that  $\text{C}_4\text{H}_8\text{NO}^+$  is also formed by reactions of ethylenic ions with nitric oxide.

Ion-molecule reactions in water vapor at ion source pressures up to 1 torr were studied. Clustering of water molecules around the hydronium ion  $\text{H}_3\text{O}^+$ , were the predominant reactions so that essentially the only product ions observed were of the general formula  $\text{H}_3\text{O}^+ \cdot n\text{H}_2\text{O}$ . At pressures above 0.3 torr, clustering near equilibrium was probably achieved, indicating that clustering equilibrium is achieved very rapidly.

In the system methanol-water, it was found that at methanol concentrations above 2%, methanol preferentially solvates the  $\text{CH}_3\text{OH}_2^+$  core, ahead of



water. For larger clusters (more than seven molecules solvating) water is taken up preferentially. By comparison with equilibrium experiments, with an ionic reaction time of 1 millisecond, it was shown that near equilibrium clustering was achieved very rapidly, possibly in about  $10^{-5}$  seconds.





## ACKNOWLEDGEMENTS

The author expresses his deep appreciation for the guidance and encouragement of Dr. Paul Kebarle in all phases of this work.

The helpful discussions and assistance of many graduate students in Chemistry is acknowledged.

The author would like to acknowledge the assistance of the technical staff of the Chemistry Department and of the Technical Services Machine Shop.

The author wishes to thank Mrs. Lea Watson for typing part of this thesis.

The understanding and encouragement of the author's wife, Maxine, is sincerely appreciated. Her care and speed in typing the main part of the thesis was invaluable.



## TABLE OF CONTENTS

	Page
ABSTRACT	i
ACKNOWLEDGEMENTS	iii
TABLE OF CONTENTS	vi
LIST OF FIGURES	xii
LIST OF TABLES	xv
1. INTRODUCTION	1
PART I. IONIZATION AND DISSOCIATION OF ATOMS AND MOLECULES BY HIGH ENERGY PROTONS	1
1.1 Classification of Inelastic Collisions	1
1.2 The Collision Cross Section	2
1.3 Measurement of Inelastic Collision Cross Sections	4
1.4 General Description of Ionization and Charge Transfer by High Velocity Atomic Ions	6
A. Ionization	6
B. Charge Transfer	8
1.5 The Bethe-Born Approximation	12
1.6 Scope of Present Project	14
A. Mass Spectral Studies	14
B. Ionization Cross Section Studies	16
PART II. ION-MOLECULE REACTIONS IN GASES	17
1.7 Processes Occurring at Elevated Ion Source Pressures	17



	Page
1.8 Ion-Molecule Reaction Cross Sections and Rate Constants	19
1.9 The Trend Toward Increased Pressures in Ion-Molecule Reactions	23
1.10 Scope of the Present Study	24
A. Advantages of a 100 kev proton beam compared to other ionizing media	24
B. Systems studied	26
C. References to previous research	26
2. EXPERIMENTAL	28
2.1 Proton Generator	28
A. Apparatus description	28
B. Principles of operation	32
C. Safety precautions	36
D. Operating procedure and maintenance	36
2.2 The Mass Spectrometer	39
2.3 Sample Inlet System	43
2.4 Cross Section Measurements	45
2.5 Low Pressure Mass Spectral Measurements (Primary Proton Impact Spectra)	48
2.6 Ion Molecule Reactions - (High Pressure Mass Spectra)	49
A. Ion Source	49
B. Thin foils in the ion source	49
C. Secondary electron multiplier	53
D. "Metastable" suppressor	55
E. Ion source pressure measurements	56
F. Sample inlet system	56





	Page
3. IONIZATION CROSS SECTIONS; PRIMARY PROTON MASS SPECTRA	
PART I. Cross Section Measurements	58
1.1 Cross Section Evaluation from Experimental Results	58
1.2 Comparison with Previous Results	61
1.3 Errors in Cross Section Measurements	61
A. Pressure measurement	61
B. Influence of $\text{H}_2^+$ in the proton beam	64
C. Secondary electron effects	64
1.4 New Cross Section Values	65
1.5 Discussion of Ionization Cross Section Results for Molecules	69
PART II. Mass Spectra	70
4. ION-MOLECULE REACTIONS IN METHANE	86
4.1 Introduction	86
A. Previous results	86
B. Scope of present study	88
4.2 Results	89
4.3 Determination of Reaction Cross Sections	92
4.4 Discussion of Results	98
4.5 Conclusions	104
5. ION-MOLECULE REACTIONS IN ETHYLENE	106
5.1 Introduction	106
A. Previous studies	106
B. Present investigation	110
5.2 Results	110





	Page
5.2 Reaction Cross Sections, Q	115
5.3 Discussion of Ionic Polymerization in Ethylene	117
A. Variation of ionic intensities with pressure	117
B. Agreement of totals of assigned product R.A.'s with the R.A. of their (initial) primary precursors	123
C. Influence of external factors on the observed mass spectra	127
5.5 Conclusions	130
5.6 Suggestions for further research	132
6. GASEOUS IONIC REACTIONS IN ETHYLENE-NITRIC OXIDE MIXTURES	133
6.1 Introduction	133
6.2 Results and Discussion	137
A. Ionic reactions in ethylene contain- ing a high concentration of nitric oxide	137
B. NO-ethylene mixtures at low (1% and 4%) NO concentration	141
6.3 Conclusions	143
7. ION-SOLVENT MOLECULE INTERACTIONS IN THE GAS PHASE	144
7.0 General Introduction	144
A. Previous work	144
B. Present research	145
PART I. The System $(\text{H}_2\text{O})_n \text{H}_3\text{O}^+$	145



7.1	Introduction	145
7.2	The Higher Pressure Mass Spectrum of Water Vapor	147
7.3	Reactions of the Primary Ions, $\text{H}_2\text{O}^+$ and $\text{OH}^+$	149
7.4	The "Beam Model" of Consecutive Hydration Steps	149
7.5	Equilibrium in the Hydration of $\text{H}_3\text{O}^+$	154
7.6	Conclusions	160
7.7	Suggestions for Further Experiments	161
PART II	Competitive Solvation in the Gas Phase, The System Water-Methanol	163
7.8	Introduction	163
7.9	Results	164
7.10	Calculation of the Preferential Take Up of Methanol into the Water-Methanol Clusters	172
7.11	Equilibrium in the Solvation of $\text{MH}^+$ by Water and Methanol	176
	A. Qualitative model	177
	B. Comparison with other equilibrium Results	177
7.12	Further Discussion of the Solvation of $\text{MH}^+$ by Methanol and Water	178
	A. Variation of $\gamma$ with increasing $n$	178
	B. Use of the "electrostatic theory" in the interpretation of competitive solvation	181



	Page
C. Evidence for shell structure in competitive solvation of $MH^+$ by methanol and water	182
7.13 Conclusions	182
7.14 Suggestions for Further Research	183
BIBLIOGRAPHY	184
APPENDIX	189





## LIST OF FIGURES

FIGURE		Page
1.1	Cross-Sectional View of an Ion Source with Elevated Gas Pressure	18
2.1	The Proton Accelerator	29
2.2	Schematic View of the Proton Accelerator	31
2.3	The Proton Accelerator Ion Source	
2.4	The Ion Source Section of Proton Beam Mass Spectrometer	33 35
2.5	The Mass Spectrometer	41
2.6	The Mass Spectrometer Ion Source	42
2.7	Sample Inlet System	44
2.8	Typical Saturation Current Curve for Collection of Both Positive Ions and Electrons	47
2.9	The Mounting of Ion Source Foils	51
2.10	Schematic View of Secondary Electron Multiplier (SEM) Collection	54
3.1	Plot for Evaluation of $\sigma_+$ and $\sigma_-$ by 100 kev Protons in Krypton	59
3.2	Plot for Evaluation of $\sigma_+$ for n-Butane for 40 kev Protons	60
3.3	Simple Ionization Cross Sections, $\sigma_-$ , of Neon, Nitrogen and Krypton with 40 to 100 kev Protons	62
3.4	Gross Ionization Cross Sections, $\sigma_+$ of Krypton, Nitrogen and Neon for 40 to 100 kev Protons	63





FIGURE		Page
3.5	Total (or Gross) Ionization Cross Sections and Charge Transfer Cross Sections of Methane, Ethylene and n-Butane for 40 to 100 kev Protons	66
3.6	Simple Ionization Cross Sections ( $\sigma_-$ ) for Methane, Ethylene, and n-Butane for 40 to 100 kev Protons	67
3.7	Correlation Between Cross Sections $\sigma_+$ and $\sigma_-$ with 100 kev Protons and Number of Valence (Outer Shell) Electrons	71
3.8	Correlation between Polarizabilities of Compounds and Ionization Cross Sections with 100 kev Protons	72
3.9	Fragmentation Pattern Dependence on Proton Velocity (Energy) for Ethylene	81
4.1	Relative Abundances of Product Ions in Methane as a Function of Ion Source Pressure	90
4.2	Variations with Pressure of Relative Abundances of Some Ions in Methane	91
4.3	Comparison of Ionic Product Variations in Methane	99
4.4	Comparison of Ionic Product Variations in Methane	100
5.1	Mass Spectra of Ethylene at Various Ion Source Pressures	112
5.2	Comparison of High Pressure Mass Spectra of Ethylene	113
5.3	Mass Spectra of Ethylene at Different Ion Source Pressures	116
5.4	Variations with Pressure of Main Product Ions in Ethylene Formed from a $C_2H_4^+$ Precursor	119



FIGURE	Page
5.5 Variations with Pressure of Main Product Ions in Ethylene Due to a $C_2H_3^+$ Precursor	120
5.6 Variations with Pressure of Main Product Ions in Ethylene Due to a $C_2H_2^+$ Precursor	121
6.1 Mass Spectrum of 20 torr Ethylene with 0.1% NO	136
6.2 Mass Spectra of 21% NO-Ethylene Mixtures	138
6.3 Mass Spectra of Ethylene-NO Mixtures at Low Concentration of Nitric Oxide	142
7.1 Intensities of Hydrate Ions in Water Vapor at Pressures up to 1 torr	148
7.2 Fit of Experimental Water Vapor Mass Spectra to the Successive Reaction Scheme Calculated from Equation (7.8)	153
7.3 Fit of Experimental Water Vapor Mass Spectra to the Equilibrium Mass Spectra	156
7.4 Effect of Increasing Ion Exit Energy in the Mass Spectrum of Water Vapor at 0.36 torr	159
7.5 Mass Spectra of Water and Water-Methanol Mixture	165
7.6 Mass Spectrum of Methanol-Water Mixture	166
7.7 Mass Spectra of Water-Methanol Mixture and Pure Methanol	167
7.8 Variations of Summed Cluster Groups of $L_nH^+$ in Methanol-Water Mixtures	171
7.9 Variation of $\log \gamma$ versus Number of Solvated Molecules (n)	179



LIST OF TABLES

Table		Page
3.1	Normalized Cross Sections for 100 kev protons	69
3.2	Comparative Mass Spectra of Hydrocarbons Ionized by 50 and 100 kev Protons and 55 ev Electrons	73-75
3.3	Comparison Between 55 ev Electron and 100 kev Proton Spectra Percentage of Ion Yields of Fragments for which Deviation is $\leq 0.1$	77
4.1	Total Reaction Cross Sections of Ions with Methane	95
4.2	Rate Constants of Reaction of Product Ions with Methane	97
4.3	Primary (low pressure) Mass Spectrum of Methane	103
5.1	Total Cross Sections for Reactions of Ions with Ethylene	118
5.2	Ion Product Balance for Selected Ethylene Pressures (repeller = 11 V/cm)	124
7.1	Mass Spectra of Water-Methanol Mixtures at 0.36 torr Water and Varying Methanol Concentrations	169







Table		Page
7.2	Mass Spectra of Methanol-Water Mixtures Showing Competitive Solvation of the Proton by Methanol and Water Molecules.	173
7.3	Coefficients of Preferential Methanol take up ( $\gamma$ ) in the Water-Methanol Clusters.	175



## 1. INTRODUCTION

This thesis describes experimental work done with a mass spectrometer in which the ionizing medium is a 40 to 100 kev proton beam. The mass spectrometer is coupled to a Cockroft-Walton type proton accelerator. The proton beam mass spectrometer was constructed by the author for investigations into two somewhat different areas in the field of ionization phenomena. The first area deals with the ionization cross sections and ionic fragmentations of molecules induced by high energy protons. The second field is that of ion-molecule reactions at high pressures. A discussion of the background information and the areas which will be investigated is given below. The two main areas of the research mentioned above will be discussed separately in Parts I and II of this introduction.

### PART I. IONIZATION AND DISSOCIATION OF ATOMS AND MOLECULES BY HIGH ENERGY PROTONS

Ionization and dissociation of gas atoms and molecules by fast protons falls in the general area of inelastic collisions between ionic particles and atoms or molecules. An inelastic collision involves conversion of kinetic energy of the incident beam of fast ions to internal energy of the target species

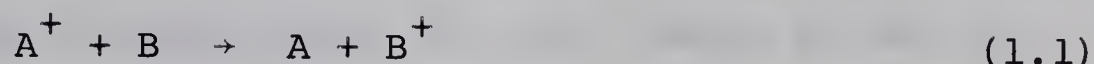
(atoms or molecules). <sup>Transfer of internal energy between the collision</sup> A classification of some of the pheno- <sup>partners</sup> can also occur. mena due to inelastic collisions between these systems is first given.

#### 1.1 Classification of Inelastic Collisions

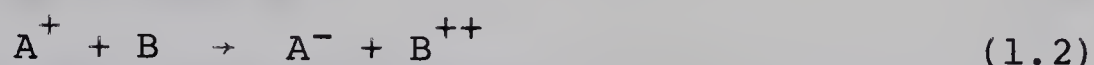
Considering the impact of a simple atomic ion  $A^+$  on



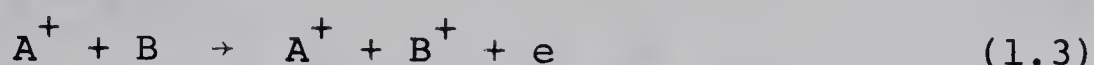
a stationary atom B, a variety of types of inelastic reactions can occur. Some of these are single charge transfer:



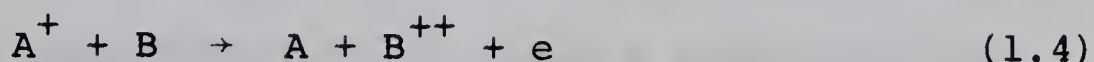
double charge transfer:



ionization:



transfer ionization:



and stripping:



The stripping of electrons from the incident particle ( $A^+$ ) as in reaction (1.5) cannot occur using incident protons.

In molecular systems dissociation to yield fragment ions by both charge transfer and ionization can occur as in reactions (1.6) and (1.7), respectively.



Since the probability of occurrence of these phenomena due to inelastic collisions may be described and measured by collision cross sections, this concept will now be discussed.

## 1.2. The Collision Cross Section $\sigma$

Consider a monoenergetic beam of  $N_0$  particles per second incident upon a gas whose concentration is  $n$  particles per  $\text{cm}^3$ . It can be considered that the target particles present







an effective area,  $\sigma$ , (in  $\text{cm}^2$ ) to the incident beam. After travelling a small distance  $dx$  (cm) in the gas, the unreacted component of the incident beam,  $N$ , will change by  $dN$ , as given by

$$dN = -nN\sigma dx \quad (1.8)$$

Integrating Eq. (1.8) we obtain

$$N = N_0 e^{-\sigma n x} \quad (1.9)$$

A knowledge of  $N_0$ , and the value of  $N$ , the unreacted component after the beam has travelled a distance  $x$  through a gas of concentration  $n$  particles/cc will yield a value for the collision cross section in  $\text{cm}^2/\text{target atom or molecule}$ . If incident particles of unit charge are used, then we can substitute currents into Eq. (1.9) to give

$$i_p = i_p^0 e^{-\sigma n x} \quad (1.10)$$

where  $i_p$  is considered to be the primary (incident) ion beam current after traversing a distance  $x$ , and  $i_p^0$  is the initial incident beam current at  $x = 0$ .

If ionization is being measured then

$$i_p^0 = i_p + i_s \quad (1.11)$$

where  $i_s$  is the ion current produced due to the target ionization. Therefore upon substitution of Eq. (1.11) into Eq. (1.10) we obtain

$$\frac{i_s}{i_p} = e^{\sigma n x} - 1 \quad (1.12)$$

and

$$\sigma = \frac{\ln(1 + i_s/i_p)}{n x} \quad (1.13)$$



If  $i_s/i_p \leq 0.05$ , then Eq. (1.13) can be approximated to be

$$\sigma = \frac{i_s}{i_p n x} \quad (1.14)$$

with an error of only 2% for  $i_s/i_p = .05$ .

### 1.3 Measurement of Inelastic Collision Cross Sections

Most experimental studies of ionization and charge transfer by high velocity ions include the total collection of the slow ions and/or electrons produced when the primary beam traverses a "thin" gas target,<sup>1, 2</sup> (i.e. low gas concentration). The method that has commonly been used is the "condenser" method in which saturation currents of positive ions or electrons produced are collected on two parallel plates by use of appropriate potentials. The incident ion beam will be essentially undeflected by these potentials unless it is of very low energy. The <sup>effective</sup> length of the condenser electrode defines  $x$  in equation (1.14).

These measurements are usually conducted at "thin target" conditions (about  $10^{-5}$  to  $10^{-3}$  torr). At these pressures, when  $x$  is not too large, the incident beam remains essentially unattenuated over the whole path length  $x$ , since the probability is small that an incident ion will undergo even one collision in traversing the gas target region. In this case Eq. (1.14) accurately applies.

For primary ions which consist of a bare nucleus as protons and deuterons, three apparent cross sections can usually be determined: (1) the cross section for production of slow positive





ions  $\sigma_+$ , which will include contributions from processes (1.1) to (1.4) and also (1.6) and (1.7). Since multiply charged ions may be produced and collected, the measured cross section is really the weighted sum

$$\sigma_+ = q^+ + 2q^{++} + 3q^{3+} + \dots \quad (1.15)$$

where  $q^{n+}$  is the sum of the cross sections for all events involving ejection of  $n$  electrons from a target molecule.

(2) The cross section for production of slow electrons  $\sigma_-$ , which will include contributions from processes (1.3), (1.4) and (1.7) if no stripping of the incident ions is involved.

This apparent cross section is in fact equal to the cross section for ionization, since only electrons from ionizing events are measured. The probability of negative ion formation as in Eq. (1.2) is usually very small. The cross section  $\sigma_-$  will also be a weighted sum of the type in Eq. (1.15). Under thin target conditions, an inappreciable number of secondary electrons are usually produced in the gas by electrons ejected from the projectile or target. (3) The charge transfer cross section  $\sigma_c$ , which will include contributions from processes (1.1), (1.2), (1.4) and (1.6), may be evaluated from the equation

$$\sigma_c = \sigma_+ - \sigma_- \quad (1.16)$$

These three cross sections could not be so readily separated if stripping of incident ions, process (1.5), occurred.

For molecular targets, it may be noted that, the individual cross sections,  $\sigma_+$  's, for all the various slow ion





fragments produced could be evaluated by mass spectrometric analysis, assuming all slow ions from the target molecules are extracted and mass analysed <sup>with equal</sup> efficiency. The separate assessment of contributions due to charge transfer and pure ionization, however, cannot be made if both processes are occurring.

#### 1.4 General Description of Ionization and Charge Transfer by High Velocity Atomic Ions.<sup>1-4</sup>

##### A. Ionization

A fast atomic ion in passing through a gas makes ionizing collisions, loses little energy and is scattered through only small angles. The ions produced (from the target species) are scattered at nearly 90° to the projectile beam and will normally receive only very small "knock on" kinetic energy. In a very small fraction of the collisions, ions produced may receive up to the full kinetic energy of the projectile, with the latter being scattered through a large angle.

The cross sections for ionization by atomic particles behave analogously to cross sections for electron impact ionization in that they increase to a maximum with increasing impact energy, whence the cross section then falls off at sufficiently high energies. Ionization of atoms by atomic particles can take place even at tens of ev, where the energy threshold is given by

$$E_{\min} = \frac{E_i (m_1 + m_2)}{m_1} \quad (1.17)$$



where  $m_1$  and  $m_2$  are the masses of the incoming and target particles, and  $E_i$  is the ionization potential of the target atom. This minimum energy  $E_{\min}$  would only be twice the ionization potential of a hydrogen atom for ionization of a hydrogen atom by protons.

For simple systems involving atomic and diatomic molecule targets that have been studied, the cross section peaks in the 20 to 100 kev region.<sup>2</sup> In general, simple ionization by atomic particles is not important at energies below a few kev since the cross section here is usually at least 3 orders of magnitude smaller than at its maximum. Above the maximum, the cross section gradually decreases with increasing projectile energy but remains sizeable up to about 1 Mev. This wide energy range spanned in considering ionizing collisions of atomic particles is in contrast to that for electron impact. The electron impact ionization cross section rises from zero at the appearance potential of the target and then rapidly rises to a peak value near 100 ev. The cross section then monotonically decreases with increasing electron energy so that at 3000 ev the values are less than one-tenth the maximum value.

As will be shown later (see Sec. 1.5), the velocity of the incident particle is an important parameter in considering ionization by various media. The classical Thomson theory of ionization<sup>5</sup> predicts that electrons and protons of equal velocity on a given target should have the same cross section for ionization. The same prediction is made by quantum theory,





but with the important qualification that the comparison is valid only if the projectile velocities are high, so that the Born approximation<sup>3</sup> may be applied. This will be discussed more fully in Sec. 1.5.

A qualitative explanation may be given for the fact that ionization cross sections by fast atomic projectiles reach their maxima at such high energies compared to electron impact. At impact energies well below the peak energy, the relative velocity of the colliding particles is small compared to the velocity of the orbital electrons in the target atom. Therefore the cross section is small because the orbital electrons have sufficient time to adjust adiabatically to the slowly changing perturbation. At energies far above the peak (of the cross section curve) the interaction is of such short duration that electron ejection is improbable. The maxima for both heavy particle and electron impact are dependent on the velocity of the projectile and generally the ionization cross section maxima by various ionizing charged projectiles occur at velocities of about  $5 \times 10^8$  cm/sec.

#### B. Charge Transfer

In general, as for ionization, charge transfer has been studied mostly for atoms.<sup>3, 4</sup> In the single charge transfer process, Eq. (1.1), one electron and very little kinetic energy is transferred from the target atom to the projectile ion. The collision is a glancing one, taking place at comparatively large impact parameters (the interaction distance



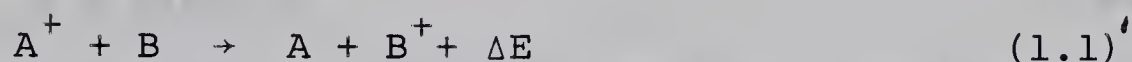


between projectile and target), except at very high energies. The product ion is scattered nearly perpendicularly to the projectile path.

One can distinguish between symmetrical resonance charge transfer reaction



and the more general asymmetric reaction as given by Eq. (1.1)'



Here  $\Delta E$ , which represents the energy change in the electronic transition (1.1)', is called the energy defect of the reaction. For atoms,  $\Delta E = \text{I.P. (A)} - \text{I.P. (B)}$ , where I.P. is the ionization potential of the atom. The energy defect is, of course, zero for resonance charge transfer. According to Massey<sup>6</sup> the cross section for charge transfer at very low relative velocities of approach will be extremely small unless  $\Delta E$  is small. The energy dependence of the charge transfer cross section can be considered in terms of Massey's adiabatic hypothesis<sup>3</sup>. At low velocities between the colliding particles, the perturbation of the neutral particle by the passing ion changes sufficiently slowly so that no electronic transition between the particles occurs. Therefore, the value for the cross section will be small. The adiabatic region of velocities is that range in which the time of electronic transition,  $\frac{h}{|\Delta E|}$  ( $h$  is Planck's constant) is much smaller than the time of collision  $\frac{a}{v}$ , where  $v$  is the velocity of the projectile and  $a$  is the



"adiabatic parameter" which is a distance of the order of atomic dimensions over which the charge transfer is deemed possible. Therefore the inequality

$$v \ll \frac{a|\Delta E|}{h} \quad (1.19)$$

marks the adiabatic region. When the time of collision becomes comparable with the time of the electronic transition, i.e. when

$$v = a|\Delta E|/h \quad (1.20)$$

the charge transfer cross section is a maximum. This marks the end of the adiabatic region. This criterion has been found to be valid<sup>1</sup> for collisions of protons (and similar light projectiles) with atoms. After the cross section maximum is reached, the cross section will decrease with increasing kinetic energy, since the interaction time ultimately becomes too short for the transition to be likely.

The energy defect can be exothermic or endothermic. There will be an energy threshold for endothermic charge transfer below which the cross section is zero. Tal'roze<sup>7</sup> has shown experimentally that this threshold is practically similar to that calculated from conservation of energy and momentum. For symmetrical resonance charge transfer, Eq. (1.18), the maximum cross section will occur at zero velocity.

The charge transfer cross section has been found to fall off much more rapidly at high energies past the maximum cross section than do the ionization cross sections<sup>1</sup>. In certain very simple cases (eg. the collisions  $H^+$  with  $H_2$  etc.), the





charge transfer cross section is found to fall off as  $\sigma \propto v^{-x}$  where  $x = 4$  to  $10$ . For ionization the cross section falls off only as  $\sigma \propto v^{-2} \ln v$ .

Charge transfer cross section data on molecules more complicated than  $N_2$  or  $CO$  are almost nonexistent for medium and high ion velocities, i.e. for  $v > 10^7$  cm/sec (corresponds to proton energies greater than 1 kev). With regard to the fragmentation pattern induced by charge transfer of molecules with high velocity particles, there is an absolute lack of theoretical and experimental information. Charge transfer to polyatomic molecules is a case in which "accidental" resonance is nearly always present. This is because the molecular ions of polyatomic molecules have a very large number of excited states and near resonance can be obtained as long as the recombination energy (R.E.)\* of the incident ion is higher than that of the molecule. Considerable studies of charge transfer to molecules at low projectile velocities ( $v < 10^7$  cm/sec), have been done by Lindholm<sup>8</sup> and others.<sup>9</sup> At these velocities the ionization cross sections are very small and charge transfer is dominant. It is found that the fragmentation pattern depends on the nature of the projectile only through its recombination energy (R.E.), i.e. through the excitation energy deposited in the charge acceptor. Ionic breakdown diagrams for a number of molecules have been constructed with the use of projectiles with different R.E.'s. It is generally observed that a given fragment  $R_1^+$  from the molecule  $R_1R_2$  is produced in maximum abundance when the R.E. of the projectile

---

\* R.E. of incident ion P for the process  $P^+ + S \rightarrow P^* + S^+$  equals  $I.P.(P) - E_x$ , where  $E_x$  is the excitation of  $P^*$  over the ground state of  $P^*$ .





is about 1 to 1.5 ev higher than the energy required for the fragmentation leading to  $R^+$ , i.e. higher than  $A_p(R^+)$ . The question as to what happens to the charge transfer mass spectrum when the velocity of the projectile is increased does not seem to have been considered.

### 1.5 The Bethe-Born Approximation

Ionization cross sections cannot be calculated exactly for a complete energy range, even for a simple system such as a proton incident upon a hydrogen atom. Basically, this is because of the extreme difficulty in solving the time-dependent Schrodinger wave equation for the system of colliding particles. Therefore more approximate methods based on the time-independent wave equation have been used. One of the most useful methods is the Born approximation<sup>3,6</sup> which is valid for high impact velocities. The basic assumption of the Born approximation is that there is little interaction between the projectile and the target. The following specific assumptions can then be made: (1) the projectiles may be represented by a plane wave since the incident wave is undistorted by the interaction, (2) excitation to any final state comes only as the result of a direct transition from the initial state, (3) distortion of the wave of the scattered projectile may be neglected since the potential energy of the interaction between the scattered projectile and the target in its final state is small. Even with these assumptions, extremely difficult calculations remain, and in fact the results cannot be obtained in closed analytical form. A further approximation of Bethe<sup>3,10</sup> has been used to



simplify somewhat the mathematics involved. Bethe obtained an equation for the general cross section  $\sigma_{n\ell}$  for the ejection into the continuum of a single electron from the  $n, \ell$  shell of the target atom by a point charge ion of charge  $+Z_e$  to be

$$\sigma_{n\ell} = \frac{2\pi Z^2 e^4 c_{n\ell} Z_{n\ell}}{m_e v_o^2 |E_{n\ell}|} \ln \frac{2m_e v_o^2}{c_{n\ell}} \quad (1.21)$$

where  $Z$  and  $v_o$  are the charge and velocity of the projectile,  $m_e$  and  $e$  are the mass and charge of the electron,  $c_{n\ell}$  is the dipole matrix element for the electronic transition,  $c_{n\ell}$  is an energy of the order of  $|E_{n\ell}|$ ,  $Z_{n\ell}$  is the number of electrons in the  $n, \ell$  shell and  $|E_{n\ell}|$  is the ionization energy of this shell. An identical expression can be written for the electron impact ionization cross section for ejection of a single electron from the outer shell of this atom.

It is readily seen that only the charge and velocity of the projectile is explicitly introduced into Eq. (1.21). Thus for projectiles of the same velocity the individuality of the impacting particle is only indicated by  $Z^2$ . The ionization cross section for a proton and electron of identical velocities should be identical.

It has been shown theoretically<sup>4,10,11</sup> and experimentally<sup>13</sup> that the Born-Bethe approximation holds for impacting particles of velocities four times that of the Bohr velocity\*, which is  $2.2 \times 10^8$  cm/sec. This would correspond to 400 kev protons and 220 ev electrons. The deductions that may be made from the Bethe equation apply only for simple ionization (no charge transfer)

\* The Bohr velocity, which is defined as the orbital electron velocity in a ground state hydrogen atom (in the Bohr model) is equal to  $2\pi e^2/h$ , where the symbols have been defined previously.





and for point-charge (i.e. bare nuclei) projectiles.

Kebarle and Godbole<sup>14</sup> suggested that the cross section for removal of a given electron from a molecule by different charged particles of the same velocity should be the same. It might be expected that for molecules, therefore, the cross sections for removal of various electrons from the various molecular orbitals, and thus for the production of excited ions, should be proportional for charged particles of the same velocity. Thus, Kebarle and Godbole and later Wexler<sup>15</sup> have proposed that the mass spectra due to charged particles such as electrons, protons, deuterons, alpha particles etc. at the same velocities, should be very similar at sufficiently high projectile velocities.

Kebarle and Godbole found that the mass spectra obtained with electrons change little from 50 ev to 30 kev electron energies. They suggest that a major simplification, at least from the standpoint of radiation chemistry, may be introduced for ionization by simple charged particles. This may be stated as follows: the mass spectral fragmentation patterns change little with the velocity and nature of the charged impacting particle for the velocity range in which the Bethe-Born approximation applies.\*

## 1.6 Scope of Present Project

### A. Mass Spectral Studies

Because of the deductions which can be made from the Bethe-Born approximation, Sec. 1.5, the author decided to measure the mass spectra of several molecules due to the im-

\* Takacs and Freeman<sup>12</sup> found that the electron impact mass spectra of hydrocarbons were essentially invariant for incident electron velocities down to double those of the valence electrons in the molecules.





pact of 40 to 100 kev protons. This was undertaken partly with the intention of showing the independence of the mass spectra, and therefore the ionic fragmentation process, from the nature of the ionizing particle.

Before this work was completed, three other investigations<sup>15-17</sup> were published in which results had been obtained with similar intention. Thus Wexler<sup>15</sup> using 2.25 Mev protons was able to show that the mass spectra from a number of hydrocarbons show only small deviations from the mass spectra obtained with electrons of the same velocity. He found that in general the protons gave lower yields of high appearance potential fragment ions than did the electrons of the same energy. The overall conclusions in Schuler's<sup>16</sup> work, in which a similar proton energy was used, were the same, although in many cases it was found that the protons gave increased fragmentations than did electrons of the same velocity. Abbé's<sup>17</sup> experiments extended the energy range downward from 1200 to 200 kev. Very recently Rudolph and Melton<sup>18</sup> carried out another comparative study using 2.2 Mev alpha particles and electrons of the same velocity as the alpha particles. Similar conclusions could be made from their study as in those of Wexler and Schuler and Stuber. The present work covering the range 100 to 40 kev is complementary to these studies and gives mass spectra in a range where the Born approximation begins to fail.

The range of proton energies below 100 kev is also of special interest, because charge transfer from the proton to



the molecules becomes an important process. As mentioned previously, no studies of ionic fragmentations due to charge transfer have been made above 2 kev ion energy. Therefore, the question as to what happens to the charge transfer mass spectrum when the velocity of the projectile is increased does not seem to have been considered. This is, however, a question of practical and theoretical importance. The mass spectrum, after all, is a fingerprint of the internal energy imparted to the charge accepting molecule.

#### B. Ionization Cross Section Studies

The studies of ionization cross sections of 10 to 200 kev protons have only been done for certain atoms and diatomic molecules.<sup>1-3</sup> Measurements for more complex molecules are needed, however, since such data are required by a number of fields under investigation such as plasma physics<sup>19</sup>, physics of the ionosphere<sup>1</sup>, radiation chemistry and astrophysics. Because of this, ionization cross sections were measured for several hydrocarbons with 40 to 100 kev protons. Charge transfer cross sections were also obtained in this energy range. The relative ionization cross sections for some paraffins, olefins, acetylenes, chloroalkanes and benzene with 100 kev protons were also measured. After this research was completed, a study<sup>20</sup> appeared recently with ionization cross section measurements for a few simple hydrocarbons with 30 to 100 kev protons. These results will be mentioned in the discussion of results.





## PART II. ION - MOLECULE REACTIONS IN GASES

The mass spectrometer and associated apparatus in the present study was designed with the intention of also doing studies at more elevated ion source pressures.

### 1.7 Processes Occurring at Elevated Ion Source Pressures

In primary ionization processes previously considered (Part I of this Chapter), an ion formed in the mass spectrometer ion source at low gas pressure ( $10^{-5}$  torr), will undergo essentially no collisions with neutral gas molecules before leaving the ion source. As the pressure is increased the probability that an ion will undergo collisions with unionized gas molecules is increased. In Fig. 1.1 a schematic diagram of a typical mass spectrometer ion source is shown to help us visualize the phenomena occurring as gas pressure is increased. The ionizing beam of energetic electrons, protons, etc., which is usually pre-collimated, is directed between, and parallel with, the repeller plate and the ion source exit slit. The primary ions formed in the track of the ionizing beam are impelled downward by the positive (with respect to ion box and exit slit) potential, and will collide with the unionized molecules if the gas pressure is sufficient. The primary and secondary ions exit from the ion source and are further accelerated and mass analysed as in conventional work at low pressures.

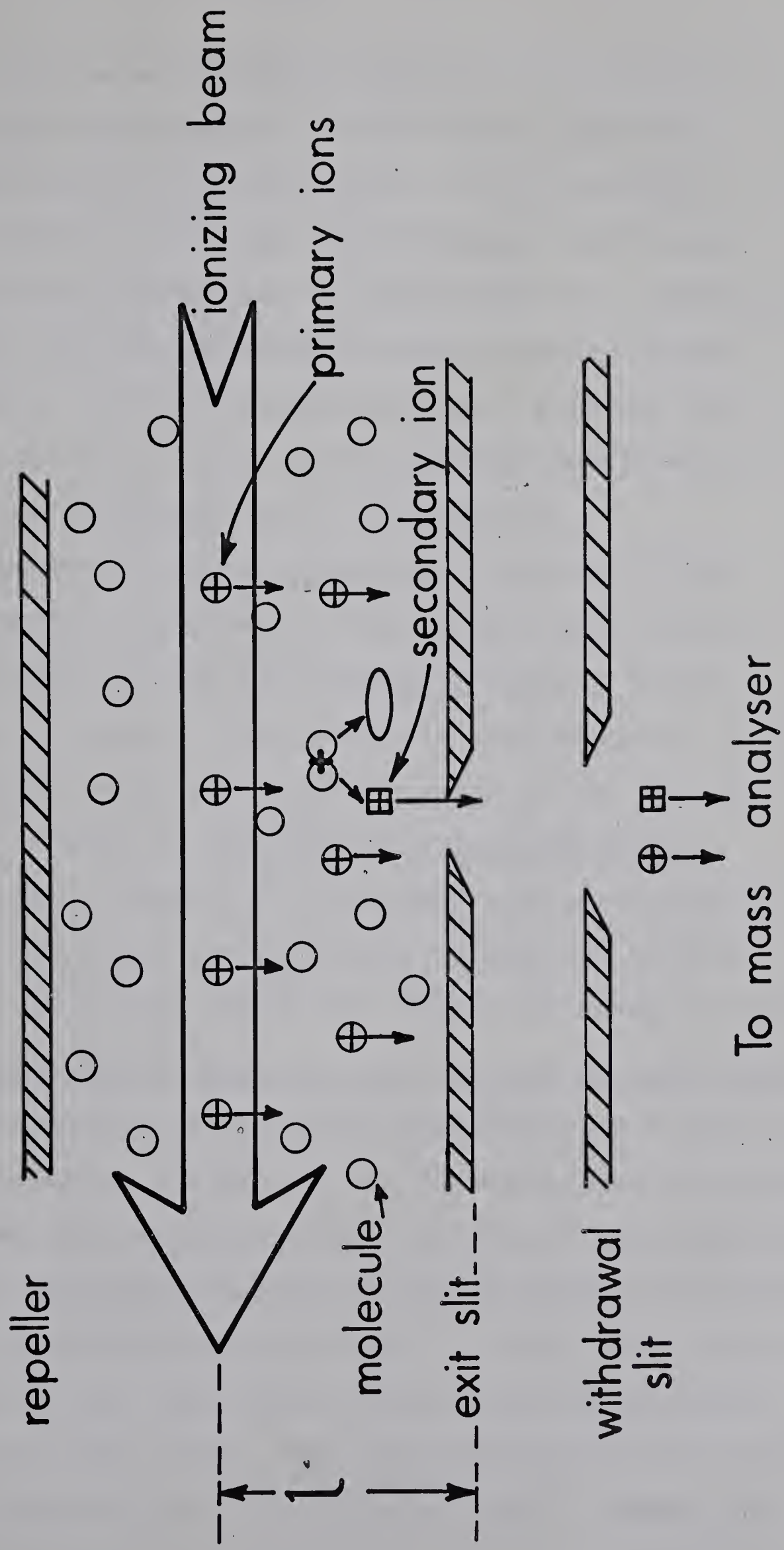
Now at a pressure of  $10^{-5}$  torr the mean free path,  $\lambda$ , of a typical small mass ion will be about 1000 cm. The number of collisions a primary ion undergoes in the distance  $l$  (the distance from central plane of ionizing beam to the ion source



FIGURE 1.1

Cross-Sectional View of an Ion Source with Elevated  
Gas Pressure.

The distance between the plane of the ionizing  
beam and the exit slit is  $\ell$  .





exit slit) will be approximately equal to  $\ell/\lambda$ . At  $10^{-5}$  torr this would correspond to  $5 \times 10^{-4}$  collisions for a typical  $\ell = 0.5$  cm. At one millitorr  $\ell/\lambda$  will be 0.05 collisions and at 1 torr about 50 collisions could occur. Thus as pressures are raised, it can be seen that collisions of secondary ions with molecules to form tertiary product ions can occur. Even at one millitorr gas pressure some secondary ions due to ion-molecule reactions should occur, if many of the collisions result in reactions.

This method of forming primary ions directly in the ion source and allowing them to react further with neutral molecules has been called the internal ionization method. Another method, which is more difficult experimentally, is to use a collimated primary ion beam in place of the ionizing beam. This is known as the external ionization method<sup>7</sup>, since the primary reactant ions are generated separately and are then directed into the ion source or reaction chamber. The internal ionization method was used in the present study.

### 1.8 Ion-Molecule Reaction Cross Sections and Rate Constants

The importance of ion-molecule reactions in the gas phase under conditions when ions are formed such as gas phase radiolysis was not recognized until the 1950's. With the start of systematic mass spectrometric studies of these reactions by Tal'roze<sup>21</sup> and Stevenson and Schissler<sup>22</sup> it was shown, especially by Stevenson et al., that these reactions can proceed with extraordinarily high rates. The high bimolecular rate constants determined (typically  $10^{-9}$  cc molecule<sup>-1</sup> sec<sup>-1</sup>), showed that





these ion-molecule reactions must be proceeding with a high efficiency, possibly with reaction upon every collision. The reaction cross sections  $Q$ , of known ion molecule processes are within the range of  $10^{-13}$  to  $10^{-18}$   $\text{cm}^2$  and reaction rate constants  $k$ 's, determined at temperatures of 400 to 500°K are within  $10^{-9}$  to  $10^{-13}$   $\text{cc}/\text{molecule-sec}$ . Consequently, the upper limits of observed  $Q$  and  $k$  values are about one to two orders of magnitude higher than the usual gas kinetic values for bimolecular processes.

The phenomenological or macroscopic cross section  $Q$ , for the reaction of a primary ion  $P^+$  with molecules  $M$  to form a secondary ion  $S^+$  as in the reaction



can be determined. The primary ion intensity,  $i_p$ , will be attenuated due to reaction to form secondary ions as the primary ions, under the influence of the positive repeller field, move toward the exit slit, as given by

$$i_p = i_p^0 e^{-\ell n Q} \quad (1.23)$$

where  $i_p^0$  is the initial primary ion intensity,  $\ell$  is the distance from plane of ionization to exit slit, (see Fig. 1.1), and  $n$  is the number of gas molecules/cc in the ion source.

At low ion source pressures where  $i_p^0 - i_p$  is very small, Eq. (1.23) can be approximated to give

$$Q = \frac{i_s}{i_p n \ell} \quad (1.24)$$



where  $i_s$  is the primary ion intensity. Equation (1.24) is valid when the gas concentration is sufficiently low that few of the primary ions can react, and those that do can interact only once.

Gioumousis and Stevenson<sup>23</sup> rederived the microscopic reaction cross section  $\sigma_g$ , based on Langevin's<sup>24</sup> classical considerations of the ion-molecule reaction taking place through a polarization interaction model, to be

$$\sigma_g = \left( \frac{2\pi e}{g} \right) \left( \frac{\alpha}{\mu} \right)^{\frac{1}{2}} \quad (1.25)$$

where  $e$  is the charge of the electron,  $g$  is the relative velocity of the reactant ion-molecule pair (and is equal to the primary ion velocity when the ion velocity is higher than thermal velocities),  $\alpha$  is the polarizability of the neutral molecule and  $\mu$  is the reduced mass of the ion-molecule pair. These workers were also able to derive an expression for the phenomenological cross section  $Q$ , by assuming that the ion velocity  $\bar{v}$  is larger than thermal, i.e. the ion velocity is much greater than the neutral molecule velocity. Now  $\bar{v}$  may be readily calculated for electrostatic considerations to be

$$\bar{v} = \left( \frac{eE_r \ell}{2m_p} \right)^{\frac{1}{2}} \quad (1.26)$$

where  $E_r$  is the repeller field strength in the mass spectrometer ion source and  $m_p$  is the mass of the primary ion.

Equating  $\bar{v}$  with  $g$  and inserting Eq. (1.26) into (1.25) they obtained

$$Q = 2\pi e \left( \frac{\alpha}{\mu} \right)^{\frac{1}{2}} \left( \frac{2m_p}{eE_r \ell} \right)^{\frac{1}{2}} \quad (1.27)$$

This equation predicts that the cross section  $Q$  is proportional to  $(E_r \ell)^{-\frac{1}{2}}$  and this has been found to be true for several but not all ion molecule reactions.<sup>25</sup> Equation (1.27)





is not expected to be valid at near thermal ion velocities.

Gioumousis and Stevenson<sup>23</sup> were also able to derive a theoretical rate constant  $k_t$  for ion-molecule reactions such as reaction (1.22) to be

$$k_t = 2\pi e \left( \frac{\alpha}{\mu} \right)^{1/2} \quad (1.28)$$

which is independent of repeller field strength.

This specific reaction rate  $k$  can be related to the phenomenological cross section  $Q$  by a comparison of Eqs. (1.27) and (1.28) and is given by

$$k = Q \left( \frac{eE_r \ell}{2m_p} \right)^{1/2} \quad (1.29)$$

It can readily be noted that

$$k = Q\bar{v} \quad (1.30)$$

or that

$$kt = Q\ell \quad (1.31)$$

where  $t$  is the ionic residence time and is equal to  $\ell/\bar{v}$ .

The derivation of Eqs. (1.25) and (1.28) assumes that reaction occurs on every collision. This has been shown to be true for many ion molecule reactions.<sup>25</sup> These observed reactions also have no temperature coefficient, i.e.  $Q$  and  $k$  are independent of temperature.<sup>25</sup> In order for a secondary ion  $S^+$  to be detected at conventional ion source pressures (e.g. up to a few torr) it is necessary that the rate of reaction be within a few orders of magnitude of the collision frequency. To an accuracy of about 5 kcal/mole it can be shown that a necessary condition for the observability of a secondary reaction in a mass spectrometer is that the





reaction must not be endothermic.<sup>25</sup> For example, an activation energy of 5 kcal/mole at conventional ion source temperatures of about 200°C would indicate a collision efficiency of about  $10^{-3}$ . Collision efficiencies lower than  $10^{-3}$  would render the reaction unobservable even at ion source pressures of a few torr.

### 1.9 The Trend Toward Increased Pressures in Ion-Molecule Reactions

Until the mid-1950's ion molecule reactions were not studied at pressures higher than about 10 millitorr. With the advent of good differential pumping between the ion source and analyzer regions and the use of larger (and faster pumping speed) pumps the pressures studied were gradually elevated. Thus, in 1958 Saporoschenko<sup>26</sup> was able to study ion-molecule reactions in nitrogen at pressure up to 0.2 torr. Melton<sup>27</sup>, Field<sup>28</sup> and Wexler<sup>29</sup> studied ion-molecule reactions in some hydrocarbons at ion source pressures up to 0.3 torr. With the thought in mind that mass spectrometric studies of ion-molecule reactions can be correlated with gas phase radiolysis studies, ion source pressures have been increased so that ionic reactions at essentially atmospheric pressure can be studied in the mass spectrometer.<sup>30</sup>

Some of the reasons why mass spectrometric studies of ion-molecule reactions in the gas phase have been conducted at ever increasing pressures can be summarized as follows. As mentioned, at intermediate ion source pressures (1 to 100 millitorr) information can be provided on the reactivity of



ions in bimolecular reactions. Studies at higher pressures can provide information on high order, consecutive ion-molecule reactions. It is also necessary to check the ion-molecule reaction rate constants which might be affected by cluster formation. At higher pressures other interesting points could be collisional deactivation of excited ions and excited ion-molecule reactions not observed at lower pressure because of decomposition of the ion in the relatively long time between collisions. Information must be obtained on these points before correlations with conventional gas phase radiolytic studies at near atmospheric pressure become really meaningful.

At higher pressures (above 1 torr), electron beams of conventional energies (70 - 200 ev) have too low a penetrating power. Kebarle and coworkers<sup>30</sup> use 5 Mev alpha particles in the near atmospheric mass spectrometer. The ion source of this mass spectrometer is different from the conventional one described earlier, in that ions are sampled from the high pressure region through a pinhole or series of pinholes without aid of a repeller field in the ion source.

#### 1.10 Scope of the Present Study

##### A. Advantages of a 100 kev proton beam compared to other ionizing media.

The vast majority of mass spectrometric studies at elevated source pressures have involved the use of an electron beam (emitted from a heated filament and accelerated by electric fields) to provide the initial or primary ions.







The penetrating power of electrons is not sufficient at pressures of about 1 torr and higher to provide a well-collimated beam of well-defined energy. Even when the electron energy is increased above the conventional energy of 70 ev, attenuation and scattering of the electron beam by the high gas pressure results. There are also instrumental difficulties, due to the pressure, resulting in reduced electron emission and burn-out of the filament.

In ion sources using an electron beam, a weak magnetic field of  $\sim 200$  gauss is conventionally used to provide collimation of the electron beam, but mass discrimination of the ions sampled from the ion source may result. Since the distance between the plane of ionization and exit slit of the ion source chamber,  $l$ , is an important parameter for calculating reaction cross sections and rate constants, the distortion of the electron beam by the repeller field may give an unreliable value for this distance. Studies with electron beams are therefore somewhat limited in variation of repeller field strength.

The alpha particle mass spectrometer of Kebarle and co-workers mentioned earlier suffers from lack of collimation of the alpha particles, thus leading to somewhat poorly defined ionic reaction times.

To try to overcome some of these problems, a 100 kev beam of protons from a Cockcroft-Walton accelerator was used as the ionizing radiation. This beam is of sufficient intensity and penetrating power that higher pressures can be studied



with ease and with little attenuation or scattering. If desired, very high repeller fields could be used without influencing beam position. No mass discrimination due to collimating magnets will exist since none are used. The source is also at room temperature in contrast to the electron-beam sources which are at  $\sim 200^{\circ}\text{C}$ . By using this method we could possibly show if the results obtained by the conventional ionizing media were influenced by some artifacts of the experimental method. These studies are also another attempt to partially bridge the pressure gap in order to approach conditions of conventional gas phase radiolytic studies.

#### B. Systems studied

Ion-molecule reactions in methane, ethylene, and ethylene-nitric oxide mixtures at pressures over 2 torr have been studied in this thesis. Some studies of hydration or clustering have been carried out for water vapor. Competitive solvation studies between methanol and water in the gas phase have also been undertaken. No attempt has been made to make an exhaustive and comprehensive study of all five systems mentioned. Rather, all were more in the nature of exploratory studies to indicate the feasibility of using this new type of ionizing medium (100 kev protons), and to point the way to further experiments along these lines.

#### C. References to previous research

All previous work on the topics mentioned in Subsection B. have been omitted here. These reference will be found in





the introductions in Chapters 4,5,6 and 7 so as to provide more continuity.

For general referral to the subject of ion-molecule reactions in gases there are several fairly recent and excellent reviews,<sup>7,25,31-33</sup> and a recent and extensive bibliography<sup>34</sup> (covering the period January 1900 to March 1966).





## 2. EXPERIMENTAL

The apparatus used consisted of a mass spectrometer which used a proton beam as the ionizing medium. The various parts of the apparatus are described below.

### 2.1 Proton Generator

#### A. Apparatus description

The source of protons was a 100 kev (variable voltage) Cockcroft-Walton<sup>35</sup> type Texas Nuclear Corporation (Austin, Texas) Model no. 100-1H proton accelerator. This particular machine was a prototype model which was available to us at a substantially reduced price. Since the proton accelerator was a prototype it will be described in some detail. The accelerator beam tube, vacuum system, and associated electrical components all are mounted on a sturdy steel chassis as shown in Fig. 2.1.

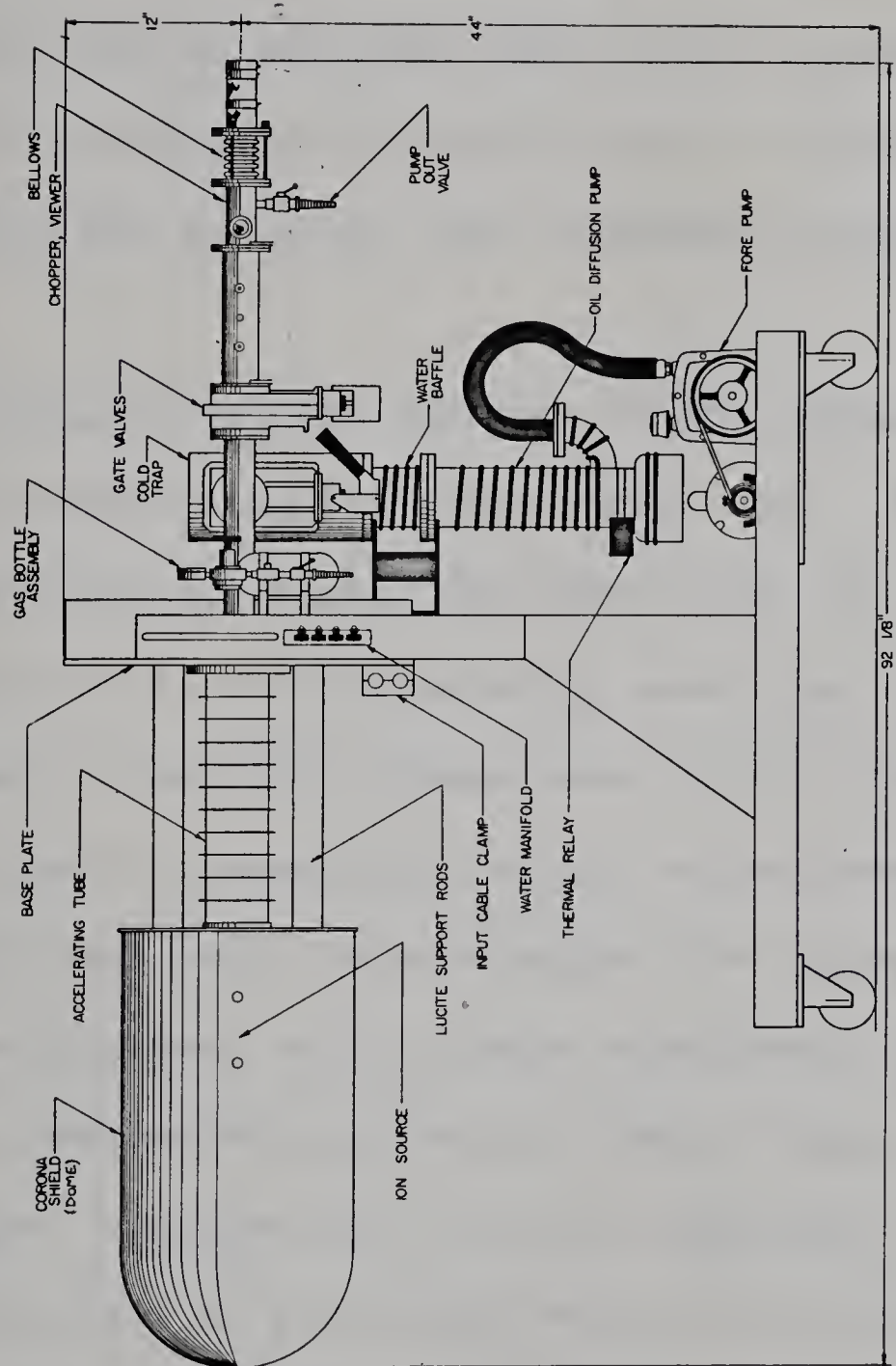
The proton accelerator consists of an ion source where the protons are generated by a radio-frequency (r-f) discharge in hydrogen gas. The protons are extracted, <sup>whence the beam is</sup> focused and accelerated by a system of electrodes. The accelerated proton beam then enters the mass spectrometer housing where, after collimation, it passes through the ion source.

The vacuum system of the proton accelerator consists of a mechanical forepump which backs a four-inch diameter oil diffusion pump. A cold water baffle and liquid nitrogen cooled cold trap are mounted above the diffusion pump. An extended range Phillips type (cold-cathode) vacuum gage is located near the cold trap.

FIGURE 2.1

The Proton Accelerator

Main features of the 100 kev Texas Nuclear Corporation proton accelerator are shown.







The beam accelerating tube is bolted directly to the heavy aluminum faceplate and consists of eleven cylindrical ceramic rings bonded, sandwich style, directly to the disc shaped accelerating electrodes. The electrostatic lens assembly is situated at the end and the ion source bottle (inside terminal dome) is coupled directly to it. These two components will be described more fully in section 2.1(B). On the other side of the faceplate, the drift tube is aligned with the accelerator beam tube and the drift tube ultimately connects with the mass spectrometer.

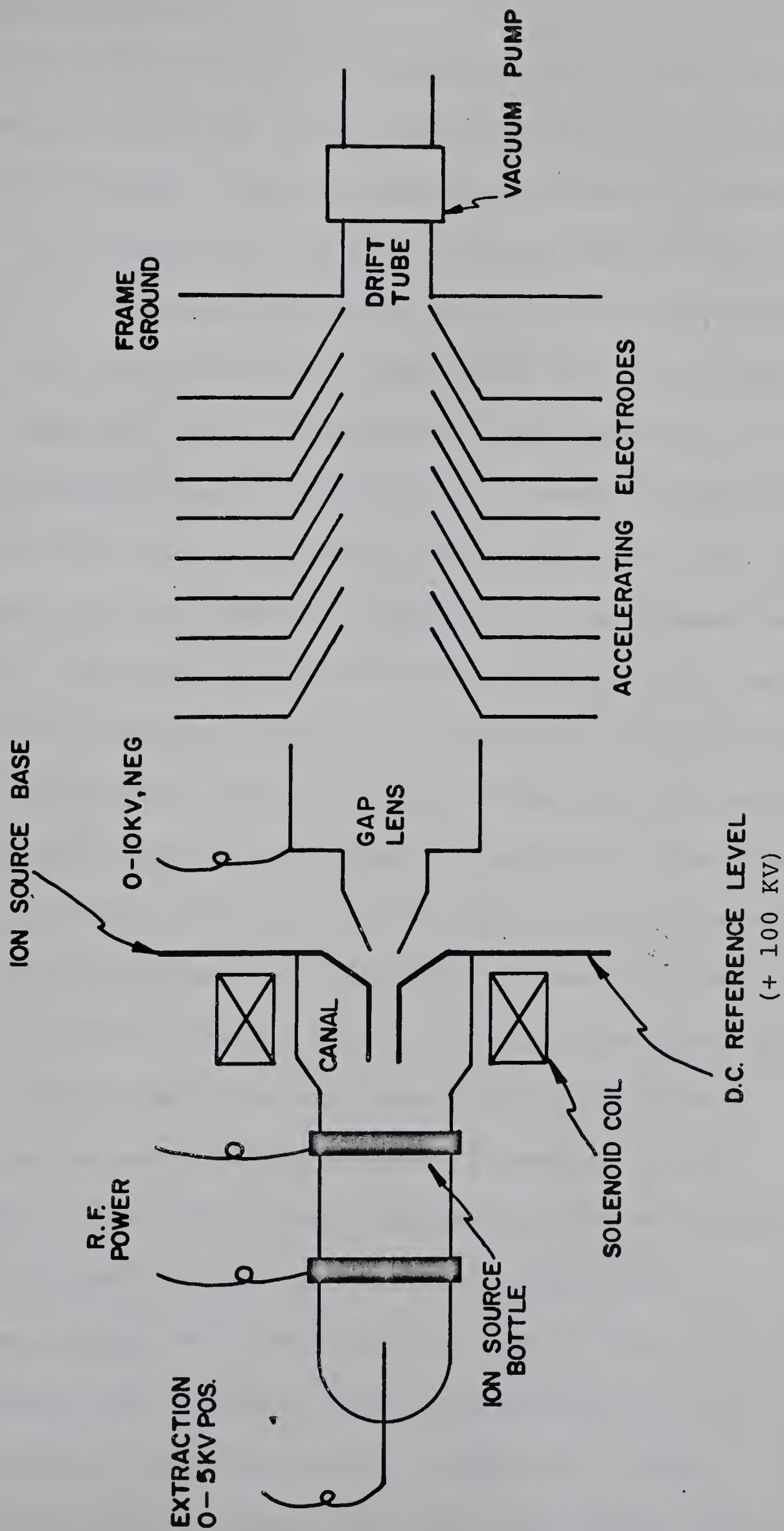
Electrically, the machine consists of the terminal dome charged to 100 kV positive potential by the power supply with a divider string of twenty 10 megohm resistors tapped off every other one to provide 10 kV steps of potential to the accelerating beam tube. An isolation transformer situated in the high voltage power supply provides 117 volts AC terminal power for operating the ion source power supplies and components associated with the accelerator ion source (see Fig. 2.2).

The ion source used in the proton accelerator is the Oak Ridge<sup>36</sup> type which produces 90% protons and 10%  $H_2^+$  ions. Two small variable high voltage supplies of 0 to 10 kV (negative) for the focus electrode (gap lens) and 0 to 5 kV (positive) for the extraction electrode are supplied by the isolated 117 VAC as well as a 0 to 30V DC power supply for the ion source solenoid and a variable AC powerstat for the palladium leak heater. Each of these variable controls is operated by means of an insulating nylon shaft connected to control servo-mechanisms on the main frame. Another rod operates a beam switch controlling power to the radio-frequency oscillator. Controls for each of these functions are on the operator's console as well

FIGURE 2.2

Schematic View of the Proton Accelerator

Protons formed in the ion source bottle are extracted, focussed and then accelerated by 100 kV.







as the control panel for the accelerating high voltage power supply.

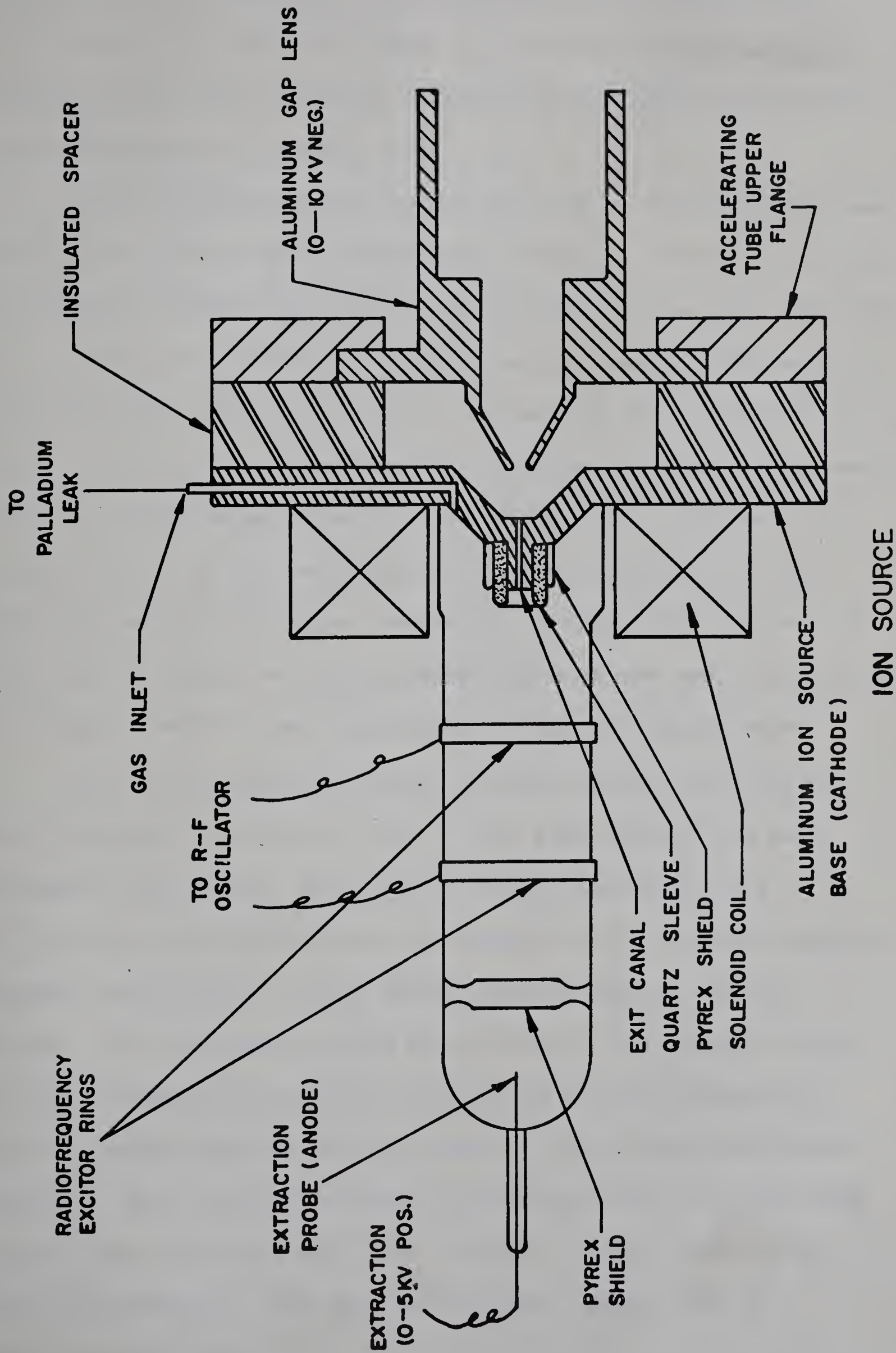
## B. Principles of operation

Hydrogen is admitted into the ion source bottle (see Fig. 2.3) through the heated palladium leak whose temperature can be varied thus varying the flow of hydrogen. Since the heated palladium is permeable only to hydrogen, other impurities (if any) are kept from the ion source bottle. An r-f field applied to the two excitor rings initially accelerates stray electrons within the source which dissociate and ionize hydrogen. Secondary electrons released upon ionization of hydrogen and accelerated by the r-f field start a steady discharge in the hydrogen. Since the hydrogen is mainly dissociated into hydrogen atoms which are then ionized, almost all the ions in the plasma are protons. The power (100 watts) delivered by the r-f oscillator maintains the discharge at hydrogen pressures of about 10 - 100 millitorr. The solenoid coil, which fits around the base of the pyrex ion bottle, produces a longitudinal magnetic field thereby restricting the electron paths to the center portion of the ion bottle and causing the electrons to spiral. The ionization density is therefore increased in the central longitudinal part of the ion bottle. The protons formed in the discharge are forced toward the exit canal by the positive (with respect to the ion source aluminum base) potential of the extraction electrode. The quartz sleeve surrounding the exit canal becomes positively charged and acts as an electrostatic lens to partially focus the protons being extracted as shown in Fig. 2.3. Protons passing through the end of the canal are focused by the negative potential of the gap lens as shown in Fig. 2.3. After the beam leaves the gap lens it enters the beam accelerating tube to



FIGURE 2.3

The Proton Accelerator Ion Source





be accelerated up to 100 kev. The accelerated proton beam then passes through the field-free region of the drift tube until it is collimated by the first tantalum collimation slit near the entrance to the mass spectrometer (see Fig. 2.4).

This collimation hole is water cooled to dissipate the heat produced by the proton beam striking the tantalum. Since this is the only connection between the proton accelerator and the mass spectrometer section, differential pumping is maintained between the two sections. At operating pressures in the proton accelerator of 1 to  $2 \times 10^{-5}$  torr, measured close to the drift tube by the Phillips pressure gage, the pressure in the mass spectrometer is still only  $1 \times 10^{-7}$  torr. Although the ion source bottle of the accelerator operates at about 10 to 100 millitorr pressure of hydrogen, pressures in the drift tube section are kept low by virtue of the low conductance of the small cylindrical (1/16" diameter and 1" long) exit canal of the ion source base.

The collimated beam passes through another circular 1mm diameter tantalum collimating hole to then pass through the mass spectrometer ion source. The beam is finally collected on a heavy tantalum lined Faraday cup (surrounded by a secondary electron suppressor guard ring at -67 V) where the beam current can be monitored. The collimating holes were lined up with respect to the holes (1/8" diameter) through the ion source and with respect to the 1/16" diameter hole of the exit canal of the proton accelerator ion source. This was done by means of sighting with a transit from the proton beam collector end (with collector flange removed) of the mass spectrometer. The mass spectrometer proper will be described later in Sec. 2.2.

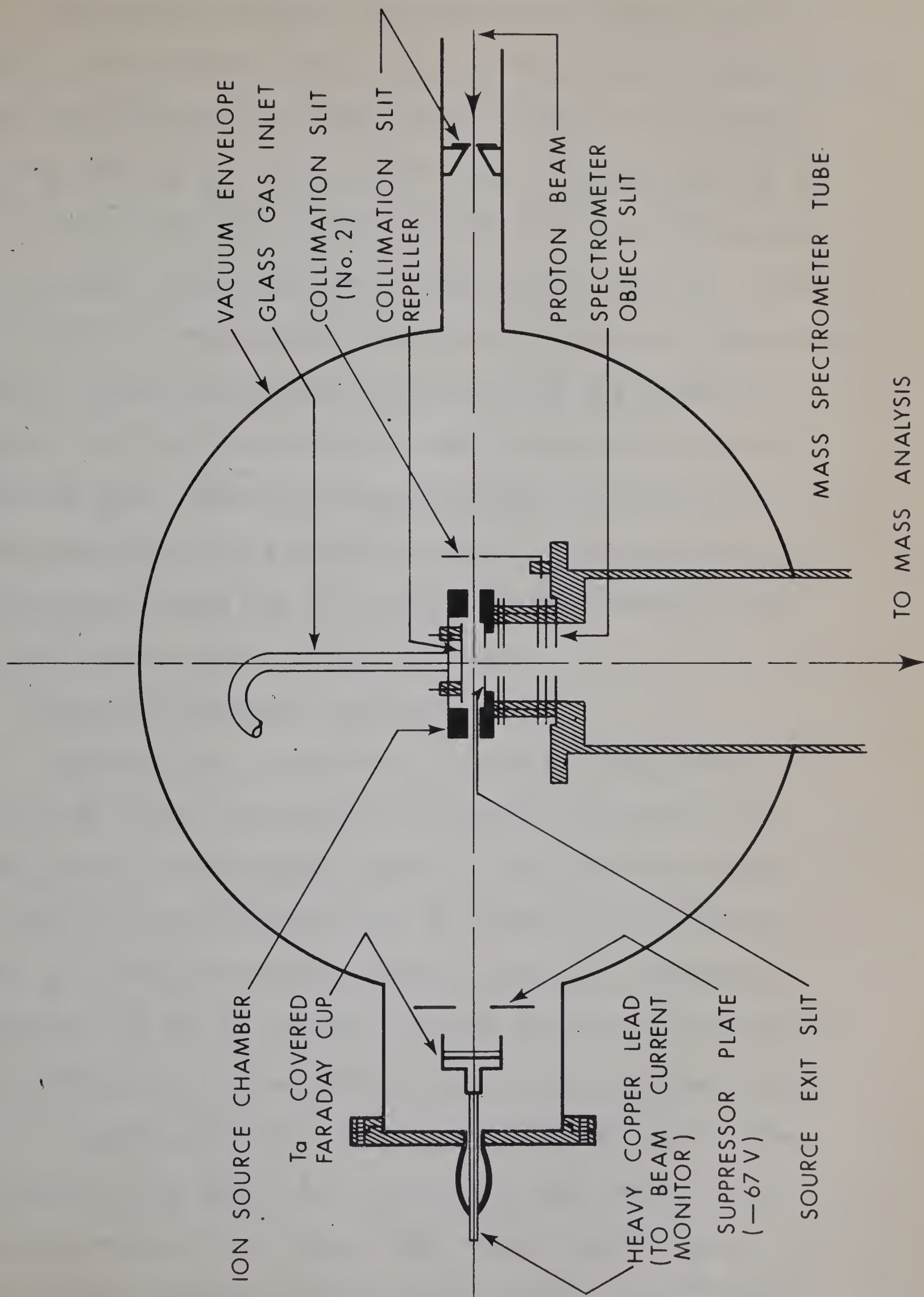
FIGURE 2.4

The Ion Source Section of Proton Beam  
Mass Spectrometer

The proton beam is collimated by the first collimation slit at the far right of the diagram. The beam is further collimated by the 2nd slit and passes through the mass spectrometer ion source to be collected in the heavy tantalum lined Faraday cup.

The view is looking down at the mass spectrometer







### C. Safety precautions

The proton accelerator was effectively walled off with a lead-lined plywood barrier with a door for access to the accelerator. This door was equipped with a microswitch connected to an interlock on the accelerator console so that high voltage could not be turned on without the door closed. If the door was accidentally opened the high voltage would be automatically turned off. Flashing red lights for warning were mounted on the barrier. These were switched on automatically when the high voltage was turned on. The barrier was lead-lined to absorb soft X-rays emitted at the high voltage dome. These X-rays most probably originate from secondary electrons in the drift tube being accelerated back up the acceleration plates and ultimately striking a metallic part in the ion source assembly of the accelerator.

### D. Operating procedure and maintenance

Terminal power is activated by means of key switch. This is turned on and the machine is allowed to warm up for at least one minute. The hydrogen supply in the evacuated teflon tubing leading to the palladium must be brought up to pressure ( $15 \text{ lbs/in}^2$ ) before the high voltage is turned on, otherwise a discharge will be set up in which the high voltage will arc through the low pressure gas in the teflon tubing to the hydrogen cylinder which is at ground potential. Then hydrogen is allowed to bleed to the ion bottle by means of the palladium leak control. The background pressure of the machine was usually  $1 \times 10^{-6}$  torr or less and hydrogen pressure was adjusted to about  $1.5 \times 10^{-5}$  torr as monitored by the Phillips pressure gage. The beam switch (r-f





discharge) is turned on, thus giving a bright pinkish-red plasma glow in the ion source bottle. The high voltage is then turned on and brought up to the desired accelerating potential. The solenoid can be turned on and extraction and focus controls increased until the desired beam current is reached. To shut down, the procedure should be followed in exact reverse order. Although the operating procedure to obtain a beam is quite simple, there were quite a number of factors that had to be learned, mostly by trial and error, for successful day to day operation with a steady beam current.

It was found that the hydrogen should be allowed to bleed for at least 5 minutes and up to 1/2 hour if the machine had just been freshly pumped down from atmospheric pressure. Then the r-f oscillator (beam switch) is turned on with another 15 to 30 minute wait.

Hydrogen pressure (in the ion bottle), extraction, focus and solenoid controls must all be adjusted and manipulated to achieve maximum beam current. It was found that working at maximum current is not to be recommended since both the noise (short-term fluctuation) and drift (long-term fluctuation) of the beam current was found to be higher here. If the gas pressure is set too low the plasma will not "fire" but just above this pressure the plasma will blink on and off at approximately 10 cps. The optimum pressure was found to be just above this oscillatory mode — partial pressure of hydrogen  $1.5 \times 10^{-5}$  torr as measured at the Phillips cold cathode pressure gage. The beam was found to be slightly more stable with the solenoid off. Different magnetic field settings of the





solenoid also influenced the beam position at the first collimating slit. The beam could be observed by the fluorescence on the first collimation slit through a special plexiglass window mounted at an angle to the slit. A small moveable circular magnet mounted around the drift tube could be used to bend the proton beam slightly to align it more closely with the collimation slit.

As mentioned previously, working with controls set for a beam current maximum produced a fluctuating beam. The extraction voltage seemed to be most critical control with regard to a reduction of the fluctuations, and working with it set below maximum current conditions (ie. approximately 10 to 14 turns of the extraction control) resulted in a steadier beam. With the extraction voltage control set to its maximum, arcing from the extraction electrode to the plasma could result with possible overheating of the ion bottle and ultimate failure in the vacuum due to the ion bottle chipping or cracking.

The beam current was found to become more unstable than usual after approximately 300 "beam on" operating hours. Cleaning of the ion bottle and quartz sleeve restored the stability of the beam. The ion bottle and quartz sleeve could usually be successfully cleaned with a dilute HF solution (5 parts water: 1 part HF), followed by very thorough rinsing with distilled water and drying. The quartz sleeve must be inspected very carefully for pit marks which result from ionic sputtering and bombardment. Sometimes aluminum sputtered from the exit canal became imbedded in the inside of the quartz sleeve and could not be removed by the acid treatment. In such cases the old sleeve had to be replaced. The exit canal of





the aluminum ion source base plate must also be carefully inspected. If it is pitted and out of round the canal must be plugged and remachined. The dimensions given by the manufacturer are critical for the exit canal and must be followed exactly.

In efforts to obtain optimum beam current, attempts were made to maintain a tight, well focussed beam of approximately 2mm diameter centered on the first collimation slit. The internal diameter of the exit canal of the ion source base of 1/16" (.0625") was reduced to 0.040" and the focus setting was adjusted for a tight beam. A small, well focussed beam of reasonable intensity was obtained and many experiments were done in this way. However it was found that a more stable proton beam trap (collector) current could be obtained from exactly the opposite mode of operation i.e. allowing a wide and diffuse beam to hit the first collimating slit. A diffuse beam was achieved by having the focus control at a low voltage setting and keeping the exit canal internal diameter at 1/16". In this manner the proton trap current was cut down by nearly a factor of ten but was much steadier. The trap current fluctuations under good conditions were 1%, under usual conditions 1 - 5%, going up to 10 - 15% on certain days. Beam current drift could usually be kept to 1 or 2% after stable conditions were reached.

## 2.2 The Mass Spectrometer

The mass spectrometer parts were built by the University of Alberta Machine Shops to the designs and specifications of the Research Director and the author. It was assembled and made functional by the author. The instrument is a conventional 60° sector field





magnetic mass spectrometer with 15cm radius of curvature. A diagram of the main mass spectrometer set-up is shown in Fig. 2.5. see also Fig. 2.4 Theory of the mass spectrometer is not new and may be found readily elsewhere.<sup>37</sup>

The ion source utilized a Nier-type electrode system (Fig. 2.6) that is very similar to that used in the AEI MS2 mass spectrometer. Voltages to the various electrodes (slits) of the ion source were distributed from a voltage divider which was fed by a highly regulated ( $\pm .005\%$  ripple) commercial high voltage supply. Typical voltages at the various ion source slits and dimensions of slits and spacers between slits are given in Fig. 2.6.

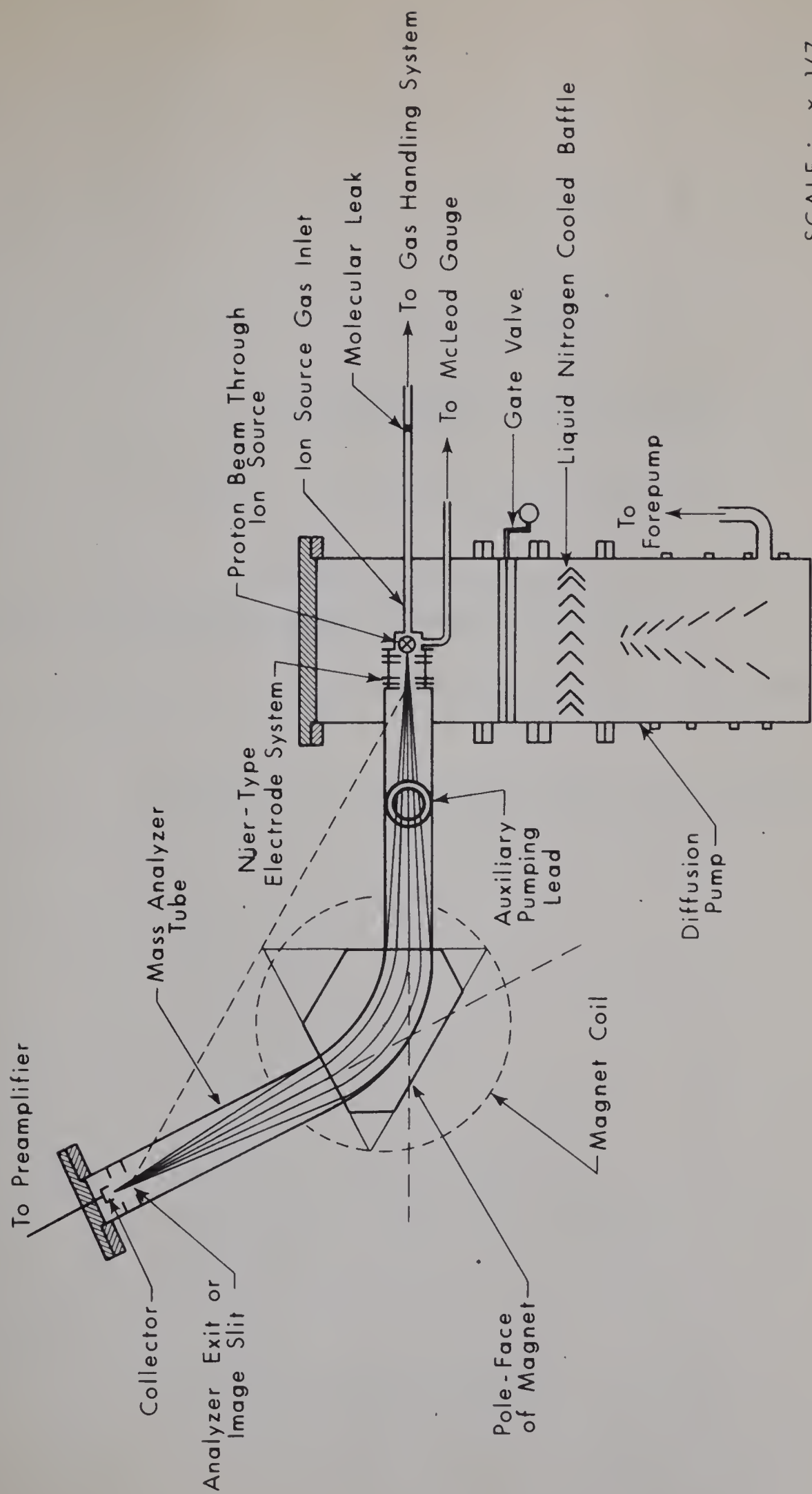
The vacuum system of the mass spectrometer consisted of a 1400 liter/sec. 6" diameter oil diffusion pump (Model PMC-1441, Consolidated Vacuum Corp.) backed by a 425 liter/sec. Welch Duo-Seal forepump. Above the diffusion pump was mounted a 6" diameter liquid nitrogen cooled baffle (Consolidated Vacuum Corp.) and a 6" diameter (Consolidated Vacuum Corp.) gate valve. These components were all mounted directly below a six inch diameter tube which surrounded the mass spectrometer ion source. The ultimate pumping speed at the ion source was calculated to be 400 liter/sec. Separate differential pumping of the mass spectrometer analyzer tube was obtained with a 30 liter/sec. Model PDV-30A Dri-Vac ion pump. (Consolidated Vacuum Corp.) Background pressures in the mass spectrometer were about  $1 \times 10^{-7}$  torr.

The basic operation of the mass spectrometer was as follows: Ions formed upon collisions of protons with gas molecules were

FIGURE 2.5

The Mass Spectrometer

The proton beam passes through the ion source in a direction perpendicular to the ion source as shown. This is a side view.



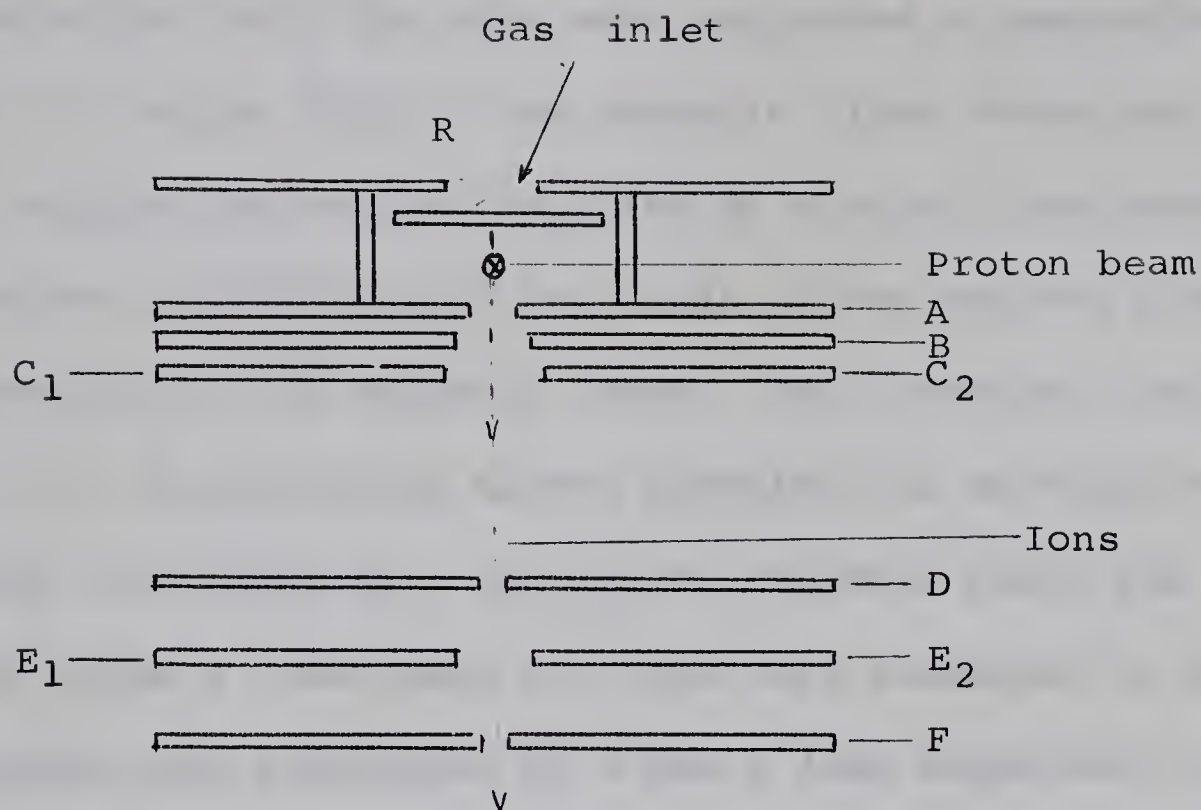
SCALE : x 1/7

CROSS-SECTIONAL VIEW OF MASS SPECTROMETER

FIGURE 2.6

The Mass Spectrometer Ion Source

The view shown is perpendicular to the proton  
beam.



### Typical Potentials of Electrodes (slits)

R : Ion repeller +2010V. (variable)

A : Ion source +2000V  
exit slit

B : Withdrawal slit +1988 to 1750V  
(draw-out)

C<sub>1</sub>: Focus half- +270V  
plate

C<sub>2</sub>: Focus half- +100 to +250V  
plate

D : Defining slit 0V (ground)

E<sub>1</sub>: Beam center half- 0V (ground)  
plate

E<sub>2</sub>: Beam center half- 0 to +150V  
plate

F : Exit slit 0V (ground)  
(analyzer object slit)





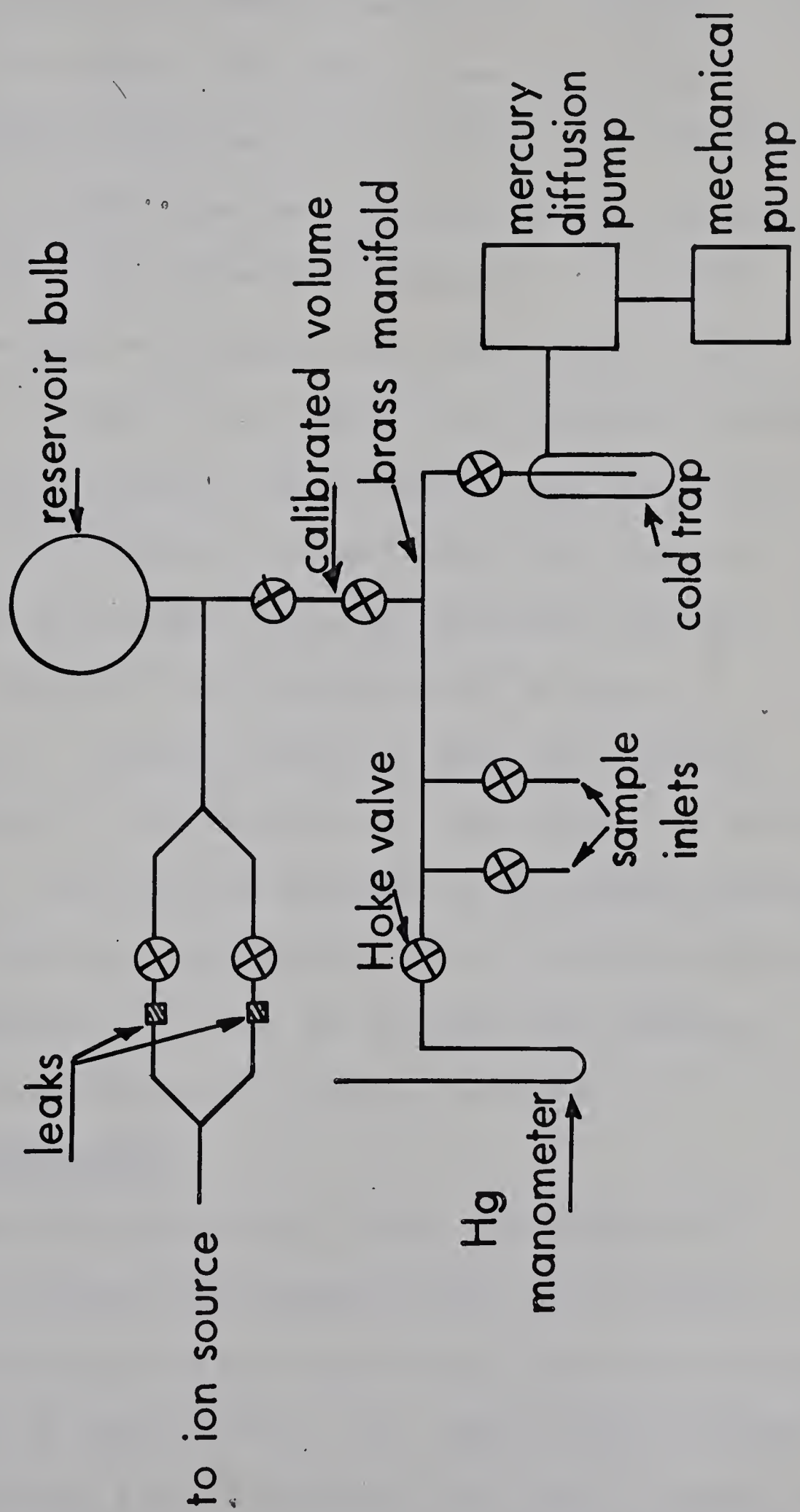
extracted by a positive repeller field through the ion source exit slit (whose dimensions could be varied by inserting different sized slits - typically 1mm x 15mm for low pressure mass spectra), to be accelerated by 1850 V through the Nier-type ion gun. Upon leaving the .25mm x 15mm object slit the ions were subjected to magnetic analysis by the  $\pi/3$  sector field. The magnetic field variation is obtained by varying the current (supplied by a highly regulated NJE constant current supply) through the coils of the magnets, thereby increasing or decreasing the magnetic field. This scanning could be done manually or automatically either downfield or up-field at will. Upon coming into focus at a particular magnetic field the ions entered the 0.5mm x 15mm image slit and were collected in a deep grooved Faraday cup surrounded by a 5mm x 15mm suppressor slit at -22 1/2 V. The currents to the Faraday cup were measured by a vibrating reed amplifier (a Cary Model 31 Amplifier was first used and later a Victoreen Model 475R Femtometer was used). The output of the amplifier was fed to a 10 mV potentiometric recorder (Honeywell) to be automatically recorded. Later on a secondary electron multiplier (SEM) was added to increase the sensitivity. This addition will be described more fully later (see Sec. 2.6). The resolving power of the mass spectrometer was approximately 200 as measured experimentally with the isotopes of mercury.

### 2.3 Sample Inlet System

Although modified slightly for different experiments, the basic design for gas introduction to the mass spectrometer was as shown in Fig. 2.7. All valves used were teflon gasketed Hoke (helium leak tested) brand. The whole system was pumped by liquid

FIGURE 2.7

Sample Inlet System







nitrogen cold trapped 10 liter/sec. mercury diffusion pump backed by a Welch Duo-Seal forepump. Gases or vapors could be introduced via a 12/30  $\frac{1}{8}$  ground joint or an Edwards metal "O" - ring-seal joint. A 2 liter reservoir was used for low pressure mass spectra and cross section measurements whilst an 11 liter pyrex bulb reservoir was used for the high pressure spectra. Pressure in the reservoir could be measured directly by the mercury manometer. A cathetometer was used for readings at pressures less than 10mm. If the pressure required in the bulb was too small to be measured accurately on the manometer, a larger pressure was introduced into one of the smaller volumes (eg. the calibrated volume between the reservoir bulb and the manifold) and expanded into the evacuated reservoir. The pressure in the reservoir was then calculated by means of Boyle's Law ( $p_1 V_1 = p_2 V_2$ ). Several molecular leaks (of sintered ceramic material sealed into the pyrex glass inlet tubing) of different leak rates were used. The leak used depended on the pressure desired in the ion source of the mass spectrometer and the convenient pressure to be used in the reservoir. For the low pressure mass spectra a leak with a measured conductance of 0.1cc/sec. was used.

#### 2.4 Cross Section Measurements

As mentioned previously, upon leaving the second slit or collimation hole the proton beam passed through the ion source at a point almost midway between the exit slit of the ion source chamber and the repeller plate as shown in Fig. 2.4. After passing through the source chamber the beam was finally collected in a large tantalum coated Faraday cup as described previously. The beam defining slit 2 was kept at +300 V, during cross section measurements. The ion box



was maintained at -160 V. The slow positive ion currents were collected at the plate which in normal mass spectrometric operation is the repeller. A voltage of -80 V on the repeller with respect to the ion box was found to give a saturation current for positive ions. This saturation current was amplified by a vibrating reed electrometer (Cary Model 31) floated to the potential of the repeller. The electrometer was mounted in a lucite box and 115 V. A.C. was fed through an isolation transformer.

The proton trap current was monitored simultaneously with a D.C. electrometer (Keithly Model 610B) attached to the Faraday cup. Typical currents measured at the repeller were  $1 \times 10^{-11}$  to  $10^{-9}$  Amp. while proton currents to the Faraday cup varied from  $1 \times 10^{-8}$  to  $10^{-6}$  Amp. depending on conditions of the experiment.

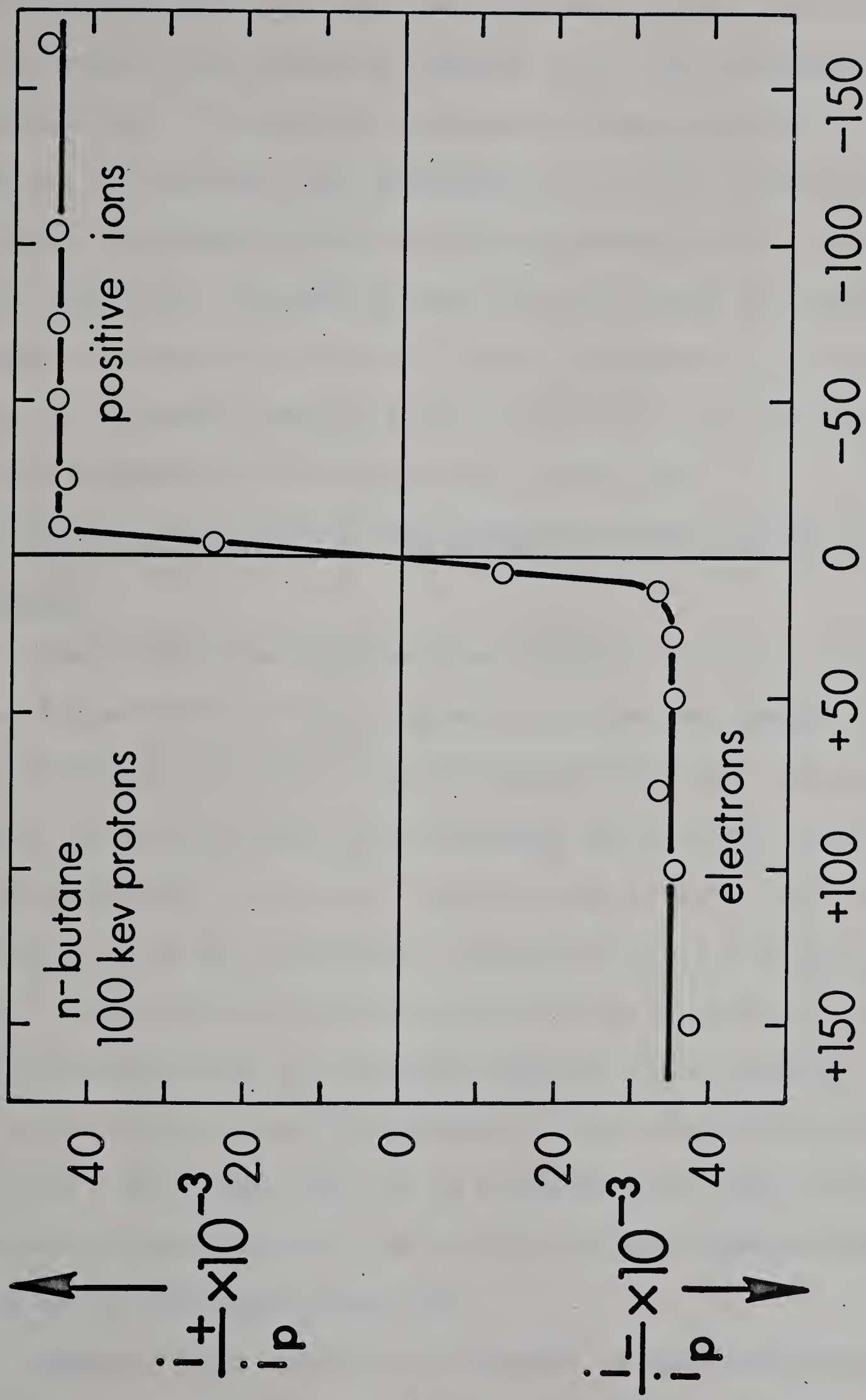
The electron current in the ion source chamber could also be measured by maintaining the repeller at +80 V with respect to the source chamber. Some typical saturation current curves for collection of both electrons and positive ions are shown in Fig. 2.8. These were measured for several compounds at different proton energies in the linear pressure region (i.e. thin target conditions). The background saturation currents to the repeller were always measured first, with no gas in the ion source. Because of beam intensity limitations, cross sections below 40 kev could not be successfully measured.

The absolute pressure of gas in the source chamber was measured by a cold-trapped (Dry Ice-Acetone) McLeod gage of  $525\text{cm}^3$  volume and 1/2mm diameter capillary, which was connected directly to the ion source chamber. Pressures in the 2 liter bulb

FIGURE 2.8

Typical Saturation Current Curve for Collection of both  
Positive Ions and Electrons









upstream from the molecular leak were accurately known. The pressure in the ion source (for a certain pressure in the bulb) was measured by the McLeod gage. A linear relationship between pressure in bulb and pressure in ion source was obtained for a series of gases, giving a calibration relating pressure in bulb to pressure in the ion source. During an actual run, pressure in the ion source could be determined from the known pressure in the bulb, without recourse to the McLeod gage. At the pressures used ( $5 \times 10^{-5}$  to  $2 \times 10^{-4}$  mm) reproducibility of pressure measurements was rather poor, being  $\pm 15\%$ .

## 2.5 Low Pressure Mass Spectral Measurements (Primary Proton Impact Spectra)

The proton beam after passing through the final collimation slit (maintained at +150 V with respect to the source chamber to suppress secondary electrons) passed through the source chamber as before and was then collected on the Faraday cup with the beam current monitored by feeding the current through an appropriate resistor — this potential drop was continuously monitored with a 1 mV Sargent recorder. The ions formed upon collision of the protons with gas molecules were extracted by a positive repeller field (usually ca. 15V/cm) adjusted for maximum ion current of the parent molecular ion peak through a 1mm x 15mm slit, to be accelerated by 1850 V through a Nier-type electrode system. The distance between repeller and exit slit of the ion source was 0.6cm.

Magnetic mass analysis was obtained as described previously. The ion source pressures used were  $10^{-5}$  torr. Secondary electron currents to the repeller and source chamber were measured by floating



a vibrating reed electrometer to the acceleration potential used in the ion chamber. The ratio of secondary electron current to primary proton current was approximately 1% for the ion source chamber and less than 1% for the repeller plate. This was much higher than for cross-section measurements since the high positive potential of the mass spectrometer ion source probably attracted more stray electrons.

The electron impact mass spectra at 55 e.v. were taken with a Nier-type filament arrangement and electron beam focussing magnets. This set-up unfortunately does not completely duplicate the proton beam geometry. However such a duplication is really quite difficult, especially with acceleration energies as low as 55 volts.

All hydrocarbon gases used were Phillips research grade. The rare gases and nitrogen were Airco research gases.

## 2.6 Ion Molecule Reactions - (High Pressure Mass Spectra)

### A. Ion source

In order to maintain a low pressure outside the ion source and in the analyzer tube at ion source pressures of about one torr, a few modifications were made to the mass spectrometer ion source. The exit slit was shortened to 5mm and its width was decreased to 25 microns. This small slit was made by spotwelding 1 mil thick tantalum foil on a larger slit to give the aforementioned dimensions. To maintain the high ion source pressure the proton beam entrance and exit holes were sealed with thin nickel foils in a somewhat special manner.

### B. Thin foils in the ion source







Thin nickel foils (Chromium Corp. of America) of  $10^{-5}$  inch thickness and less, were mounted on hexagonal copper grids (kindly donated by Varian Associates, Palo Alto) which in turn were mounted on 1/4" diameter circular stainless steel plug (as shown in Fig. 2.9) which made a smooth gas tight fit in the entrance and exit holes of the ion source. The copper grids were used for dissipation of the heat produced in the foil by the passage of the proton beam to prevent burnout of the thin nickel foils. The copper grids which are 0.012" thick have a heavier outer rim. They were soft soldered to the stainless steel plug with a light bead of solder. All flux was then removed and the plug was set on a hot heavy brass block. The slight excess of solder on the edge of the grid soldered the outer diameter of the foil to the rim of the grid. Since the foils were copper backed for ease in handling, they were mounted copper side out and the copper layer was removed by a chromic acid solution. Foils of  $5 \times 10^{-6}$  inch thick were successfully used with no burn-out. The success of the method seems to be partly due to the fact that a very thin copper layer was left on the foil. The proton beam sputtered off the excess copper\* where it struck the foil but the rest of the foil retained the layer thus allowing more mass for heat conduction. This is illustrated by the fact that a thicker foil ( $1 \times 10^{-5}$  inch) was tried and burned out in about a weeks' operation. The copper was completely cleaned off this foil.

---

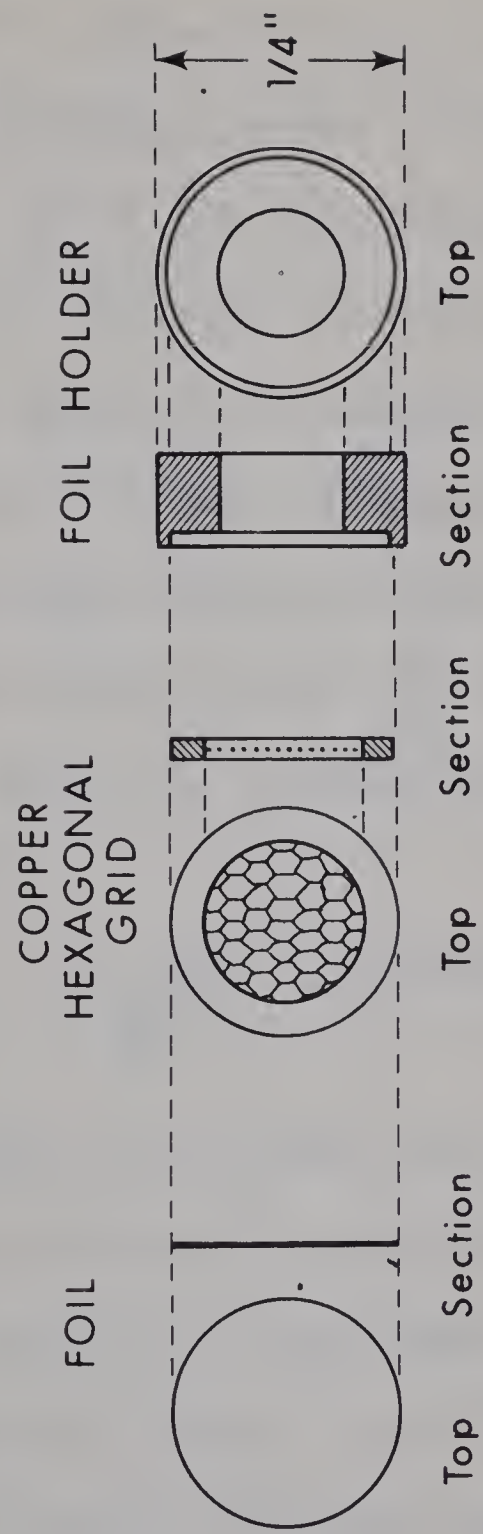
\* It has been found that for 70 kev ions, the sputtering rate of copper is higher than that of nickel (O. Almén and G. Bruce, Trans. 8th Vac. Symp. Vol. 1, p. 245, 1961)

FIGURE 2.9

The Mounting of Ion Source Foils

The thin ( $0.5$  to  $1 \times 10^{-5}$  inch) nickel foil is punched to  $\frac{1}{4}$ " diameter and mounted on copper hexagonal grid. The latter is first soldered to heavy stainless steel foil holder. The entire assembly (of which two are used) makes a gas tight push fit into both sides of the mass spectrometer ion source.

The copper hexagonal grids have a heavier outer rim which is  $0.012$ " thick. There are approximately 150 holes in the gridded portion. The vanes of the grid are only  $0.0006$ " thick.





The proton beam remained well collimated through the ion source since a uniform carbon spot of 1mm diameter was burned on the second (exit) foil. This diameter is the same as the diameter of the 2nd collimation hole. An estimate can be made of the energy of the proton beam after it leaves the first foil. The energy loss can be estimated from the stopping powers (in kev/mg/cm<sup>2</sup>) for copper in the energy range of 50 to 100 kev protons.<sup>38</sup> Since the densities of copper and nickel are identical (8.9 gm/cc) and their atomic numbers differ by only one, we will assume the data for copper apply equally well to nickel. The rate of energy loss in kev/mgm/cm<sup>2</sup> can be converted to kev/cm since density (mgm/cc) x thickness of foil (cm) = mgm/cm<sup>2</sup>. Since the stopping power  $-\frac{dE}{dx}$  for nickel changes only gradually from 100 to 50 kev to a reasonable approximation we can say

$$\frac{\Delta E}{-\frac{dE}{dx}} = \text{thickness (cm)}$$

where we consider a 5 kev slice under the  $-\frac{dE}{dx}$  vs. E curve and then calculate the thickness of foil required to give this energy loss. By consideration of a series of these small slices of area under the stopping power versus proton energy curve<sup>38</sup> we find that a  $\Delta E = 25$  kev (starting with 100 kev protons incident upon the foil) corresponds to the manufacturer's thickness of the foil ( $5 \times 10^{-6}$  inch). Thus 100 kev protons incident upon the foil would lose 25 kev in the foil to yield 75 kev protons on the ion source side of the foil. However a carbon film is built up on the ion source side of the first foil, presumably from hydrocarbon gases used. The energy of the proton





beam is therefore probably lower than 75 kev. Without knowing the true thickness of the foil plus carbon layer the energy loss is somewhat indeterminate.

### C. Secondary electron multiplier

Since the small ion source exit slit cuts down sensitivity considerably, a 17 stage Cu-Be secondary electron multiplier (SEM) was installed as a collector instead of the Faraday cup (see Fig. 2.10). The multiplier structure was obtained from the Technical Physics Section of the Federal Institute of Technology, Zürich. It was supplied in an evacuated glass envelope. The multiplier was mounted on a flange fitted to the collector end of the Mass Spectrometer. In operation the first dynode voltage was between -1000 to -1850 V (supplied by a highly regulated Hamner constant voltage supply). Araldite-coated 1 megohm resistors were connected between each successive dynode with the last dynode (collector) being at ground potential. Thus the voltage was distributed in a series of steps down to zero volts with the first dynode at the highest (negative) potential. The SEM was surrounded by alternate sheets of "Netik" and "Conetik" material for shielding from stray magnetic fields. The electron suppressor slit was replaced by a grid of 85% transparency nickel mesh. This was at the potential of the first dynode for SEM operation.

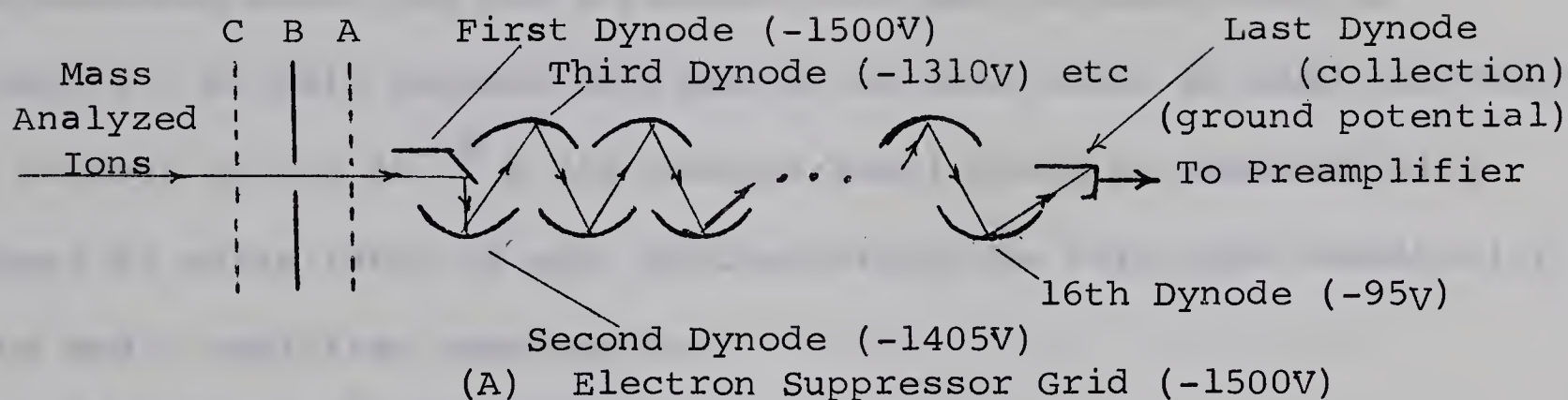
Ions could also be collected without multiplication on the first dynode [Fig. 10 (b)]. In this mode of operation the first dynode is connected to the preamplifier (at ground potential) and the second dynode and electron suppressor grid are at -45 V. The change from SEM to 1st dynode collection was made readily with

FIGURE 2.10

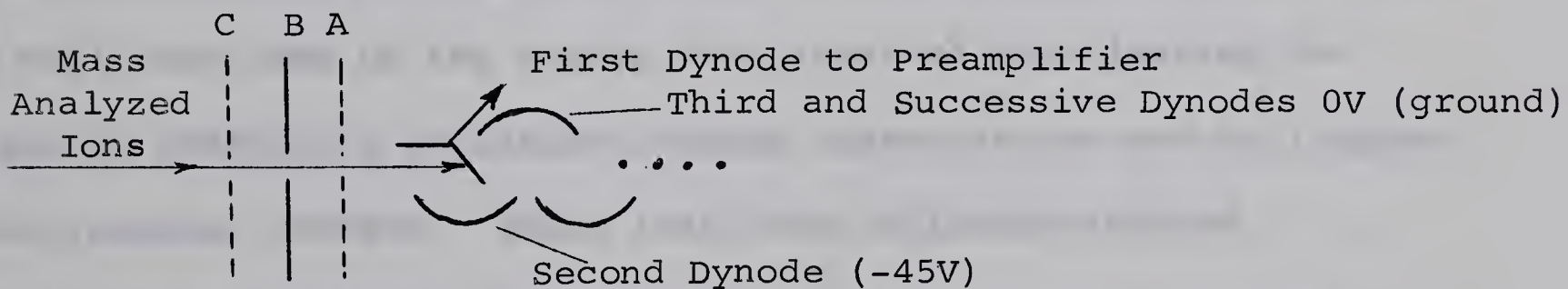
Schematic View of Secondary Electron Multiplier (SEM)  
Collection

The mass analyzed ions focus on the analyzer exit slit (B) and strike the first dynode, whence the current can be either multiplied as shown in part (a) or fed directly to the preamplifier and amplifier as in part (b)

(a) SEM COLLECTION of IONS



(b) FIRST DYNODE COLLECTION of IONS







two switches. Multiplication factors were determined by comparison of signals from SEM and 1st dynode collection. Useable SEM voltages were -1000 V to -1800 V which corresponded to multiplication (or gain) factors of 1000 (for - 1000 V) to  $1.5 \times 10^6$  for -1800 V. Experimentally, noise was not a problem with SEM voltages even up to -1800 V. At this highest multiplication that could be used conveniently, a current of  $1 \times 10^{-18}$  A (50 charges/sec.) could be measured with a signal to noise ratio of one, demonstrating the very good sensitivity of the SEM - amplifier combination.

#### D. "Metastable" suppressor

At the highest ion source pressures used (2 torr) the pressure in the analyzer tube was about  $1 \times 10^{-4}$  torr. (In the water experiments the analyzer tube pressures were much lower due to the very large pumping speed of the liquid  $N_2$  cooled baffle for water vapor. For example at 0.5 torr  $H_2O$  ion source pressure, the analyzer tube pressure was about  $1 \times 10^{-5}$  torr.) At these pressures some ions can make collisions with gas molecules in the analyzer tube. These ions will lose some of the energy they received upon leaving the ion gun by undergoing collision-induced dissociations and will appear at non-integral masses. These ions from collision-induced dissociations complicate and confuse the mass spectrum produced. Since their acceleration energy is lower than that of normal ions, it is possible to suppress these ions with an appropriate potential on a grid or slit placed before the collector of the mass spectrometer.<sup>39</sup> Therefore a suppressor grid (shown in Fig. 10 (a) ) was installed immediately before the analyzer exit slit. The voltage on this suppressor grid could be varied from about +900 to +1800 V.





Space limitations precluded mounting the grid after the analyzer tube exit slit. Since these suppressor grids or slits will suppress true metastable ions from a primary mass spectra they are often used for this purpose in analytical mass spectrometers. They are commonly called "metastable" suppressors even when used for both suppression of true metastable ions and ions of collision-induced dissociations.

At higher pressures, the "metastable" suppressor helped narrow the pressure broadened peaks and to reduce the observation of non-integral mass peaks due to collision-induced dissociation. Scans were taken with the suppressor at zero volts and at a positive suppressing potential at a few pressures. The relative intensities of the ions in the mass spectra were identical for both settings of the suppressor.

#### E. Ion source pressure measurements

Pressure in the ion source was measured with either a 0 to 5 mm tilting McLeod gage connected with short glass tubing to the gas inlet at the ion source or a large calibrated McLeod gage hooked directly to the ion source. Since water has a low vapor pressure (condenses readily) its pressures could be read only on the smaller tilting McLeod gage which has a small compression factor. Pressures up to 1 mm could be read without inaccuracies due to condensations, etc.

Once the pressure in the reservoir was at a steady state, the McLeod gage was shut off to prevent mercury vapor from entering the ion source.

#### F. Sample inlet system

A modified version of the inlet system described in Section 2.3 was used for the higher pressure mass spectra. The



sample reservoir was an 11 liter Pyrex bulb. Some of the inlet leaks used had measured conductances of 0.1cc/sec., 0.25cc/sec. and 1.1cc/sec. Because of the lower vapor pressure of water a larger conductance leak of 70 - 100  $\mu$  sintered glass was used.

For the water - methanol mixture experiments, a separate inlet system similar that described utilizing a 0.1cc/sec leak and a 2 liter reservoir was added for admitting methanol vapor to the ion source. The two vapors mixed on the low pressure (mass spectrometer inlet) side of the leaks.

#### G. Compounds used

The gases and liquids used were thoroughly degassed before use except ethylene which was used directly in the high pressure experiments.

The methane was passed through Linde 5A molecular sieves at -78° C to remove any water impurities in the gas.

Phillips (research grade) ethylene and Matheson (research grade ultra pure) methane was used. Nitric oxide (Matheson) was carefully purified by bulb to bulb distillation. Water was doubly distilled and the methanol was Mallinckrodt reagent grade.





### 3. IONIZATION CROSS SECTIONS; PRIMARY PROTON MASS SPECTRA

#### PART I Cross Section Measurements

##### 1.1 Cross Section Evaluation from Experimental Results

The total ionization cross section  $\sigma_+$  for production of slow positive ions (see Secs. 1.2 - 1.3) is given by

$$\sigma_+ \text{ (cm}^2\text{/molecule)} = \frac{i_+}{i_p n \ell} \quad (3.1)$$

where  $i_+$  is slow positive ion current

$i_p$  is primary proton beam current

$\ell$  is path length in cm (along which ions are formed)

$n$  is number of molecules/cc

and 
$$n = \frac{p}{kT}$$

where  $p$  is the pressure

$k$  is Boltzmann's constant

$T$  is the temperature (taken as room temperature)

The cross section for production of free electrons,  $\sigma_-$ , (the simple or "pure" ionization cross section) was measured in the same way by measurement of negative saturation current ( $i_-$ ) to the repeller. The probability of formation of negative ions is very small and negative current measured is almost entirely due to electrons.

The fractions  $\frac{i_+}{i_p}$  or  $\frac{i_-}{i_p}$  were plotted versus varying gas pressure for most of the compounds studied. Two examples of these plots are given in Figs. 3.1 and 3.2. Linear relationships were obtained, demonstrating single collision conditions. The

FIGURE 3.1

Plot for Evaluation of  $\sigma_+$  and  $\sigma_-$  by 100 kev Protons in  
Krypton

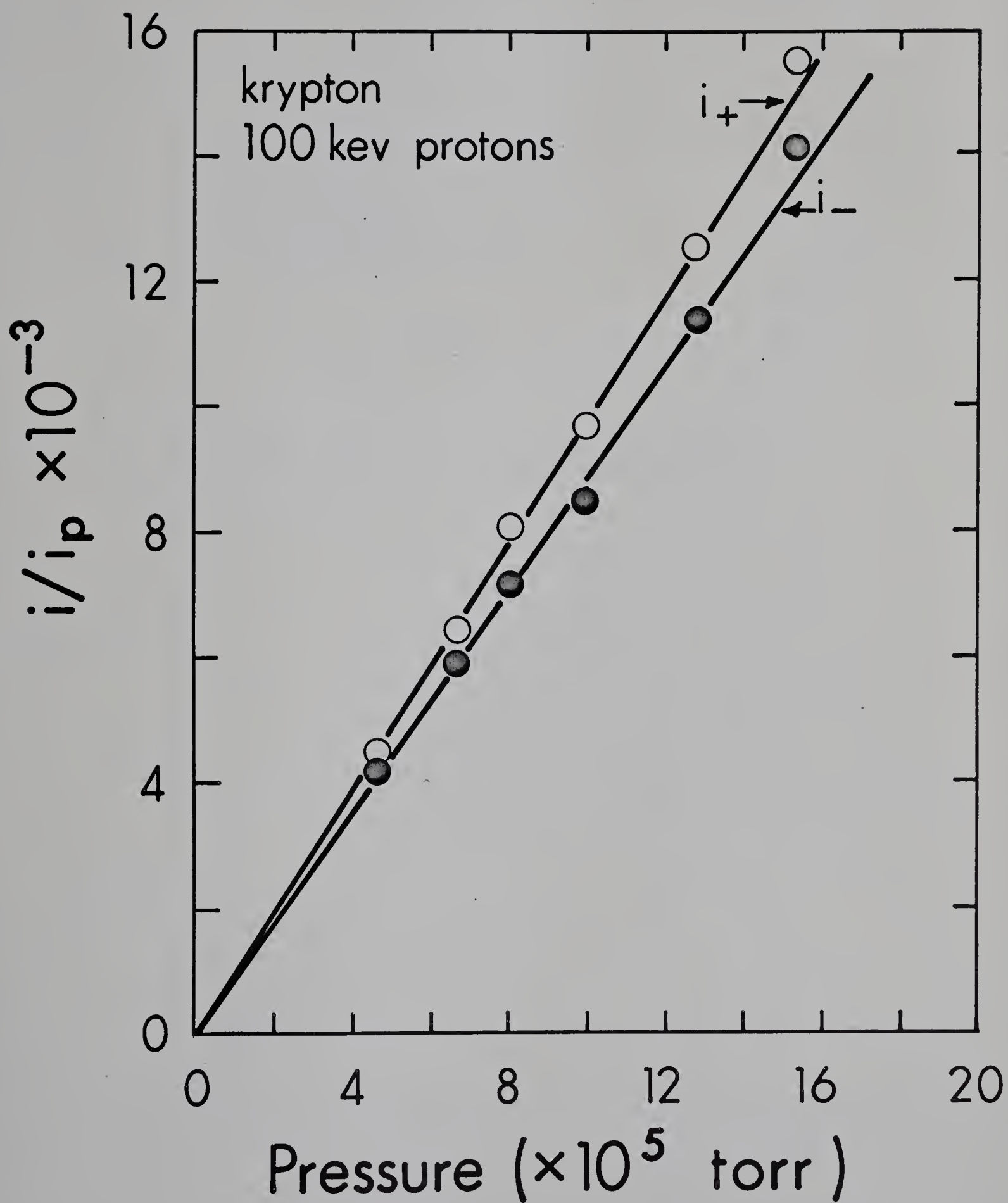
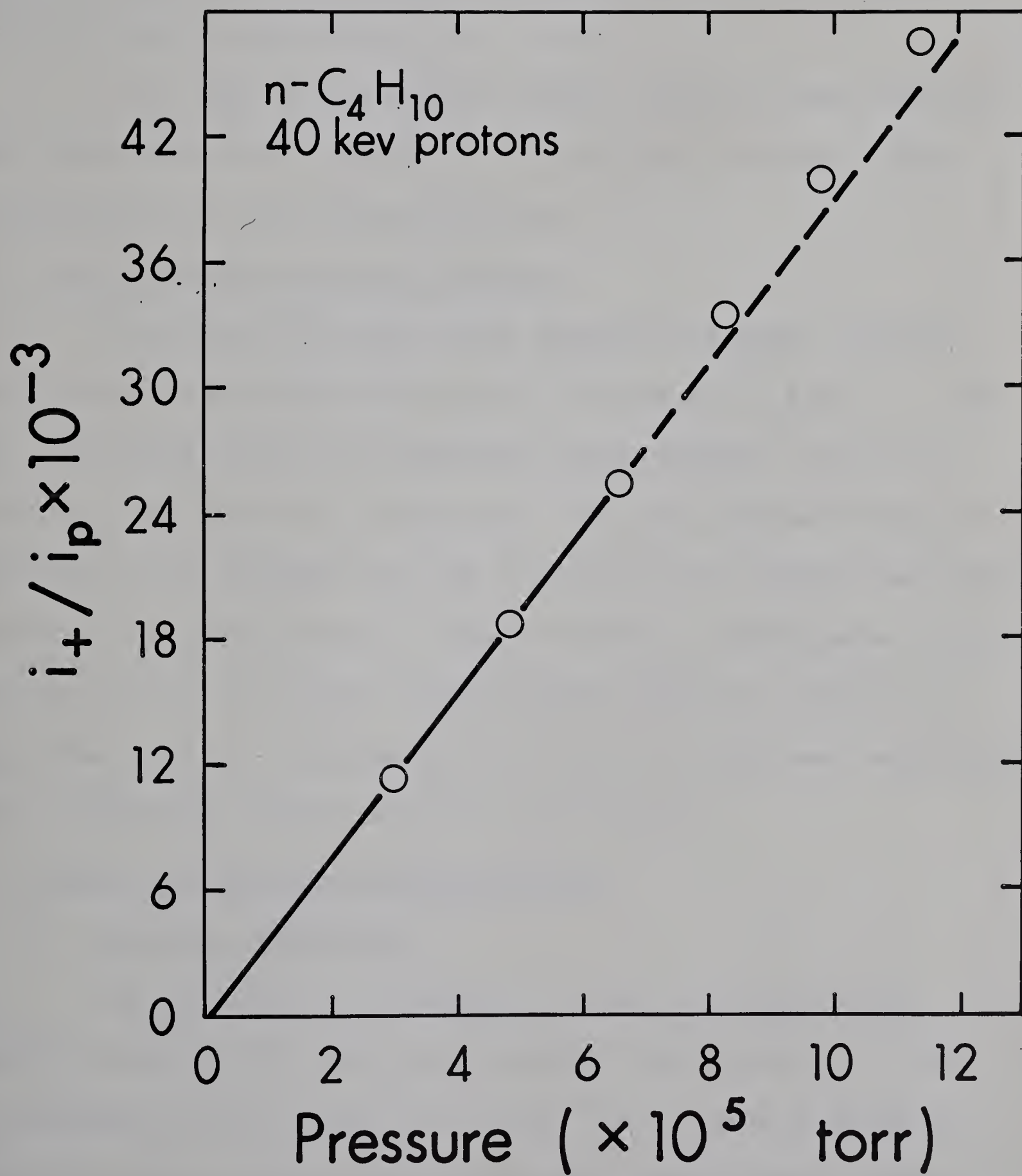




FIGURE 3.2

Plot for Evaluation of  $\sigma_+$  for n-Butane for 40 kev Protons





cross sections presented in Figs. 3.3 - 3.6 were evaluated from the slope of  $\frac{i}{i_p}$  versus gas pressure plots, such as those given in Figs. 3.1 and 3.2. The charge transfer cross section  $\sigma_c$  may be obtained from the equation  $\sigma_c = \sigma_+ - \sigma_-$ .

As a test of the general method, certain cross sections were redetermined for comparison with published results. These are mentioned in the following section.

## 1.2 Comparison with Previous Results

The results for the cross sections for neon, nitrogen and krypton are plotted versus energy of protons in Figs. 3.3 and 3.4. Published results by Fedorenko and co-workers<sup>40</sup> are also plotted on the graphs for comparison. One can see that there is relatively good agreement for the relative cross sections and their dependence on proton energy. However there is a difference in the absolute values, our cross sections being higher by a factor of approximately 1.6. Differences by a factor of 2 between experiments done in different laboratories are not unusual.

## 1.3 Errors in Cross Section Measurements

### A. Pressure measurement

We think that a likely source of error in our absolute values is the ion source pressure measurement. At the low pressures used ( $5 \times 10^{-5}$  to  $2 \times 10^{-4}$  torr) mercury sticking and random effects due to capillary action cause faulty readings with the McLeod gage. Podgurski and Davis<sup>41</sup> estimate that pressures below  $10^{-4}$  torr measured by a McLeod gage with a

FIGURE 3.3

Simple Ionization Cross Sections,  $\sigma_{\text{I}}$ , of Neon, Nitrogen  
and Krypton with 40 to 100 kev Protons



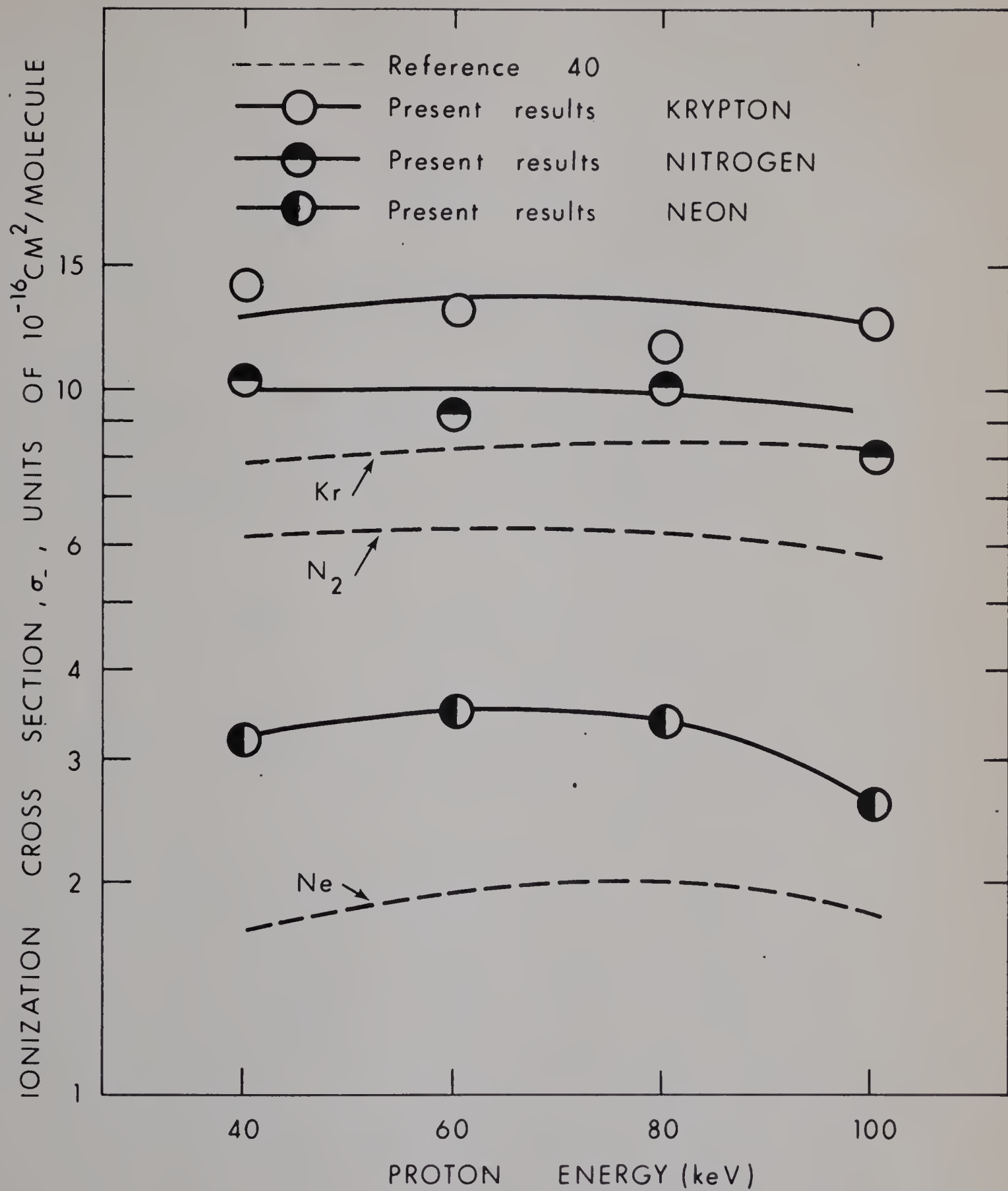
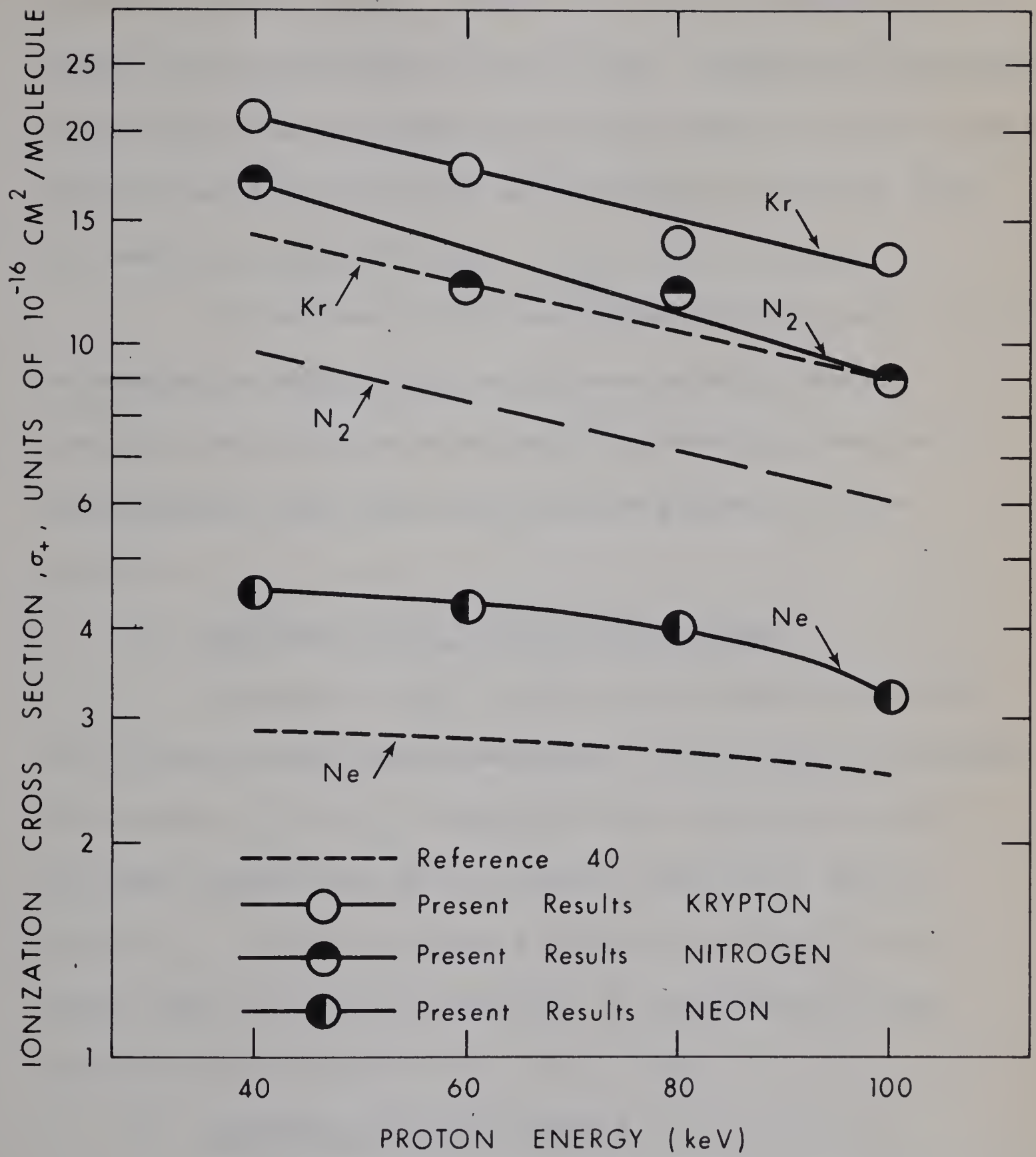


FIGURE 3.4

Gross Ionization Cross Sections,  $\sigma_+$  , of Krypton, Nitrogen  
and Neon for 40 to 100 kev Protons





capillary of 1mm diameter or less (our gage capillary was 1/2mm in diameter) could read up to 20% too low compared to the actual pressure in the system. Thus it is quite plausible that the McLeod gage measurements were too low. Schram and co-workers<sup>42</sup> found their pressure measurements were 8% too low for Ar and 14% too low for Kr because of the action of mercury vapor streaming to the cold trap.

It has been postulated<sup>43</sup> that mercury vapor streaming or pumping will occur even at much higher temperatures (room temperature) thus causing pressure measurements lower than the absolute pressure of the system.

B. Influence of  $H_2^+$  in the proton beam

Presence of  $H_2^+$  in the proton beam can increase the cross sections being measured. In the range of energies we studied,  $\sigma_+$  for  $H_2^+$  measured with a few simple gases has been found to be up to twice as high as  $\sigma_+$  due to protons. For our beam of 90%  $H^+$  and 10%  $H_2^+$  this would lead to a maximum increase in the measured cross section by a factor of  $0.9 + 2(.1) = 1.1$ .

C. Secondary electron effects

The most likely cause of secondary electrons is due to impact of protons upon metal surfaces in the ion source chamber. These electrons may be accelerated by the collecting potentials within the ion source region. Background





saturation currents with no gas within the ion source were usually about 10% of the currents measured with gas bleeding in. These background currents were always subtracted from the total saturation currents with gas bleeding. Secondary electrons are not considered to have introduced significant error into the cross section measurements.

D. End effects of the collecting electrode.

Another source of error could be due to end effects of the collecting electrode. The proton beam enters and exits the ion source through two channels (Fig. 4.2). The gas escaping the ion source through the channels is, of course, exposed to ionization by the proton beam. It is quite likely that these ions are also collected on the electrode. An estimate of this additional current can be made. The combined length of the two channels is 1.7 cm. Assuming a linear pressure drop to zero pressure at the end of the channel, we have an equivalent length of 0.85 cm at the pressure of the ion source. The length of the ion source was 2.2 cm. This length was used for the calculation of the cross sections. If we add to this length 0.85 cm due to ionizations in the channels, we have  $\ell_{\text{(effective)}} = 3.15$ . The cross sections given in Figs. 3.3 and 3.4 could thus be too high by a factor of  $3.15/2.2=1.4$ . If such a factor were taken into account, our cross sections for Ne, Kr, and N<sub>2</sub>



would become almost identical to those by Fedorenko.

It is concluded that the cross sections are probably too high by a factor of about 1.4.

The effective length of collection could have been readily made equal to the geometrical length of the collecting electrode by installing guard rings (at the potential of the collecting plate) immediately before and after this electrode. Unfortunately this was not realized at the time of the experiments and this modification was not carried out.

#### 1.4 New Cross Section Values

The total ionization cross section ( $\sigma_+$ ) and the charge transfer cross section  $\sigma_c = \sigma_+ - \sigma_-$ , for methane, ethylene and n-butane are shown in Fig. 3.5. The simple ionization cross section ( $\sigma_-$ ) values for these compounds are given in Fig. 3.6. Although the absolute values might be too high, the general trends of cross section with proton energy should be accurate. We see that these gases show trends which are similar to those observed for Kr, N<sub>2</sub> and Ne. Thus the cross sections for simple ionization ( $\sigma_-$ ) remain almost constant in the range 40 to 100 kev. On the



FIGURE 3.5

Total (or Gross) Ionization Cross Sections and Charge  
Transfer Cross Sections of Methane, Ethylene and n-Butane  
for 40 to 100 kev Protons

$\sigma_+$  is the total ionization cross section (for production of  
positive ions)

$\sigma_c$  is the charge transfer cross section



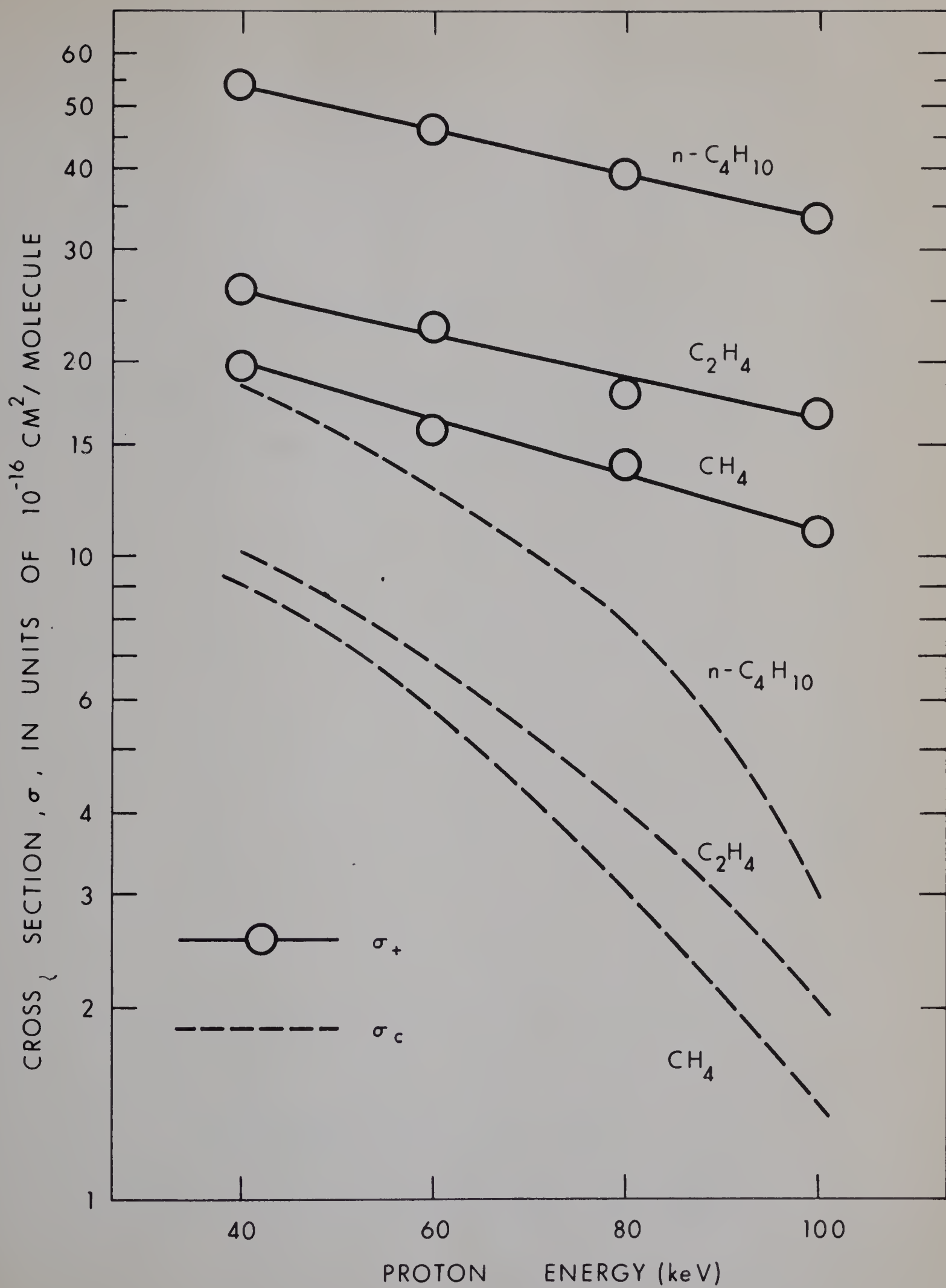
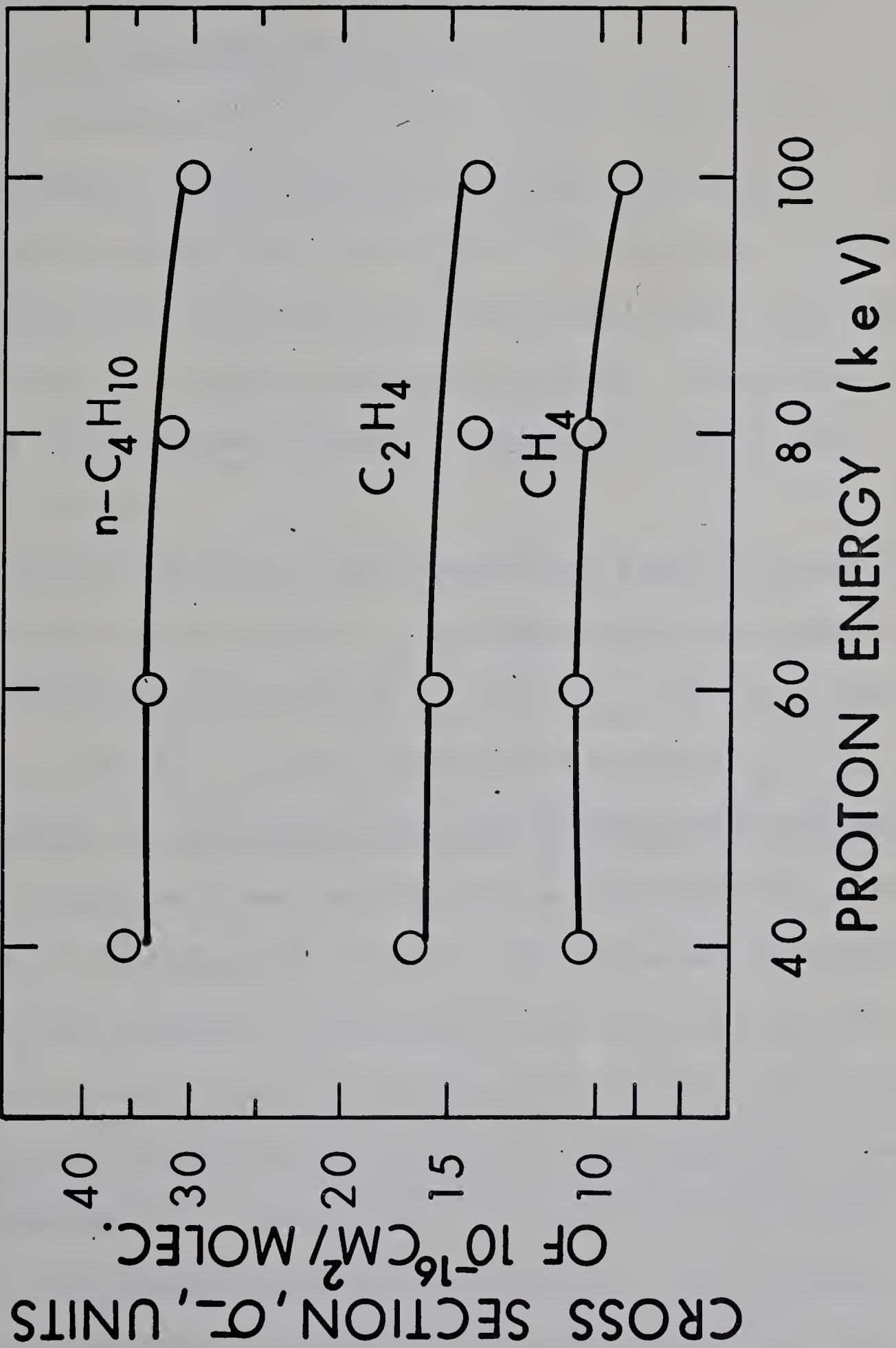


FIGURE 3.6

Simple Ionization Cross Sections ( $\sigma_{\text{I}}$ ) for Methane, Ethylene,  
n-Butane for 40 to 100 kev Protons





other hand, the charge transfer cross sections which represent only 10% of the total ionization at 100 kev increase rapidly to some 40% of the ionization at 40 kev.

The cross sections  $\sigma_+$  and  $\sigma_-$  were measured for a number of alkanes, alkenes, alkynes, chlorinated alkanes and benzene at 100 kev. For many of these compounds the ratio  $\frac{i_+}{i_p}$  was not measured at a series of pressures but at only one or two pressures within the linear pressure region. Although measured absolutely, values were all normalized to the Russian workers<sup>40</sup> values of  $\sigma_+$  and  $\sigma_-$  for krypton at 100 kev.

The values of the measurements are found in Table 3.1. Charge transfer cross sections  $\sigma_c$  are tabulated in the table and are calculated from the equation  $\sigma_c = \sigma_+ - \sigma_-$ . Of course the error for  $\sigma_c$  will be at least double the error for  $\sigma_+$  or  $\sigma_-$ .

### 1.5 Discussion of Ionization Cross Section Results for Molecules

Ionization cross sections can be correlated for various properties of the compounds ionized. Thus Otvos and Stevenson<sup>41</sup> concluded that ionization cross sections of hydrocarbons with 75 volt electrons are a constitutive molecular property and can be estimated from suitable atomic ionization cross sections. Lampe, Franklin and Field<sup>45</sup> related the 75 ev electron impact cross sections to polarizabilities of the molecules. They suggested the postulate of additivity of atomic cross sections of Otvos and Stevenson could probably be applied only within a homologous series of hydrocarbons. In a very recent and more comprehensive





TABLE 3.1

Normalized cross sections for 100 kev protons

$\sigma$ in units of $10^{-16}$ cm <sup>2</sup> /molecule			
Compound	$\sigma_+$	$\sigma_-$	$\sigma_c$
Kr*	(9.0)	(8.4)	(0.6)
CH <sub>4</sub>	7.0	6.3	0.7
C <sub>2</sub> H <sub>2</sub>	8.7	6.9	0.8
C <sub>2</sub> H <sub>4</sub>	12.3	10.4	1.9
C <sub>2</sub> H <sub>6</sub>	14.3	11.6	2.7
C <sub>3</sub> H <sub>4</sub>	16.4	14.8	1.6
C <sub>3</sub> H <sub>6</sub>	17.3	14.5	2.8
C <sub>3</sub> H <sub>8</sub>	18.9	17.0	1.9
n-C <sub>4</sub> H <sub>10</sub>	22.6	20.6	2.0
n-C <sub>5</sub> H <sub>12</sub>	29.5	27.6	1.9
n-C <sub>6</sub> H <sub>14</sub>	36.8	30.3	6.5
C <sub>6</sub> H <sub>6</sub>	29.4	27.8	1.6
CH <sub>2</sub> Cl <sub>2</sub>	20.0	19.2	0.8
CH <sub>3</sub> Cl	14.3	12.8	1.5
C <sub>2</sub> H <sub>5</sub> Cl	20.8	19.0	1.8

\* Normalized to values for krypton as determined by Fedorenko and co-workers.<sup>40</sup>



study of the cross sections for 75 ev electrons, A.G. Harrison and co-workers<sup>46</sup> concluded that the molecular ionization cross sections fit neither a simple additivity postulate nor a single linear correlation with polarizability. They find data can be correlated with polarizability or a modified additivity rule within any one homologous series.

We find that ionization cross sections by 100 kev protons can be linearly correlated with the number of valence or outer shell electrons in the molecule and with the polarizability of the molecule. Figure 3.7 shows that a satisfactory straight line correlation is obtained between  $\sigma_+$ ,  $\sigma_-$  and the number of valence electrons in the molecule for ionization by 100 kev protons. The plots in Fig. 3.8 show that a slightly better correlation is obtained with the polarizabilities.<sup>47</sup> The relationship is rather good considering that alkanes, alkenes, alkynes, benzene and chlorinated alkanes fit the same line reasonably well. Thus it should be possible with the use of Figs. 3.7 and 3.8 to estimate with good accuracy the unknown cross section of a compound from its valence electrons or its polarizability for 100 kev protons. However, considering the conclusions of Harrison et al,<sup>46</sup> these generalities should be viewed with caution.

## PART II Mass Spectra

The mass spectral fragmentation patterns for the hydrocarbons: methane, acetylene, ethylene, ethane, propane and n-butane upon bombardment of 50 and 100 kev protons are shown in Table 3.2.

FIGURE 3.7

Correlation between Cross Sections  $\sigma_+$  and  $\sigma_-$  with 100 kev  
Protons and Number of Valence (Outer Shell) Electrons

Absolute values were adjusted to cross sections of  
Krypton in reference 40.

Average vertical deviations from the straight lines were  
 $\pm 0.96 \text{ \AA}^2$  for  $\sigma_+$  and  $\pm 1.08 \text{ \AA}^2$  for  $\sigma_-$ .



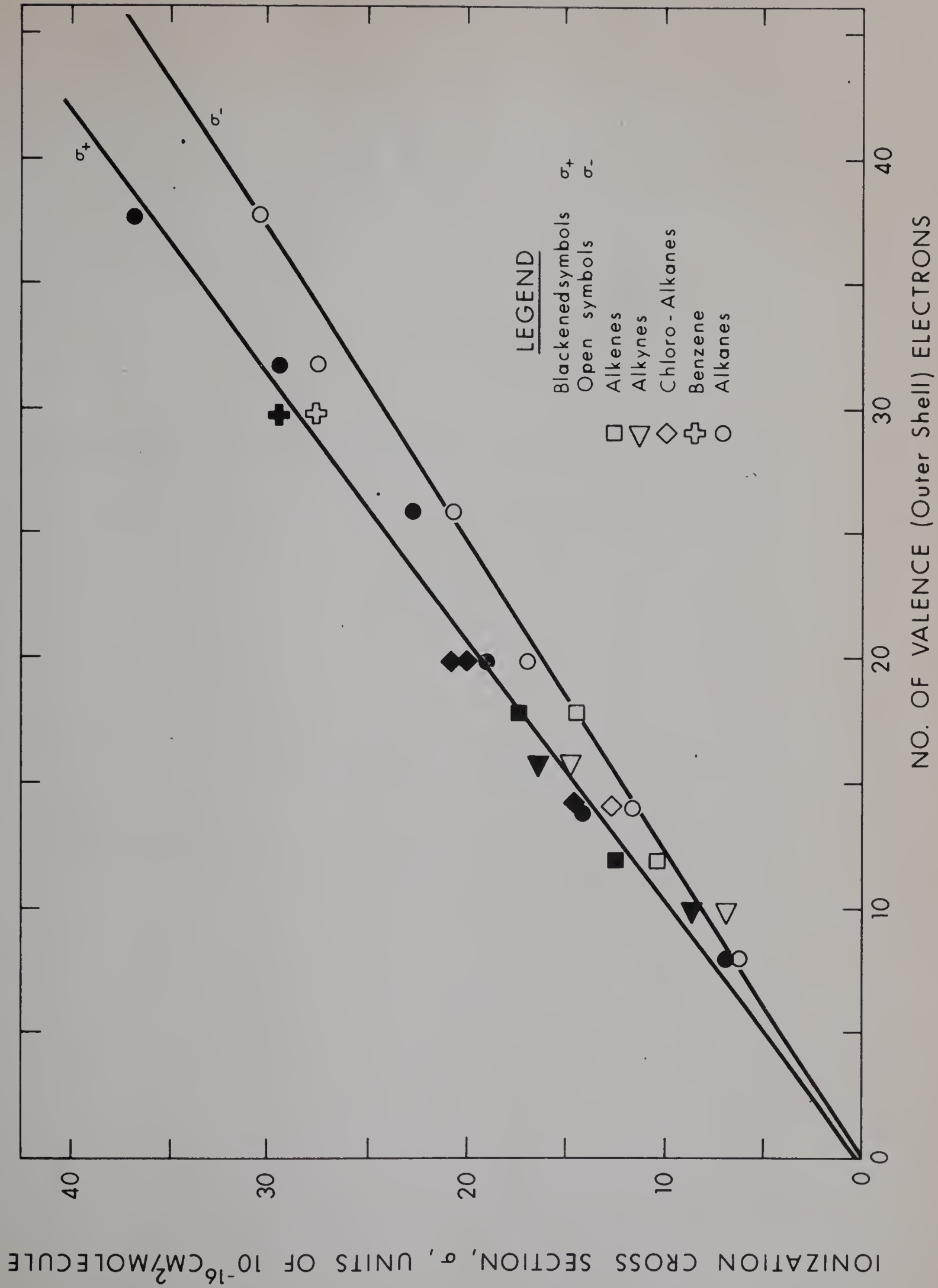


FIGURE 3.8

Correlation between Polarizabilities of Compounds and  
Ionization Cross Sections with 100 kev Protons.

Absolute values of cross sections were adjusted to cross  
sections of Krypton in reference 40.

Average vertical deviations from the straight lines were  
 $\pm 0.81 \text{ \AA}^2$  for both  $\sigma_+$  and  $\sigma_-$ .

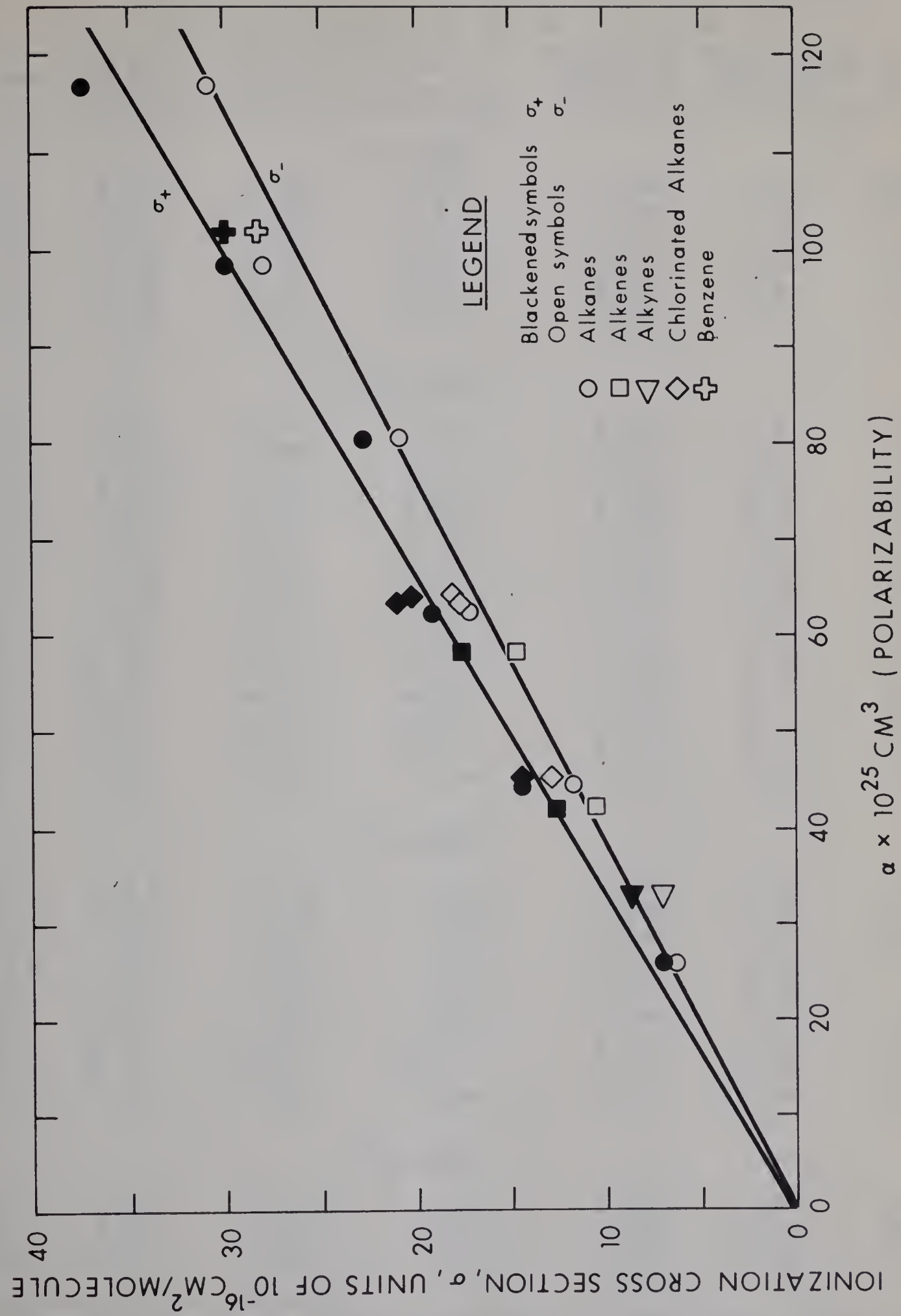




TABLE 3.2

Comparative mass spectra of hydrocarbons ionized by 50 and  
100 kev protons and 55 ev electrons

m/e	50 kev protons	100 kev protons	55 ev electrons	50 kev p 55 ev el	100 kev p 55 ev el	A.P* (ev)	computed spectrum
<u>1. CH<sub>4</sub></u>							
12	1.47	1.23	0.57	2.58	2.16	26.8	0.74
13	3.59	2.04	1.91	1.88	1.07	23.0	1.23
14	9.00	5.68	4.54	1.96	1.24	15.6	3.42
15	39.2	39.3	40.8	0.95	0.96	14.4	23.6
16	46.3	51.1	51.4	0.90	0.99	13.1	70.7
17	0.54	0.57	0.61	0.84	0.93		0.7
<u>2. C<sub>2</sub>H<sub>6</sub></u>							
12	0.28	0.17	0.07	4.00	2.4	30.5	
13	0.43	0.16	0.15	2.87	1.87	24.6	
13 $\frac{1}{2}$	0.089	0.05	0.01	8.90	5.70	35?	
14	1.83	1.59	0.68	2.69	2.38	16.3	
14 $\frac{1}{2}$	0.64	0.68	0.23	2.78	3.00	30?	
15	1.51	1.21	1.18	1.28	1.03	14.0	
24	0.72	0.60	0.17	4.24	3.59	31.6	
25	2.14	1.59	1.25	1.71	1.27	27.1	
26	11.5	9.51	9.46	1.22	1.01	15.0	
27	17.9	15.8	14.6	1.23	1.08	15.3	
28	42.3	44.2	48.3	0.88	0.92	12.1	
29	8.6	10.0	11.0	0.78	0.91	12.8	
30	11.9	14.2	12.7	0.94	1.12	11.7	
31	0.26	0.28	0.28	0.93	1.04	11.7	
<u>3. C<sub>2</sub>H<sub>2</sub></u>							
12	1.44	0.84	0.65	2.22	1.29	24.5	
12 $\frac{1}{2}$	0.06	0.04	0.009	6.89	4.40	35 - 40?	
13	7.91	5.50	2.33	3.39	2.36	22.3	
13 $\frac{1}{2}$	0.11	0.09	0.03	3.67	3.00	30 - 35?	
14	0.15	0.28	0.11	1.36	2.55		
24	5.73	4.04	4.16	1.38	0.97	23.6	
25	20.7	17.6	15.4	1.34	1.14	17.8	
26	62.5	69.6	75.7	0.83	0.92	11.4	
27	1.36	1.50	1.69	0.80	0.89	11.4	
<u>4. C<sub>2</sub>H<sub>4</sub></u>							
12	0.64	0.35	0.21	3.05	1.67	24.7	
13	0.83	0.57	0.40	2.08	1.43	23.0	
13 $\frac{1}{2}$	0.37	0.35	0.10	3.70	3.50	30?	

\* Values of the appearance potentials of the ions for electron impact are taken from F. H. Field and J. L. Franklin, ref. 48





TABLE 3.2 continued.

m/e	50 kev protons	100 kev protons	55 ev electrons	50 kev p 55 ev el	100 kev p 55 ev el	A.P. (ev)
14	1.78	1.79	0.98	1.82	1.83	19.3
15	0.14	0.13	0.13	1.08	1.00	
24	1.81	1.14	0.94	1.93	1.21	26.5
25	4.13	3.06	3.62	1.14	0.85	19.3
26	23.9	22.8	23.5	1.02	0.97	13.5
27	25.0	24.9	25.7	1.03	0.97	14.1
28	40.5	43.8	43.4	0.93	1.01	10.5
29	0.85	1.01	1.08	0.79	0.94	-

4.  $C_3H_8$

12	0.21	0.15	0.019	11.05	7.89	
13	0.24	0.16	0.045	5.33	3.56	
14	0.46	0.29	0.15	3.07	1.45	
15	1.21	0.94	0.63	1.92	1.49	~17
16	0.024	0.03	0.023	1.04	1.30	
19	1.18	not measured	0.17	6.90		
19 $\frac{1}{2}$	0.63		0.097	6.49		
20	0.91		0.23	3.96		
20 $\frac{1}{2}$	0.16		0.063	2.54		
21	0.01		0.004	2.50		
24	0.15	0.13	0.012	12.5	10.8	
25	0.42	0.26	0.11	3.82	2.36	
26	2.84	2.08	1.84	1.54	1.13	14.5
27	12.4	10.6	10.5	1.18	1.01	15.3
28	14.3	17.8	18.7	0.76	0.95	11.8
29	23.6	29.4	31.3	0.75	0.94	12.2
30	0.54	0.52	0.70	0.77	0.74	
36	0.57	0.36	0.10	5.70	3.60	
37	2.16	1.42	0.86	2.51	1.65	
38	2.74	1.84	1.39	1.97	1.32	
39	8.07	5.76	5.50	1.48	1.05	~17
40	1.10	0.88	0.67	1.64	1.31	14.8
41	5.03	4.75	4.82	1.04	0.99	14.1
42	1.56	1.72	1.79	0.87	0.96	12.3
43	7.90	9.25	9.77	0.81	0.95	11.7
44	11.1	12.2	10.6	1.05	1.15	11.2
45	0.35	0.39	0.39	0.90	1.00	

5.  $n-C_4H_{10}$

12	0.11	0.04	0.004	27.5	10.0	
13	0.10	0.06	0.01	10.0	6.00	
14	0.24	0.20	0.055	4.34	3.64	
15	1.04	0.75	0.39	2.67	1.92	16.5 - 20
16	0.015	0.015	0.013	1.15	1.15	
19	0.033	0.019	0.003	11.0	6.33	
19 $\frac{1}{2}$	0.008	0.011	0.003	2.67	3.67	

\*  
Due to an oversight, these peaks were not scanned in the mass spectrum.



TABLE 3.2 continued.

C <sub>4</sub> H <sub>10</sub> continued						
m/e	50 kev protons	100 kev protons	55 ev electrons	50 kev p 55 ev el	100 kev p 55 ev el	A.P. (ev)
20	0.015	0.019	0.003	5.00	6.33	
20 ½	0.008	-	-	-	-	
24	0.088	0.074	0.005	17.6	14.8	
25	0.45	0.30	0.031	14.5	9.68	
25 ½	0.45	0.34	0.031	14.5	11.0	
26	2.59	1.87	0.96	2.70	1.95	
26 ½	0.055	0.045	0.013	4.23	3.46	
27	10.7	9.34	9.62	1.11	0.97	14.4
27 ½	0.015	0.024	0.006	2.50	4.00	
28	8.70	8.74	9.69	0.90	0.90	11.5
29	11.5	11.9	13.5	0.85	0.88	12.1
30	0.26	0.28	0.31	0.84	0.90	
36	0.16	0.13	0.009	17.8	14.4	
37	0.76	0.47	0.19	4.00	2.47	
38	1.01	0.63	0.47	2.15	1.34	
39	5.28	3.78	3.85	1.37	0.98	15.9
40	0.71	0.57	0.55	1.29	1.04	
41	10.2	10.2	10.3	0.99	0.99	13.2
42	4.2	4.98	4.49	1.07	1.11	11.0
43	28.1	32.5	36.4	0.77	0.89	10.9
44	0.94	1.04	1.23	0.76	0.85	
45	0.007	0.011	0.017	0.41	0.65	
48	0.088	0.082	0.006	14.7	13.7	
49	0.46	0.30	0.063	7.30	4.76	
50	1.02	0.68	0.35	2.91	1.94	
51	0.61	0.41	0.35	1.74	1.17	
52	0.11	0.082	0.095	1.16	0.86	
53	0.38	0.27	0.32	1.19	0.84	
54	0.08	0.074	0.08	1.00	0.94	
55	0.44	0.42	0.38	1.16	1.11	
56	0.29	0.28	0.30	0.98	0.93	12.5
57	0.90	1.13	0.99	0.91	1.13	12.1
58	7.23	7.44	5.18	1.40	1.44	10.8
59	0.30	0.33	0.23	1.33	1.44	





The relative abundances (R.A.'s) are given as per cent of the total ionization. The mass spectra by 55 ev electrons are presented for comparison in Table 3.2 with the spectra due to 100 kev protons. At these energies the velocity of the protons and electrons are identical  $4.4 \times 10^8$  cm/sec., which is equal to twice the Bohr velocity.

It can be seen that the proton and electron impact spectra are quite similar. This is particularly true for the ions of high relative abundance. This result was expected on basis of the predictions from the Born-Bethe relationships discussed in the introduction (Sec. 1.5). In order to get a more quantitative measure of the relative agreement between the electron and proton spectra we can define the deviation:

$$\delta = \frac{\text{R.A. (protons)}}{\text{R.A. (electrons)}} - 1 \quad (3.2)$$

where R.A. (proton) is the relative abundance of a given ion in the proton spectrum and R.A. (electron) the abundance of the same ion in the electron spectrum. If we consider a deviation

$\delta < 0.1$  as an agreement with the predictions we can compute

the percent of the ions that agree with the Born-Bethe relationship. These values are shown in Table 3.3. It can be seen that

for methane, acetylene, ethylene and ethane more than 93% of

the ions show agreement. Slightly larger deviations are observed

for propane and butane. Thus we can conclude that the extension

of the Bethe equation to molecular ionization and fragmentation

is valid as a fair approximation for ionization at particle velocities

double the Bohr velocity. Similar conclusions have been derived from a



TABLE 3.3

Comparison between 55 ev electron and 100 kev proton spectra  
Percentage of ion yields of fragments for which deviation is  $\leq 0.1^*$

Molecule	% of Total Ions
CH <sub>4</sub>	93%
C <sub>2</sub> H <sub>2</sub>	93
C <sub>2</sub> H <sub>4</sub>	93
C <sub>2</sub> H <sub>6</sub>	98
C <sub>3</sub> H <sub>8</sub>	80
n-C <sub>4</sub> H <sub>10</sub>	84

---

\* The deviation  $\delta$  is defined as  $\delta = \frac{\text{R.A. (protons)}}{\text{R.A. (electrons)}} - 1$





mass spectral study using low energy (10-70 ev) electrons.<sup>12</sup>

As was mentioned in the introduction, Abbé and Adloff<sup>17</sup> have studied mass spectra in the proton energy range 200 - 1200 kev and Wexler<sup>15</sup> and Schuler and Stuber<sup>16</sup> have used 2 Mev protons. All these authors found relatively good agreement between the mass spectra obtained with protons and electrons. Furthermore, since the spectra change little with proton energy, the fragmentation patterns obtained by all workers are qualitatively very similar. Thus the A.P.I. mass spectral tables with 50 - 70 ev electrons are a guide to the ionic fragmentation induced by charged particles with velocities about  $4 \times 10^8$  cm/sec.

It is of interest to turn now to the deviations between proton and electron spectra and also to the changes resulting from a variation of the proton velocity. Considering first our own results, an inspection of Table 2.2 shows that the largest differences between the proton and electron spectra occur for fragments which are formed by a succession of decomposition reactions and have high appearance potentials. In all cases these fragments are of higher relative abundance in the proton spectra. This effect is even larger in the 50 kev spectra. Taking ethane as an example, we see that going from m/e 30 to 24 the deviations are initially relatively small, but increase rapidly with decrease of mass and increase of appearance potential (A.P.). Thus at mass 24 (A.P. 31.6 ev) the proton spectra abundances are 3.6 (100 kev) and 4.2 (50 kev) times higher than those obtained by electron impact. Similarly at m/e 15 to 12 we find nearly equal abundances at mass 15.





The deviations then gradually increase such that at  $m/e = 12$  (A.P. 30.5 ev) the proton abundances are 2.4 (100 kev) and 4 (50 kev) times higher than the electron impact values. Even bigger effects are observed with some other molecules. Thus in the proton n-Butane spectra  $m/e = 12$  is 10 (100 kev) and 28 (50 kev) times higher than in the electron spectra.

The doubly charged ions (A.P.'s = 30 - 40 ev) are also found in much higher abundances, with the effect again being larger at 50 kev than at 100 kev. The proton impact abundances are generally 2 to 3 times higher but the ratio in some cases is as high as 10. Apart from the half integral mass peaks, some integral mass peaks are undoubtedly partially due to doubly charged ions. For example, in the ethylene mass spectrum,  $m/e = 14$  could be  $C_2H_4^{++}$  or  $CH_2^+$  although one has no way to distinguish between the ions. We have one example, in the spectra of acetylene, that shows that an integral peak, namely  $m/e = 13$  is caused partially by doubly-charged ions. The ion  $m/e = 13 \frac{1}{2}$  is  $C^{12}C^{13}H_2^{++}$  of R.A. 0.09% for 100 kev protons. Since this is the doubly charged isotope peak of the acetylene molecule ion, the R.A. of  $m/e = 13$  should be 4.1% due to  $C_2H_2^{++}$  and 1.4% due to  $CH_2^+$  since  $m/e = 27$  is 2.2% of  $m/e = 26$ . Ions of  $m/e = 13 \frac{1}{2}$  and 13 increase for 50 kev protons indicating increased formation of doubly-charged ions. Doing similar calculations, we find that the R.A. of  $C_2H_2^{++}$  is 1.4% for 55 ev electron impact and 5.0% for 50 kev proton impact. In butane we observe a very small  $C_3H_5^{++}$  ( $m/e = 20 \frac{1}{2}$ ) of R.A. 0.008% for 50 kev protons. This is not observed for 100 kev protons (within limits of detectability) nor for 55 ev electron impact.

Wexler<sup>15</sup> using 2.2 Mev protons found that the fragments





of high appearance potential were produced in an abundance which was lower than that obtained with electrons of the same velocity. However, Schuler<sup>16</sup> at the same energies found quite the opposite effect, namely that these fragments are of higher abundance in the proton spectra. This brings out an unfortunate fact of mass spectral measurements, namely that the spectral patterns and particularly the abundances of ions with high initial kinetic energies are dependent on ion repeller, ion extraction and mass analysis conditions. Schuler's study was also done with a time-of-flight mass spectrometer, whereas the present study and that of Wexler was done with conventional magnetic deflection instruments. A study of the repeller effect and the kinetic energies of ionic fragments has been made by Taubert<sup>49</sup> and Bracher et al<sup>50</sup>. It is found that the high appearance potential fragments have highest initial kinetic energies so that their relative abundances might be expected to vary most with experimental conditions. Undoubtedly part of the difference between Wexler's and Schuler's results is due to such instrumental factors. Therefore a sensible comparison between experiments from different laboratories can be made only if the general experimental conditions are similar. Such similarity in conditions exists in the arrangements used by Abbé and Adloff,<sup>17, 51</sup> Wexler<sup>15</sup> and ourselves. These results have been combined for some representative ions of the ethylene spectrum in Fig. 3.9. The proton energy range covered is from 0 to 2.5 Mev. It can be seen that the points from the different laboratories are mutually consistent. The

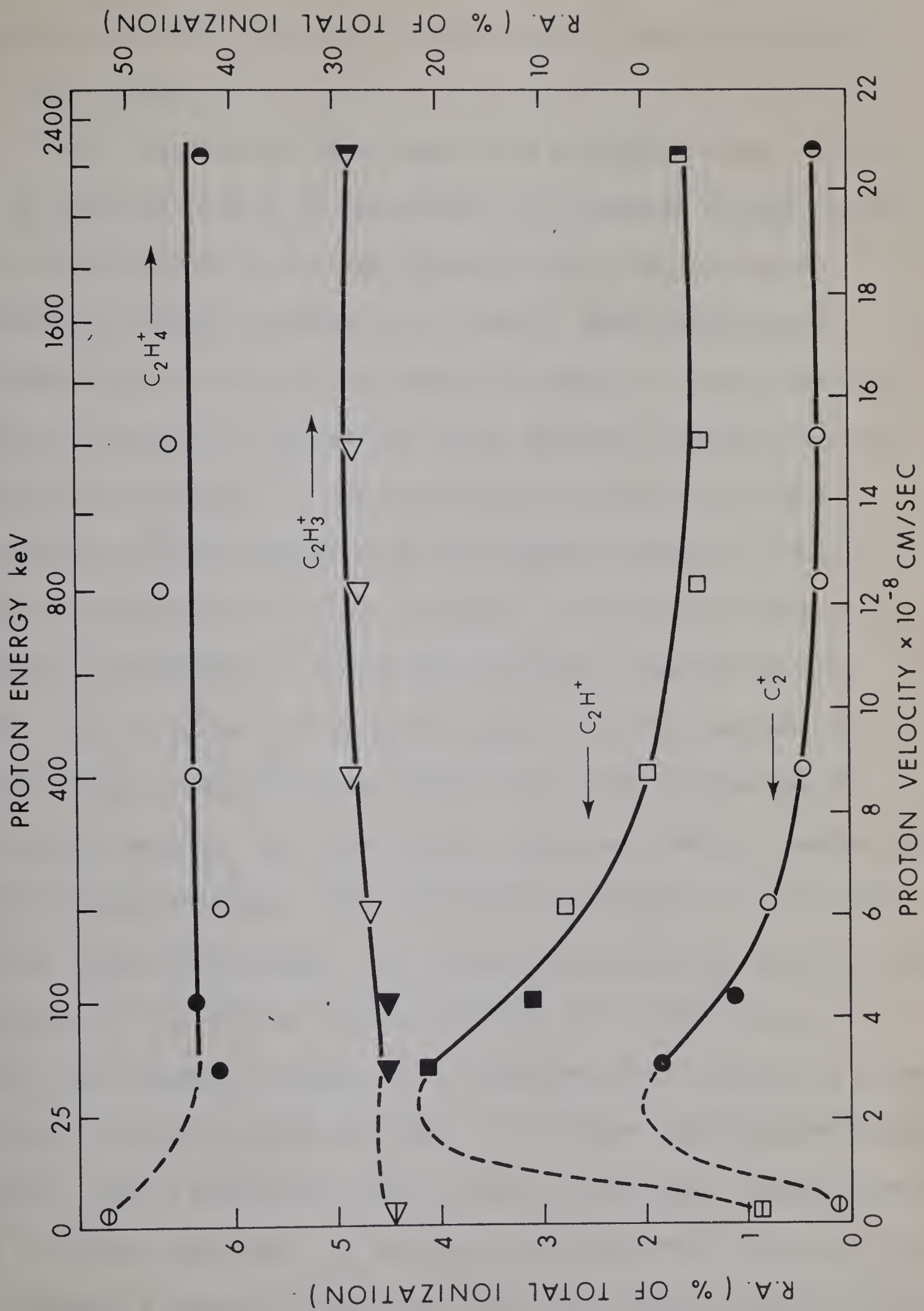
FIGURE 3.9

Fragmentation Pattern Dependence on Proton Velocity  
(Energy) for Ethylene

Legend:

$\ominus$	$\triangleleft$	$\boxminus$	Results of Abbe and Adloff <sup>51</sup>
$\bullet$	$\blacktriangleleft$	$\blacksquare$	Present Results
$\circ$	$\triangleleft$	$\square$	Results of Abbe and Adloff <sup>17</sup>
$\odot$	$\triangleleft$	$\boxplus$	Results of Wexler <sup>15</sup>







plot shows clearly the relative constancy of the high abundance peaks ( $m/e$  28 and 27) and the significant increase of the high appearance potential peaks ( $m/e$  25 and 24) in the proton energy range 100 - 10 kev.

The increase of high appearance potential peaks in the 100 - 10 kev region must be due either to a gradual change in the nature of the simple ionization process or to the increasing importance of charge transfer, or to both. With decrease of proton velocity the simple ionization can begin to occur through a "strong interaction complex" in which multiple electron excitation might be expected.<sup>52</sup> Unfortunately we can not separate the influence of this effect from the changes induced by the increased importance of charge transfer. However, some interesting general deductions on the charge transfer interaction can be made. As was shown in the first part of the discussion, Sec. (3.4) charge transfer represents some 30% of the total ionization at 50 kev proton energy. At lower proton energies charge transfer will become the major process. What are then the charge transfer mass spectra at these velocities? The charge transfer mass spectra obtained with protons up to 1000 ev energy are well known from the work of Lindholm<sup>8</sup> and others. Inspection of the spectra in Table 3.2 shows that the charge transfer spectra at some 10 - 100 kev must be drastically different. This is best seen in the case of methane. Charge transfer from  $H^+$  produces only  $CH_4^+$  at energies up to 900 ev.<sup>53</sup> Thus, one can easily compute a spectrum composed of say 40% charge transfer ionization (leading exclusively to  $CH_4^+$ ) and 60% simple ionization.





Such a computed spectrum is shown in the methane section of Table 3.2. The 100 kev proton spectrum was used to represent the simple ionization fragmentation. Comparison of the 50 kev spectrum with the computed one shows that there is no similarity between them. Another simple example that charge transfer spectra at  $10^8$  cm/sec velocities are very different can be obtained from the results of Abbé and Adloff.<sup>17</sup> These authors give spectra of ethylene obtained with  $\text{Ar}^+$  at 200 kev. The velocity of  $\text{Ar}^+$  at 200 kev is only  $0.8 \times 10^8$  cm/sec. We expect that at this velocity charge transfer should represent at least 50% of the total ionization. Charge transfer from  $\text{Ar}^+$  to ethylene at low energies (0-900 ev) produces almost exclusively  $^{51}\text{C}_2\text{H}_3^+$  (75%) and  $\text{C}_2\text{H}_2^+$  (20%). The abundance of these peaks in the 200 kev spectrum obtained by Abbe is not higher than that observed with 100 kev protons or 50 ev electrons. Therefore we conclude that charge transfer spectra with projectiles of velocities around  $10^8$  cm/sec do not depend strongly on the recombination energy of the charge acceptor but rather resemble spectra obtained by pure ionization. This observation can be partially understood on basis of the Massey<sup>6</sup> adiabatic criterion which was discussed in Sec. 1.5 B of the Introduction. The equation predicting a maximum charge transfer cross section may be written

$$\frac{h v}{a \Delta E_{\max}} = 1 \quad (3.3)$$

Here  $\Delta E_{\max}$  is the energy defect that would lead to a maximum cross





section for protons of velocity  $v$ . The situation for polyatomic molecules is special since one has almost continuous "accidental" resonance, due to the large number of available excited states in the molecular ion. Thus with increase of projectile velocity one can expect a broadening\* of the imparted energy to values higher and lower than the recombination energy of the primary ion. For protons of 50 kev acceleration, equation (3.3) predicts a  $\Delta E_{\max}$  of 25 ev. (a, the adiabatic parameter, is taken as  $7\text{\AA}$ ). Adding 13.6 ev, as a tentative recombination energy for  $H^+$ , we obtain an imparted energy of 39 ev. We do not know what the fragmentation patterns due to such a high imparted energy would look like. However, information for somewhat lower imparted energies is available from the low velocity charge transfer spectra with  $He^+$  (R.E. 25 ev). These fragmentation patterns are generally characterized by very low molecular ion abundance. For example, the charge transfer spectrum<sup>53</sup> of methane produced with low velocity  $He^+$  is:  $CH_4^+$  0,  $CH_3^+$  5,  $CH_2^+$  72,  $CH^+$  23,  $C^+$  0%. Taking such a spectrum as a rough guide to the fragmentation for even higher imparted energies we could assume that the increased abundances of the high appearance potential peaks in the 50 kev proton spectra might be due to charge transfer. Also the doubly charged ions which have appearance potentials

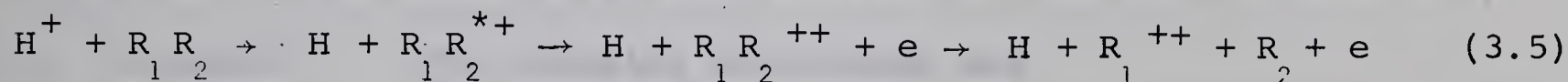
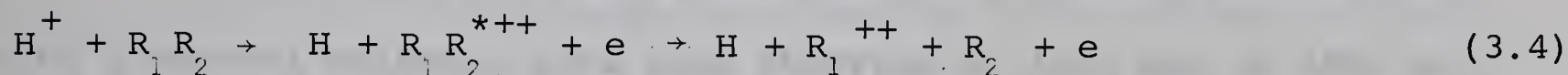
---

\* The effect of such broadening is evident already in the proton spectra of Lindholm<sup>8</sup> taken with 1 kev proton energies ( $v = 0.4 \times 10^8$  cm/sec).





in the 30 - 40 ev range might be due to transfer ionization, Reaction (3.4), and charge transfer followed by autoionization, Reaction (3.5).



The fragmentation pattern of  $CH_4$  with 50 kev protons and  $C_2H_4$  with 200 kev  $Ar^+$  is clearly incompatible with some 30 - 40% contribution from charge transfer spectra with imparted energies larger than 20 ev since it was observed that the major peaks in the high velocity charge transfer spectra must have abundances similar to those produced by simple detachment ionization. It must therefore be concluded that the energies imparted to the charge acceptor are spread over a considerable range such that the resulting energy distribution<sup>of imparted excitation</sup> is not too different from that occurring in simple ionization. The Massey criterion as we applied it to polyatomic molecules thus predicts a broad range of excitation energies but is not useful for quantitative prediction of the charge transfer mass spectra at high relative velocities.



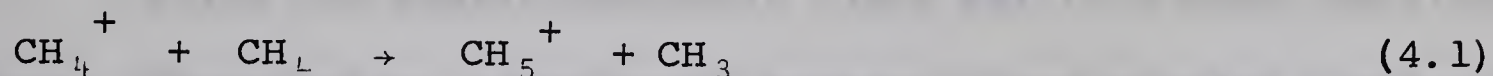


#### 4. ION-MOLECULE REACTIONS IN METHANE

##### 4.1 Introduction

###### A. Previous results

Ions which are due to reaction of a primary methane ion with a neutral molecule have been observed as long ago as 1940 by G.C. Eltenton<sup>54</sup>. The reaction discovered was



In 1952 this reaction was rediscovered by Tal'roze<sup>21</sup>. Following the rediscovery of this reaction and the reports of Stevenson and Schissler<sup>22, 55</sup> that the protonated methane ion,  $\text{CH}_5^+$ , is formed via a very large cross section ion-molecule reaction of the parent ion  $\text{CH}_4^+$  with methane, ionic reactions in methane have been extensively investigated<sup>29, 56-64</sup>. Except for the very recent studies<sup>62-64</sup> all other studies<sup>29, 56-61</sup> were done with conventional electron impact ion source mass spectrometers. Of those using electron impact ionization, Field and Munson<sup>61</sup> have reported one of the more definitive studies of the methane system to date. They also reached the highest ion source pressure (up to 2 torr) that has been studied using conventional electron impact. After the research to be reported in this chapter on the methane system was completed, a study by Wexler and co-workers<sup>62</sup> of ion-molecule reactions in methane up to 0.7 torr using a 2 Mev proton beam for the ionizing medium was published.

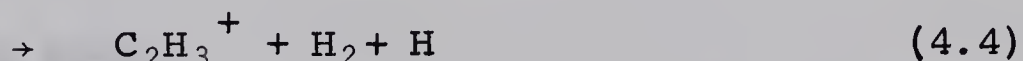
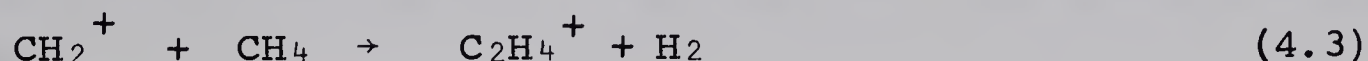
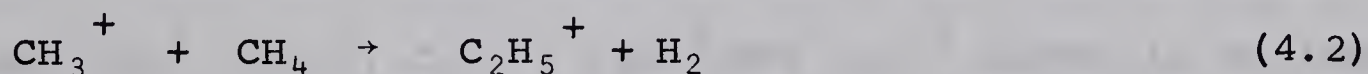
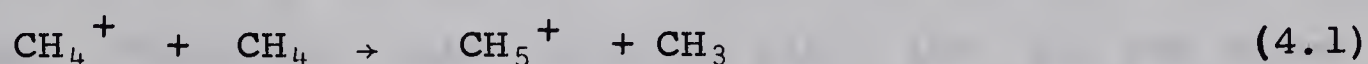
In contrast experimentally to these studies<sup>29, 56-62</sup> Abramson and Futrell<sup>63</sup> have used a tandem mass spectrometer arrange-



ment (external ionization method) in which primary ions are pre-selected by the first mass spectrometer to then enter the collision chamber (ion source) of the second mass spectrometer, where the products of ion-molecule reactions are mass analyzed. Ion source (collision chamber) pressures here are in the 1 to 10 millitorr range.

Using the near-atmospheric alpha particle mass spectrometer in these laboratories, Kebarle and Haynes<sup>64</sup> have studied the ion-molecule reactions in the alpha particle radiolysis of methane from one torr to almost 200 torr.

From all these studies it is now agreed that the three main primary ions from methane, i.e.  $\text{CH}_4^+$ ,  $\text{CH}_3^+$  and  $\text{CH}_2^+$  react rapidly with methane (with rate constants  $k$ 's  $\approx 1-2 \times 10^{-9}$  cc/molecule-sec.)<sup>59</sup> to give the secondary ions in the following reactions



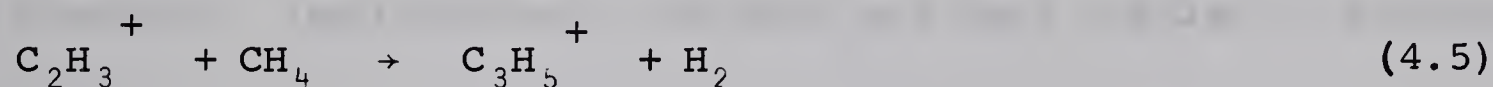
Concerning reactions of the secondary product ions, Wexler and Jesse<sup>29</sup> found, in their study at pressures up to 0.4 torr methane, that the yield of  $\text{C}_2\text{H}_5^+$  increased slowly up to 0.4 torr while the intensity of  $\text{CH}_5^+$  decreased after a maximum at 0.15 torr. It was suggested that  $\text{CH}_5^+$  was reacting with methane to yield  $\text{C}_2\text{H}_5^+$ . In contrast, Field, Franklin and Munson<sup>59</sup> found inverse behaviours in the same pressure range, suggesting that a process forming  $\text{CH}_5^+$  at the expense of  $\text{C}_2\text{H}_5^+$  was occurring. However in their recent study



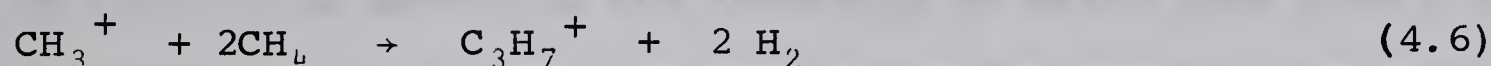


at ion source pressures up to 2 torr, Field and Munson<sup>61</sup> found no net conversion of  $C_2H_5^+$  to  $CH_5^+$  or vice versa and furthermore suggested that these main product ions if reactive at all with methane, had rate constants for further reaction of  $k < 10^{-12}$  cc/molecule-sec. Futrell and Abramson<sup>63</sup> have confirmed these results at much lower pressures showing that  $CH_5^+$  and  $C_2H_5^+$  are very unreactive in methane.

Of the secondary products ions produced by reactions (4.1) to (4.4), only  $C_2H_3^+$  appears to react further with methane as given by



Field and Munson<sup>61</sup> have suggested that  $CH_3^+$  also reacts further in the reaction



although the actual mechanism of (4.6) does not appear to have been established. Therefore, apart from the vinyl ion, all the other product ions  $CH_5^+$ ,  $C_2H_5^+$ ,  $C_2H_4^+$ ,  $C_3H_5^+$  and  $C_3H_7^+$  appear to be inert in methane.

#### B. Scope of present study

Since using the 100 kev proton beam through thin foils is a rather new method in studies of ion-molecule reactions, it was decided to study first the well-known system methane as a test and hopeful confirmation of the technique. The ion source pressure range studied was 0 to 2.2 torr. Since two recent studies<sup>61-62</sup> have been carried out in the same pressure range and also using the internal ionization method (see Chapter 1, Part II), comparisons can be made. Both the confirmation of the technique of using this new





ionizing medium and strengthening of the previous observations could be possible.

#### 4.2 Results

The main ions observed in the present work at pressures up to 2.2 torr of methane are plotted in Figs. 4.1 and 4.2. The main product ions observed are  $\text{CH}_5^+$  and  $\text{C}_2\text{H}_5^+$ , which comprise ~87% of the total ionization at pressures above 0.1 torr. Lesser amounts of  $\text{C}_2\text{H}_3^+$ ,  $\text{C}_2\text{H}_4^+$ ,  $\text{C}_3\text{H}_5^+$  and  $\text{C}_3\text{H}_7^+$  are observed with their yields varying with pressure. Qualitatively the data are very similar to previous work <sup>61-62</sup>.

Water was present as an impurity, as shown by the appearance of  $\text{H}_3\text{O}^+$  in the spectrum, the intensity of which rose from 0.3% at 0.1 torr to 5% at 1 torr. In tabulating the spectra, the contribution of  $m/e = 19$  ( $\text{H}_3\text{O}^+$ ) was omitted. Since some measures were taken to remove water from the methane coming from the cylinder (see Sec. 2.6), this impurity could possibly have come from the gas handling system which was not bakeable. Field and Munson<sup>61</sup> and Haynes and Kebarle<sup>64</sup> have also observed ions due to small concentrations of water impurities in their experiments with methane.

From Figs. 4.1 and 4.2 we can see that  $\text{CH}_5^+$ ,  $\text{C}_2\text{H}_3^+$ ,  $\text{C}_2\text{H}_4^+$ ,  $\text{C}_2\text{H}_5^+$ ,  $\text{C}_3\text{H}_5^+$  and  $\text{C}_3\text{H}_7^+$  are essentially the only product ions, since at all pressures above ca. 0.1 torr these ions total over 97% of the total ionization. Other ions of higher mass than the primary ions are also observed. These are  $\text{C}_2\text{H}_7^+$ ,  $\text{C}_3\text{H}_3^+$ ,  $\text{C}_3\text{H}_4^+$ ,  $\text{C}_3\text{H}_6^+$  and  $\text{C}_4\text{H}_9^+$ . However, these ions exhibit no particular pressure dependence and individually are never more than about 0.2% of the

FIGURE 4.1

Relative Abundances of Product Ions in Methane as a  
Function of Ion Source Pressure

The rapid decrease of the primary ions  $\text{CH}_4^+$  and  $\text{CH}_3^+$  with increasing pressure due to ion-molecule reactions is also indicated in the figure.

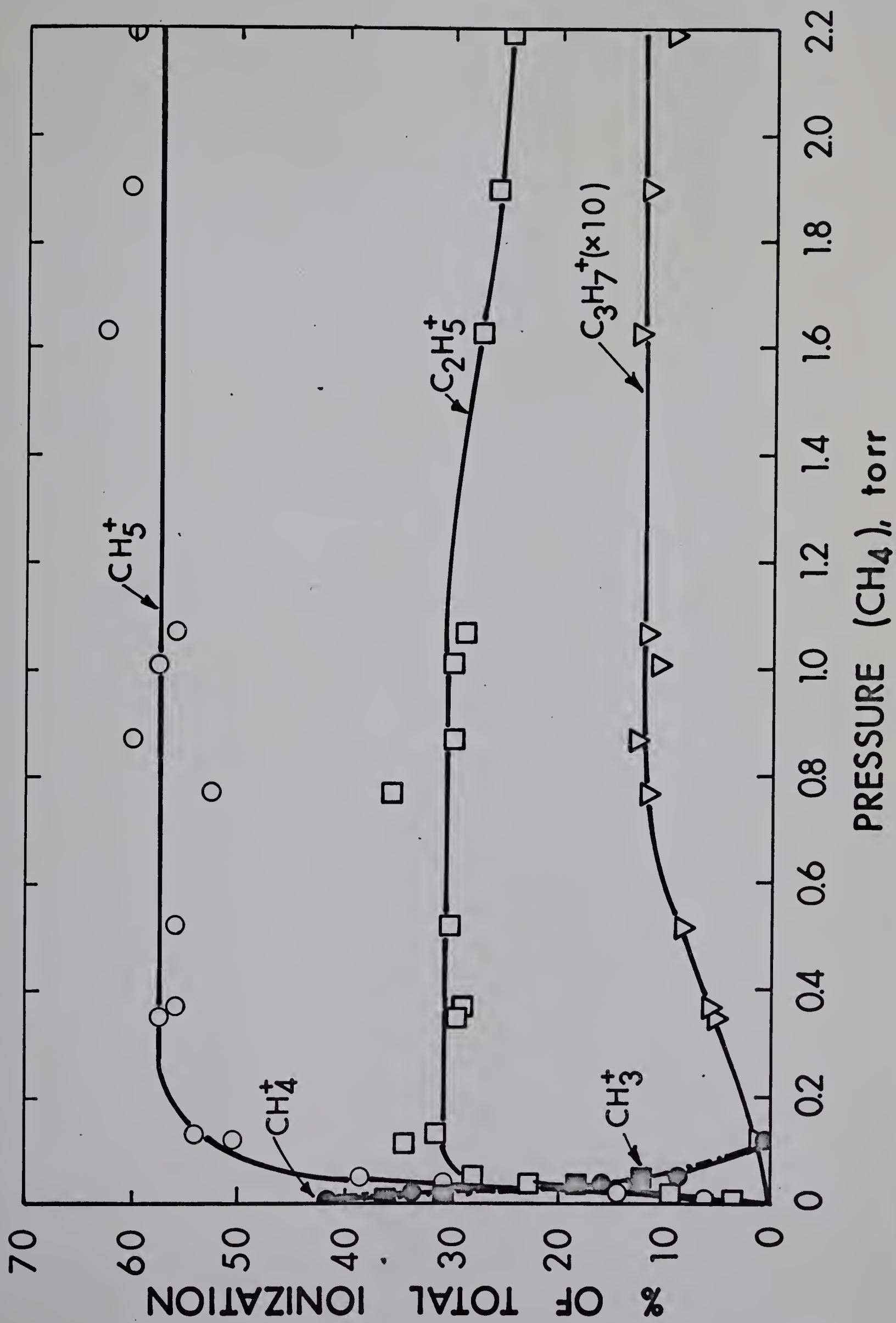
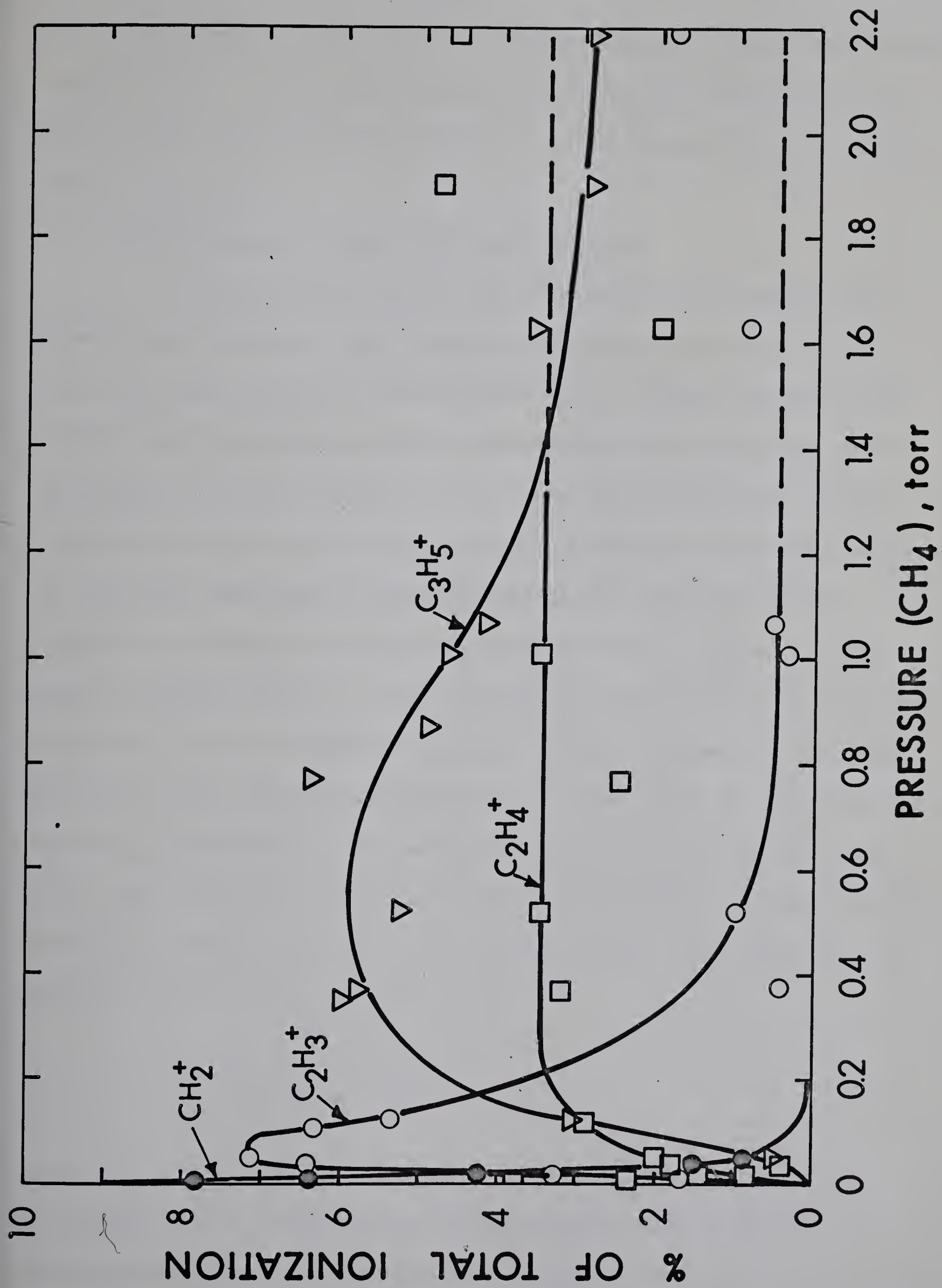


FIGURE 4.2

Variations with Pressure of Relative Abundances of some  
Ions in Methane

The rapid decrease of the primary ion  $\text{CH}_2^+$  due to ion-molecule reactions in methane is indicated, as well as variations of some lesser product ions with pressure.







total ionization. Although not in the background (no methane present) spectrum it is not certain whether these ions are actually due to ion-molecule reactions with methane or possibly with heavier hydrocarbon impurities.

#### 4.3 Determination of Reaction Cross Sections

The determinations of cross sections for reaction of primary and secondary ions with gas molecules in the ion source were made using Wexler's "beam model"<sup>29, 62</sup> Lampe, Franklin and Field<sup>31</sup> have developed a kinetic method from which reaction rate constants or ratios of these rate constants may be obtained. Their approach is based on considerations of steady-state concentrations of collision complexes. Both approaches can yield equivalent results for primary and secondary ions at least. Wexler's "beam model" possibly gives a clearer physical picture of the interactions (reactions) that take place as a beam of ions (formed in the plane of the ionizing beam of electrons or protons, etc.) is swept by the repeller field through the gas medium toward the ion source exit slit. The beam of primary ions will be decreased in an exponential fashion as these ions react with gas molecules. The intensity of primary ions at the exit slit will be

$$I_p = I_p^0 e^{-Q_p^n \ell} \quad (4.7)$$

where  $I_p^0$  is the (initial) intensity of the species in the plane of ionization at a distance  $\ell$  (cm) from exit slit,  $n$  is the concentration of gas (in molecules/cc) and  $Q_p^t$  is the total cross section





in  $\text{cm}^2/\text{molecule}$  for the reaction of primary ions with the gas.

Taking logarithms of both sides of equation (4.7) we obtain

$$\ln I_p = \ln I_p^0 - Q_p^t n \ell \quad (4.8)$$

A plot of  $\text{Log } I_p$  versus gas concentration,  $n$ , should be a straight line of slope equal to  $-Q_p^t \ell / 2.303$ .

Each species of secondary ions formed as products of reactions of primary ions with the gas will move toward the exit slit, this "beam" also being attenuated by interactions with neutral molecules. The change of intensity of a secondary product species at any point  $x$  between point of origin of primary ion and the exit is a balance between its formation and reaction

$$\frac{dI_s}{dx} = I_p Q_p n - I_s Q_s^t n \quad (4.9)$$

where  $I_s$  is the secondary ion current at exit slit,  $Q_p$  is the partial cross section of the primary ion leading to the secondary ion of interest, and  $Q_s^t$  is the total reaction cross section in  $\text{cm}^2/\text{molecule}$  of this secondary species. Upon integration between the proper limits one obtains

$$I_s = \frac{I_p Q_p}{Q_s^t - Q_p^t} \left( e^{-Q_p^t n \ell} - e^{-Q_s^t n \ell} \right) \quad (4.10)$$

According to Eq. (4.10), the yield of a secondary ion should rise with pressure, reach a maximum and then decrease. At higher pressures the first exponential term of Eq. (4.10) will be





negligible compared to the second if  $Q_s^t < Q_p^t$  and  $I_s$  will show an exponential decrease in pressure. Then the cross section  $Q_s^t$  can be obtained from a semilogarithmic plot of secondary ion intensity vs  $n$ , analogous to the treatment for primary ions.

Equations can be given for tertiary and higher order ions, but the experimental results do not yield the cross sections of interest easily from the equations relating product ion intensity,  $n$ ,  $\ell$  and cross sections.

The rate constants  $k$  can be obtained from the reaction cross section by means of the equation

$$k = Q \left( \frac{eE_r \ell}{2m_i} \right)^{\frac{1}{2}} \quad (1.29)$$

where  $e$  is the charge of the electron,  $E_r$  is the repeller field strength and  $m_i$  is the mass of the ion disappearing by further reaction.

In Eqs. (4.7), (4.8) and (4.10) the  $I$ 's are written as absolute intensities but since  $I_p^\circ$  increases with increasing gas pressure,  $I_p$  and  $I_s$  must be normalized. Thus we take the fractional intensity as <sup>the</sup> per cent of the total ionization rather than absolute intensities or peak heights. We assume that all ions are collected with equal efficiency and that the ions collected and measured are proportional to the ion concentrations at the ion source exit slit.

The cross sections for reactions of some primary and secondary ions with methane are given in Table 4.1. Also given are the results of Wexler et al<sup>62</sup> with  $\ell = 1.0$  cm, using a 2Mev proton



TABLE 4.1

Total Reaction Cross Sections of Ions with Methane

Ions	$Q^t$ (units of $10^{-16}$ cm <sup>2</sup> /molecule)			
	Present work (11 V/cm) *	Wexler <sup>62</sup> (12.3 V/cm)	Wexler <sup>29</sup> (12.5 v/cm)	Field <sup>59,61</sup> (6.25 V/cm)
CH <sup>+</sup>	45	14	45	56
CH <sub>2</sub> <sup>+</sup>	39	15	36	41
CH <sub>3</sub> <sup>+</sup>	23	21	27	29
CH <sub>4</sub> <sup>+</sup>	29	23	39	38
CH <sub>5</sub> <sup>+</sup>	very small	0.1	1.6	<0.07
C <sub>2</sub> H <sub>3</sub> <sup>+</sup>	4.0	5.0	10	6
C <sub>2</sub> H <sub>4</sub> <sup>+</sup>	very small	<0.1	1.9	<0.2
C <sub>2</sub> H <sub>5</sub> <sup>+</sup>	small	<0.06	<0.1	<0.07

\* Repeller field strength





beam, Wexler and Jesse<sup>29</sup> with  $g = 0.32$  cm and Field et al<sup>59, 61</sup> with  $g = 0.20$  cm. All studies except those of Wexler et al<sup>62</sup> used an electron beam.

There is a certain amount of scatter among the reaction cross sections measured by various workers. All these cross sections are macroscopic or phenomenological cross section which really measure weighted mean reactivities dependent on velocities and the internal energies of reactant. Experimental parameters such as repeller field strength, mean distance of travel of ions, source temperature, and space charge may influence the magnitudes of the cross sections.<sup>33</sup> Although the present cross sections agree better with the results of Field et al<sup>59, 61</sup>, the partial agreement is probably not particularly significant since none of the cross sections measured give information on what is the small scale or microscopic behaviour of ions in the mass spectrometer ion source.

In Table 4.2 the reaction rate constants calculated from our cross sections with the use of Equation (1.29)' are tabulated. The results of Field and co-workers<sup>59, 61</sup> are also tabulated for comparison. There is a close correspondence between the two sets of rate constants. As a matter of interest reaction rate constants have been calculated from Wexler's 2 Mev proton beam cross sections. The comparison of the three sets of rate constants partially confirms that there is no observable temperature dependence of  $k$  since our ion source and Wexler's is at room temperature while the ion source temperature in the experiments of Field et al is ca. 200°C.



TABLE 4.2

Rate constants of reaction of product ions with methane

k, (units of $10^{-10}$ cc/molecule sec)			
Ion	Present Results	Field <sup>59,61</sup>	Calc. from
			Wexler <sup>62</sup>
CH <sup>+</sup>	18.3	17.4	8.9
CH <sub>2</sub> <sup>+</sup>	14.5	12.4	9.7
CH <sub>3</sub> <sup>+</sup>	8.7	8.2	13.0
CH <sub>4</sub> <sup>+</sup>	10.6	10.3	13.9
CH <sub>5</sub> <sup>+</sup>	very small	0.01	
C <sub>2</sub> H <sub>3</sub> <sup>+</sup>	1.1	0.9	2.3
C <sub>2</sub> H <sub>4</sub> <sup>+</sup>	very small	<0.03	
C <sub>2</sub> H <sub>5</sub> <sup>+</sup>	small	<0.01	





#### 4.4 Discussion of Results

In general the present results are in reasonable agreement with the results of Field and Munson<sup>61</sup> and agree qualitatively with the results of Wexler and co-workers<sup>62</sup>. The present results, those of Field and Munson, and Wexler and co-workers are all studied in the same ion source pressure range but with different ion path lengths  $\ell$  (the distance between ion source exit slit and plane of ionizing beam); also different ionizing media are used (100 kev protons, 100 ev electrons and 2 Mev protons respectively). To facilitate comparison, all three sets of results are plotted together in Figs. 4.3 and 4.4 as per cent of total ionization versus  $p\ell$ , where  $p$  is ion source pressure and  $\ell$  is the ion path length defined above.

Because of the dependence of reaction cross sections on ion exit energy as  $(E_r\ell)^{-1/2}$  or  $(E_r\ell)^{-1}$ <sup>23, 25</sup> this comparison above is probably only valid for identical ion exit energies  $(E_r\ell)$ . However as an approximation, consideration of the three sets of mass spectra as a function of  $p\ell$  will be more valid than a comparison on the basis of equivalent pressures only. That is because lengthening the ion path length will raise the number of collisions an ion will undergo with gas molecules, as does an increase in pressure. Also at higher pressures,  $E_r\ell \rightarrow kT$ .

Comparing our results with those of Field and Munson first we see that positions of maxima and general shapes of curves agree quite well. The possible exceptions as far as



FIGURE 4.3

Comparison of Ionic Product Variations in Methane

Solid Lines: present results

Dashed lines: Results of Wexler et al<sup>62</sup>

Dash-dot lines: Field and Munson<sup>61</sup>

$p\ell$  is product of ion source pressure (torr) and  
ion path length  $\ell$  (mm).

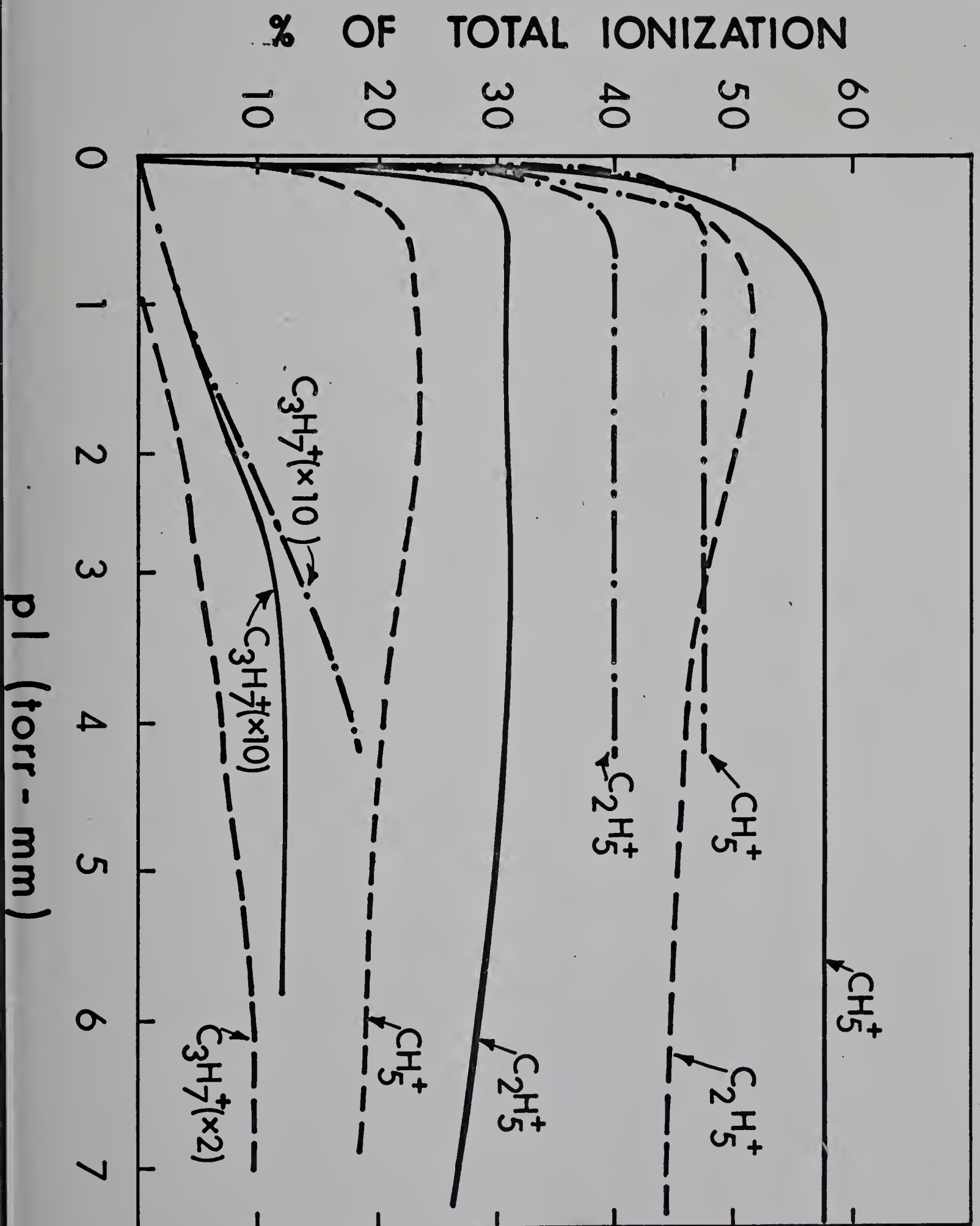


FIGURE 4.4

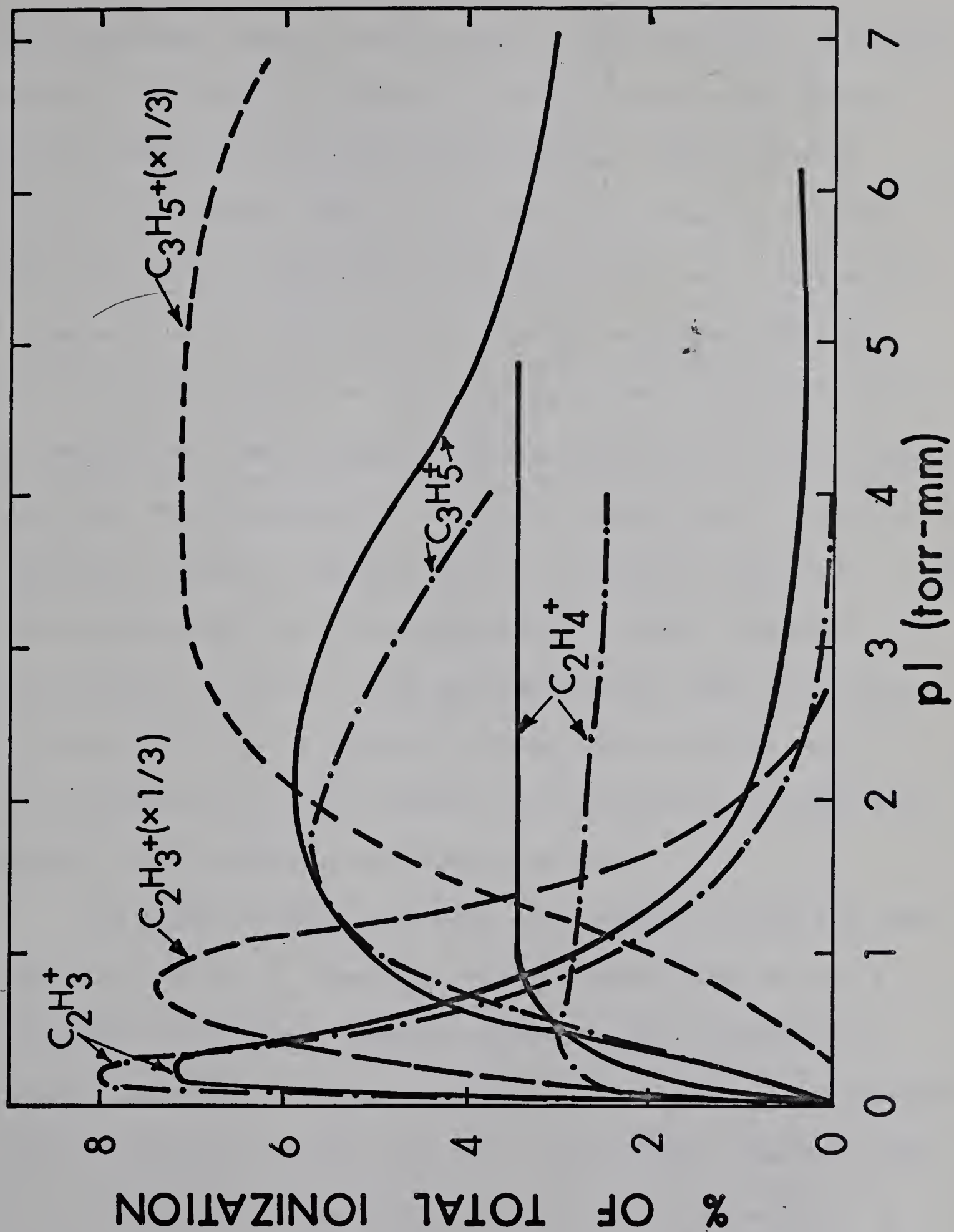
Comparison of Ionic Product Variations in Methane

Solid lines: Present results

Dashed lines: Results of Wexler et al<sup>62</sup>

Dash-dot-lines: Results of Field and Munson<sup>61</sup>

$p\ell$  is product of ion source pressure (torr) and  
ion path length  $\ell$  (mm).







absolute agreement are the intensities of  $\text{CH}_5^+$  and  $\text{C}_2\text{H}_5^+$ . Although we have not calibrated our electron multiplier detector versus Faraday cup detection for mass discrimination, from previous experience with another sector field mass spectrometer in these laboratories using an identical electron multiplier<sup>66</sup> and assuming a simple velocity discrimination we can calculate that the intensity of  $\text{C}_2\text{H}_5^+$  should be corrected by a factor of  $(29/17)^{1/2}=1.3$ . Making roughly the same correction for intensities of other higher mass ions and renormalizing the relative intensities in the spectrum, the corrected values of intensities  $\text{CH}_5^+$  and  $\text{C}_2\text{H}_5^+$  above  $p_0 = 1$  torr-mm would be about 51% and 35% respectively in good agreement with Field and Munson. However Field and Munson also used an electron multiplier detector (of a different type) and we do not know if the ion intensities in their spectra were corrected for mass discrimination in the electron multiplier or not.

All three studies indicated in Figures 4.3 and 4.4 show that reactivities of  $\text{CH}_5^+$  and  $\text{C}_2\text{H}_5^+$  with methane must be quite small, although the present results indicate  $\text{C}_2\text{H}_5^+$  intensity to be dropping somewhat at higher pressures and Wexler's data indicate that the intensities of  $\text{C}_2\text{H}_5^+$  and  $\text{CH}_5^+$  are dropping slightly with increasing pressure. It is thought that this decrease of  $\text{C}_2\text{H}_5^+$  in the present results is more apparent than real and Wexler and co-workers seem to be of the opinion that some  $\text{CH}_5^+$  and possibly  $\text{C}_2\text{H}_5^+$  is being lost through reactions with impurities and not with



methane itself. Since  $\text{CH}_5^+$  and  $\text{C}_2\text{H}_5^+$  are essentially the only product ions from reactions of  $\text{CH}_4^+$  and  $\text{CH}_3^+$  respectively, with methane, the relative abundances (R.A.'s) of  $\text{CH}_5^+$  and  $\text{C}_2\text{H}_5^+$  should correspond to those of  $\text{CH}_4^+$  and  $\text{CH}_3^+$  in the primary ion spectra (taken at low pressures) given in Table 4.3. The agreement for these two ions is excellent in the results of Field and Munson<sup>59</sup> and reasonable in our results especially considering an electron multiplier correction. While finding reasonable agreement for the R.A.  $\text{C}_2\text{H}_5^+$  compared to the R.A. of  $\text{CH}_3^+$  in Wexler's results, the R.A. of  $\text{CH}_5^+$  seems much too low and in fact R.A.  $\text{CH}_5^+$  is a good factor of two lower than R.A.  $\text{CH}_4^+$ . The R.A.'s of  $\text{C}_2\text{H}_3^+$  and  $\text{C}_3\text{H}_5^+$  at their maxima should be less than or equal to the R.A. of  $\text{CH}_2^+$  in the primary spectra. However they are some 20% while R.A.  $\text{CH}_2^+$  is only 5%. The product ion  $\text{C}_2\text{H}_4^+$  should also be included since it is a product of reaction of  $\text{CH}_2^+$  with methane. This would bring in an even larger discrepancy. Although Wexler does not give the actual low pressure (primary) mass spectrum of methane caused by protons through foils we can assume it would be very similar to his earlier 2.25 Mev proton primary mass spectra taken without foils<sup>15</sup> since there are only minor variations in the proton impact spectrum from some Mev to a few kev (see Chapter 3, Part II)

At Wexler's highest pressure plotted ( $p \approx 7$  torr-mm) the ions  $\text{CH}_5^+$ ,  $\text{C}_2\text{H}_5^+$ ,  $\text{C}_3\text{H}_5^+$  and  $\text{C}_3\text{H}_7^+$  add up to about 83% of the total ionization. If we allow some 5% for  $\text{C}_2\text{H}_4^+$  then about





TABLE 4.3

Primary (low pressure\*) mass spectrum of methane

ion	2.25 Mev protons <sup>15</sup>	100 kev protons through foil	70 ev electrons <sup>61</sup>
C <sup>+</sup>	0.7	1.8	1.3
CH <sup>+</sup>	1.9	4.2	3.8
CH <sub>2</sub> <sup>+</sup>	5.1	9.3	7.6
CH <sub>3</sub> <sup>+</sup>	42.6	39.0	40.0
CH <sub>4</sub> <sup>+</sup>	49.0	45.0	47.0

\* Pressure less than  $10^{-4}$  torr





12% of the ions are unaccounted for. These could be higher mass ions. These same five ions for the present results and those of Field and Munson add up to 95% at most higher pressures. As mentioned previously certain higher mass ions observed by us (ions not plotted in the figures) showed no particular pressure dependence and were of very low intensities. The concentration of  $C_3H_7^+$  observed by us remains constant at about 1% while it is rising in Field and Munson's data and is rising to a much higher intensity in Wexler's work. Part of this ion intensity observed could be due to impurities since Munson and Field<sup>65</sup> and Haynes and Kebarle<sup>64</sup> have shown how readily  $C_3H_7^+$  could be formed, e.g. from a propane impurity. Wexler mentions observing the concentrations of  $C_4H_7^+$ ,  $C_4H_9^+$  and  $C_4H_{11}^+$  to be increasing with pressure, while Field and Munson<sup>61</sup> observe only  $C_4H_9^+$  to be increasing. Of these ions only  $C_4H_9^+$  is formed in any measurable concentration in the present work and at higher pressures it remains constant at about 0.1% of the total ionization. Haynes and Kebarle<sup>64</sup> have shown that these  $C_4$  ions could be formed by reactions of methane product ions (such as  $CH_5^+$  and  $C_2H_5^+$ ) with paraffin impurities.

#### 4.5 Conclusions

It can be concluded that of the secondary ions formed in gaseous ionic reactions of methane ions, formed by various means (electrons, protons), only  $C_2H_3^+$  is reactive, with the main product ions  $CH_5^+$  and  $C_2H_5^+$  being unreactive. Upon



reaction with methane the vinyl ion yields  $C_3H_5^+$  which is slightly reactive. The propyl ion, whose mechanism of formation is still not completely known is also unreactive in methane. Agreement with recent results of other workers was reasonable in most cases.





## 5. ION-MOLECULE REACTIONS IN ETHYLENE

### 5.1 Introduction

#### A. Previous Studies

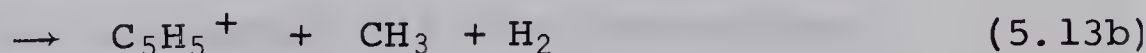
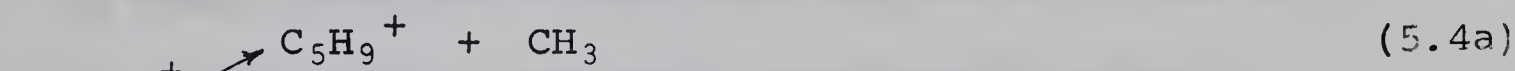
Ion molecule reactions in ethylene have been investigated by several authors. The initial<sup>55, 56</sup> studies were at low ( $\sim 10$  millitorr) pressures where only second-order reactions were observed. Later, reactions at higher pressures were studied.<sup>28 67 68</sup> Melton and Rudolph<sup>67</sup> used an uncollimated alpha-particle beam and studied ionic reactions in ethylene at pressures up to 0.1 torr. Field<sup>28</sup> and Wexler and Marshall<sup>68</sup> studied gaseous ionic reactions in ethylene using an electron-impact ion source at pressures up to 0.3 torr.

From these studies some of the main reactions for production of secondary and tertiary product ions have been well established. The main primary reactant ions are  $C_2H_4^+$ ,  $C_2H_3^+$ , and  $C_2H_2^+$  since these ions account for 90% of the total ionization in the low pressure ( $< 10^{-4}$  torr) spectrum of ethylene. By comparison of the appearance potential of the product ions with those of the primary species, Franklin et al<sup>56</sup> were able to identify several secondary product ions with their primary ion precursors. Field<sup>28</sup> confirmed the assignments of the secondary ions to the primary ion precursors and was also able to assign several tertiary ions to primary ion precursors. He used



an additive method in which the particular additive used enriched greatly the intensity of the primary ions  $C_2H_4^+$ ,  $C_2H_3^+$  and  $C_2H_2^+$  respectively.

The formal sequence of reactions suggested from Field's<sup>28</sup> results and conclusions is shown below.







Wexler and Marshall<sup>68</sup> correlated product ions with their primary ion precursor by the matching of appearance potentials and found agreement with the results of Field<sup>28</sup> with the exceptions that  $C_2H_3^+$  (upon reaction with  $C_2H_4$ ) yields  $C_4H_7^+$  and that both  $C_2H_2^+$  and  $C_2H_3^+$  could yield  $C_4H_5^+$ . The actual mechanisms proposed by Wexler and Marshall to account for the formation of higher order ions requires that the intermediate, second-order complex (i.e.  $C_4H_8^+$ ,  $C_4H_7^+$ , or  $C_4H_6^+$ ) is short-lived and dissociates before colliding with ethylene. Higher order ions would then result primarily by ethylene addition to the stable product ions by chains of simple consecutive and competitive ion-molecule reactions.

This is in contrast to the approach of Field presented above and the general model used by Lampe, Franklin and Field.<sup>31</sup> This model requires that the intermediate, second-order complex to be relatively long lived so collisions of these complexes with the neutral ethylene molecules leads to higher order reaction products.

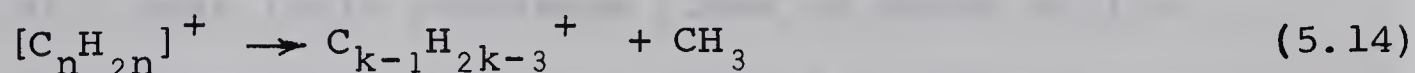
To distinguish between the two interpretations on the basis of mass spectrometric information alone is difficult and has not yet been accomplished. Neither model seems to explain completely all the observations. The ion  $C_4H_8^+$  would be a tertiary ion, if formed by decomposition of the complex  $[C_6H_{12}]^+$  and it is indeed





observed<sup>28, 68</sup> to be a tertiary ion. However its observation as a stable ion may be connected with a required stabilization of the vibrationally excited complex  $[C_4H_8^+]$  by at least one collision with an ethylene molecule.

Kebarle and co-workers<sup>69</sup> have studied the high pressure mass spectrum of pure ethylene and ethylene with rare gas sensitizers at pressures from 1 to 200 torr. These studies were done with the near-atmospheric alpha particle mass spectrometer of these laboratories. Using 20 torr xenon and 1 millitorr to 5 torr ethylene the polymer ions of formula  $C_nH_{2n}^+$  (n=even), thought to be due to a common  $C_2H_4^+$  precursor, were found to dominate the spectrum. The polymer ions up to n=14 were found in high abundance. At 4 millitorr of ethylene,  $C_4H_8^+$  was the dominant ion while at 1 torr ethylene the most intense ion was found to be  $C_{10}H_{20}^+$ . They showed that xenon collisionally deactivated the excited complexes  $[C_nH_{2n}^+]$  to yield the stable polymer ions observed. Increasing the xenon pressure effectively suppressed the decomposition reaction



where n=even and k=odd,

In pure ethylene these workers again found the  $C_nH_{2n}^+$  series of ions to be prominent but the lower mass homologues  $C_4H_8^+$  and  $C_6H_{12}^+$  were not present, even at 1 torr  $C_2H_4$  pressure.





Increasing pressures increased the complexity of the spectra observed. However the polymerization was found to effectively stop in the mass range: 200-300. The increased pressures only led to a proliferation of ionic products in the mass range 100-250. At lower pressures (below 20 torr) they were able to obtain a satisfactory ion product balance by assignment of the main product ions observed to the three main primary ions :  $C_2H_4^+$ ,  $C_2H_3^+$  and  $C_2H_2^+$ .

Very recently (while this thesis was being written) Wexler and co-workers<sup>62</sup> published a study on ion-molecule reactions in ethylene at pressures up to about 1 torr using a 2 Mev proton beam as a source of ionization. A comparison of their results will be made in the discussion Sec. 5.2.

#### B. Present Investigation

Previous studies on ethylene had been done only at pressures up to 0.3 torr using conventional electron impact sources at temperatures of about 200° C. The high pressure studies with the alpha particle mass spectrometer were done under quite different conditions-at room temperature and with mean ionic residence times of about milliseconds. The present study is an effort to partially bridge the pressure gap between these lower pressure and high pressure studies.

### 5.2 Results

In this research, ion-molecule reactions in





ethylene were studied at pressures as high as 1.25 torr. Three representative spectra at pressures from 42 millitorr to 1 torr are plotted as histograms in Figure 5.1. We can see that even at 42 millitorr, ionic polymerization is quite extensive with ions up to mass 105 (not plotted) being found. The ions  $C_2H_5^+$ ,  $C_3H_5^+$  and  $C_5H_9^+$  dominate the spectrum in agreement with previous results<sup>28, 62, 68</sup>. At 0.12 torr, the chain of reactions extends to higher mass with  $C_3H_3^+$ ,  $C_4H_9^+$ ,  $C_5H_9^+$ ,  $C_6H_{11}^+$  being the more prominent species. The general trend continues so that at 1 torr ions as large as  $C_{10}H_{20}^+$  are observed. The main series of product ions are:

$$C_nH_{2n+1}^+, C_2H_{2n}^+, C_nH_{2n-1}^+, C_kH_{2k-1}^+, C_nH_{2n-2}^+, C_nH_{2n-3}^+, C_kH_{2k-3}^+ \quad (\text{where } n = \text{even and } k = \text{odd}).$$

Kebarle et al<sup>61</sup> found all these series of ions in the rare gas sensitized alpha particle radiolysis of ethylene studied in the alpha particle mass spectrometer. They also found all these series of ions except  $C_nH_{2n-2}^+$  in studies of pure ethylene at 2 torr and higher pressures. However all these series were much more developed toward higher mass e.g.  $C_{14}H_{28}^+ \approx 2\%$  of total ionization at 2 torr ethylene in their experiments. Their 2 torr mass spectrum is shown in Fig. 5.2 for comparison with these results at 1 torr. It is seen that ions from the  $C_kH_{2k-1}^+$  series and especially the

FIGURE 5.1

Mass Spectra of Ethylene at Various Ion Source Pressures

Repeller field strength = 11V/cm.

# PERCENT OF TOTAL IONIZATION

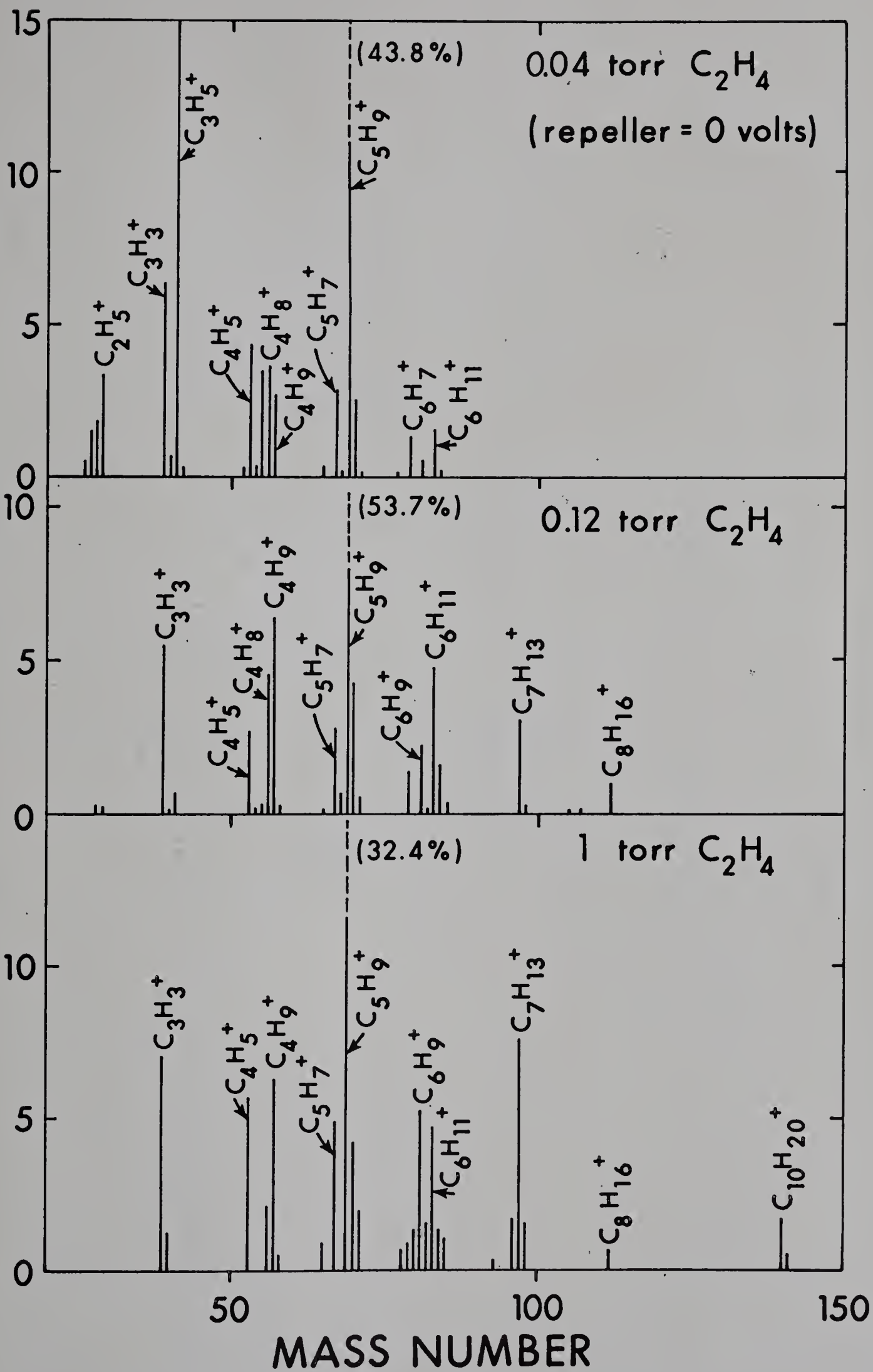
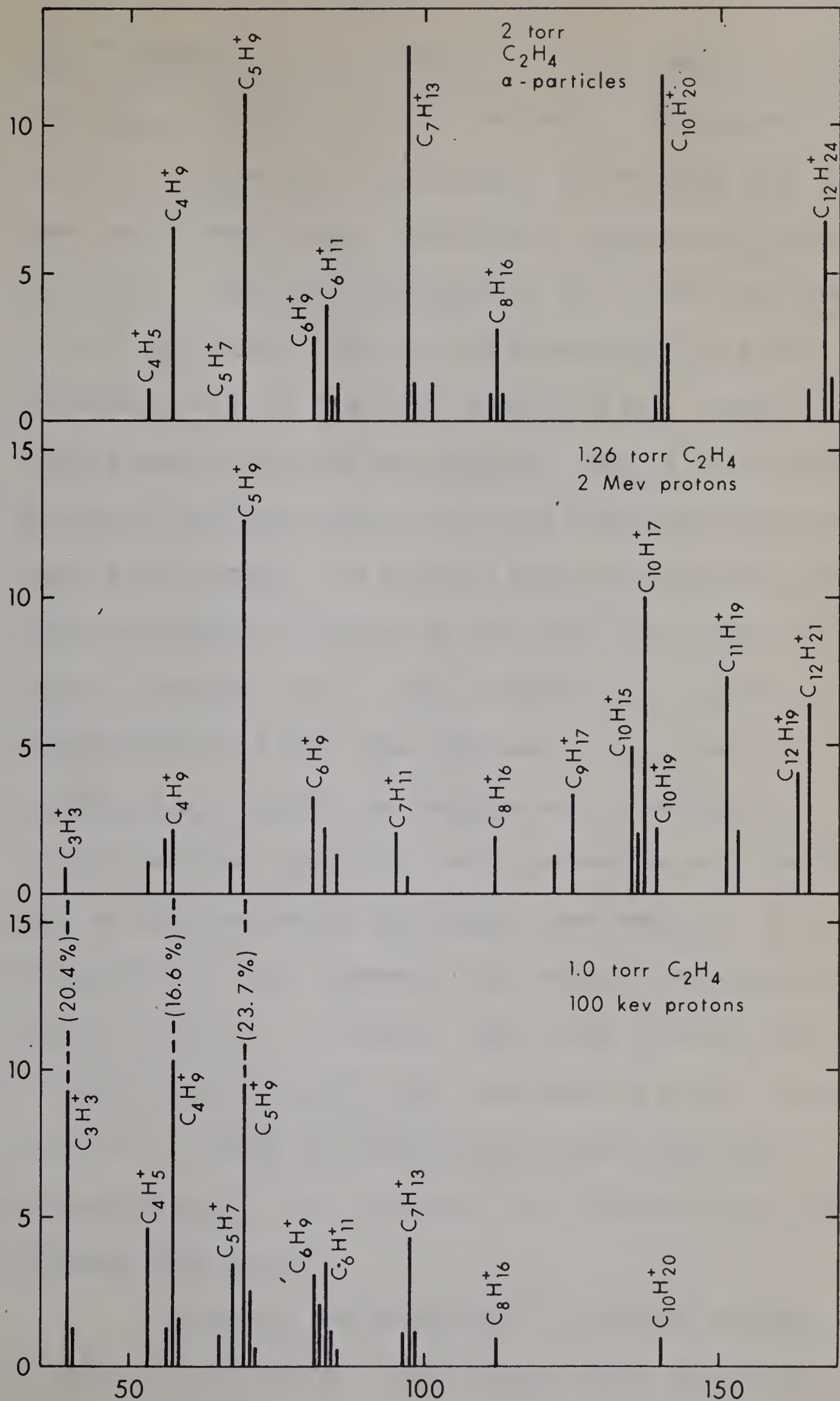


FIGURE 5.2

Comparison High Pressure Mass Spectra of Ethylene

- Top: Alpha particle mass spectrum at 2  
torr due to Kebarle et al<sup>69</sup>
- Middle: Two Mev proton mass spectrum at 1.26  
torr due to Wexler et al<sup>62</sup>
- Bottom: Present results for mass spectrum at  
1.0 torr

% OF TOTAL IONIZATION



MASS NUMBER





$C_nH_{2n}^+$  series are very prominent in their spectra. Although the  $C_kH_{2k-1}^+$  series is very prominent in the present spectra, the  $C_nH_{2n}^+$  series has not developed appreciably even at 1 torr. There would seem to be a discrepancy between our mass spectrum and theirs. Since the pressures (1 and 2 torr) are similar and both ion sources are at room temperature, the only difference would be the ionic reaction time. Since we are using a repeller field, the reaction time is ~a microsecond while the reaction time in the alpha particle apparatus is about a millisecond. The proton beam mass spectrum, therefore should represent a picture of the ionic distribution at shorter reaction times. Their results would indicate that high abundances of the lower ethylenic ion polymers  $C_4H_8^+$  and possibly  $C_6H_{12}^+$  should be observed under the condition of shorter reaction time when similar pressures are considered. This is not observed in the proton beam results. It is interesting to note, however, that Kebabian and co-workers observe no  $C_4H_8^+$  at all and a very small intensity of  $C_6H_{12}^+$ . It could be possible that the ions such as  $C_{10}H_{20}^+$  are not formed by a simple polymerization process involving successive  $C_nH_{2n}^+$  ions reacting with ethylene in the pure ethylene mass spectra.

In Wexler and co-workers<sup>62</sup> study of ethylene up to about 1 torr, using a 2 Mev proton beam, extensive ionic polymerization was also found. Although their low pressure



(22 millitorr ethylene) spectra agree well with the present results, the higher pressure (eg. 0.75 or 1.26 torr) spectra are not too similar. Their 1.26 torr mass spectrum is shown in Fig. 5.2. They find the principal series of ions to be  $C_nH_{2n-1}^+$ ,  $C_nH_{2n-3}^+$ ,  $C_nH_{2n-5}^+$  and  $C_nH_{2n-7}^+$  where  $n$ =odd or even. They do not observe ions of formula  $C_nH_{2n+1}^+$ ,  $C_nH_{2n}^+$  or  $C_nH_{2n-2}^+$ . Their spectrum is more complex than ours since the product ion intensities extend past mass 219 (not shown in Fig. 5.2) with no great reduction in abundance. We can offer no explanation for these somewhat puzzling differences.

Figure 5.3 shows three typical spectra of ethylene with the repeller at zero volts (with respect to ion chamber). In general this condition should give a longer, if somewhat ill-defined, reaction time. Even at .04 torr this can be seen since the intensities of the  $C_2$  primary ions are lower and the intensities of higher mass ions increase in intensity: eg. R.A.  $C_5H_9^+$  is 15% at 11V/cm repeller and 44% at zero repeller.

### 5.3 Reaction Cross Sections Q

Total reaction cross sections of some primary and secondary ions in ethylene were calculated as was done in Sec. 4.3 by use of semilogarithmic plots of the R.A. of ion versus ethylene pressure. From the slope of the linear portion of the curves the cross sections could be obtained since  $\text{slope} = -Q/2.303$ . The values obtained are presented

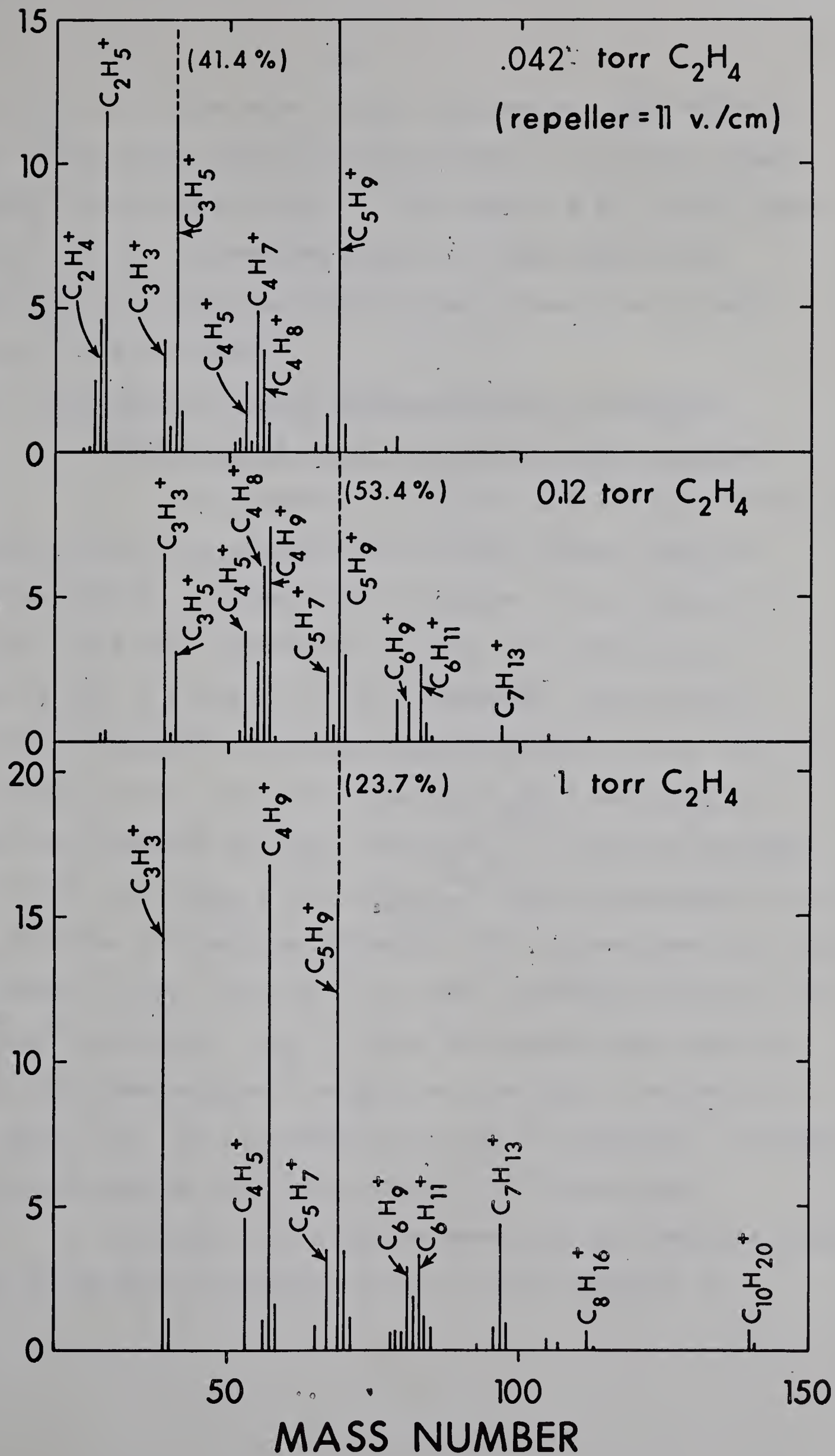
FIGURE 5.3

Mass Spectra of Ethylene at Different Ion Source Pressures

Repeller field strength is zero V/cm.



# PERCENT OF TOTAL IONIZATION





in Table 5.1 along with values obtained by other workers. All other cross sections were obtained by electron impact except those due to Wexler<sup>62</sup> who used a 2 Mev proton beam. Again, as for the methane study, in some cases cross sections from the four sets of data agree to only about a factor of two to four.

#### 5.4 Discussion of Ionic Polymerization in Ethylene

##### A. Variation of ionic intensities with pressure

In Figures 5.4 and 5.5 and 5.6 intensities of various ions from ethylene are plotted versus ethylene concentration. Product ions in Figure 5.4 are thought to be due to a  $C_2H_4^+$  precursor, in Fig. 5.5. due to  $C_2H_3^+$  and in Fig. 5.6 due to a  $C_2H_2^+$  precursor. The product ions are assigned to primary ion precursors on the basis of reactions (5.1) - (5.13). Thus the  $C_nH_{2n}^+$  and  $C_kH_{2k-1}^+$  ions are assigned to  $C_2H_4^+$ ; the  $C_nH_{2n+1}^+$  ions are assigned to  $C_2H_4^+$ ; and  $C_nH_{2n-2}^+$  and  $C_nH_{2n-3}^+$  ions are assigned to  $C_2H_2^+$ . In addition to these assignments;  $C_4H_7^+$  is assigned to a  $C_2H_4^+$  precursor,  $C_5H_7^+$  and  $C_6H_{11}^+$  to a  $C_2H_3^+$  precursor and  $C_3H_3^+$  to a  $C_2H_2^+$  precursor. All of these assignments are based on previous observations<sup>28</sup> except for the  $C_6H_{11}^+$  ion which is of small R.A. It is assigned to a  $C_2H_3^+$  precursor, although it could also be due to an initial  $C_2H_4^+$  precursor.

In Fig. 5.4 it can be seen that the dominant product ion series due to reaction of  $C_2H_4^+$  with ethylene is



TABLE 5.1

Total Cross Sections for Reactions of Ions with Ethylene

Ion	$Q^t$ in units of $10^{-16}$ cm <sup>2</sup> /molecule			
	These Results	Wexler et al. (electron impact)	Field (electron impact)	Wexler et al. (2 Mev protons)
$C_2H_2^+$	66	93	18	60
$C_2H_3^+$	47	47	17	22
$C_2H_4^+$	55	62	13	18
$C_2H_5^+$	45	28		8.5
$C_3H_5^+$	20	23		5.8
$C_4H_7^+$	9	22		4.1



FIGURE 5.4

Variations with Pressure of Main Product Ions in Ethylene  
Formed from a  $C_2H_4^+$  Precursor

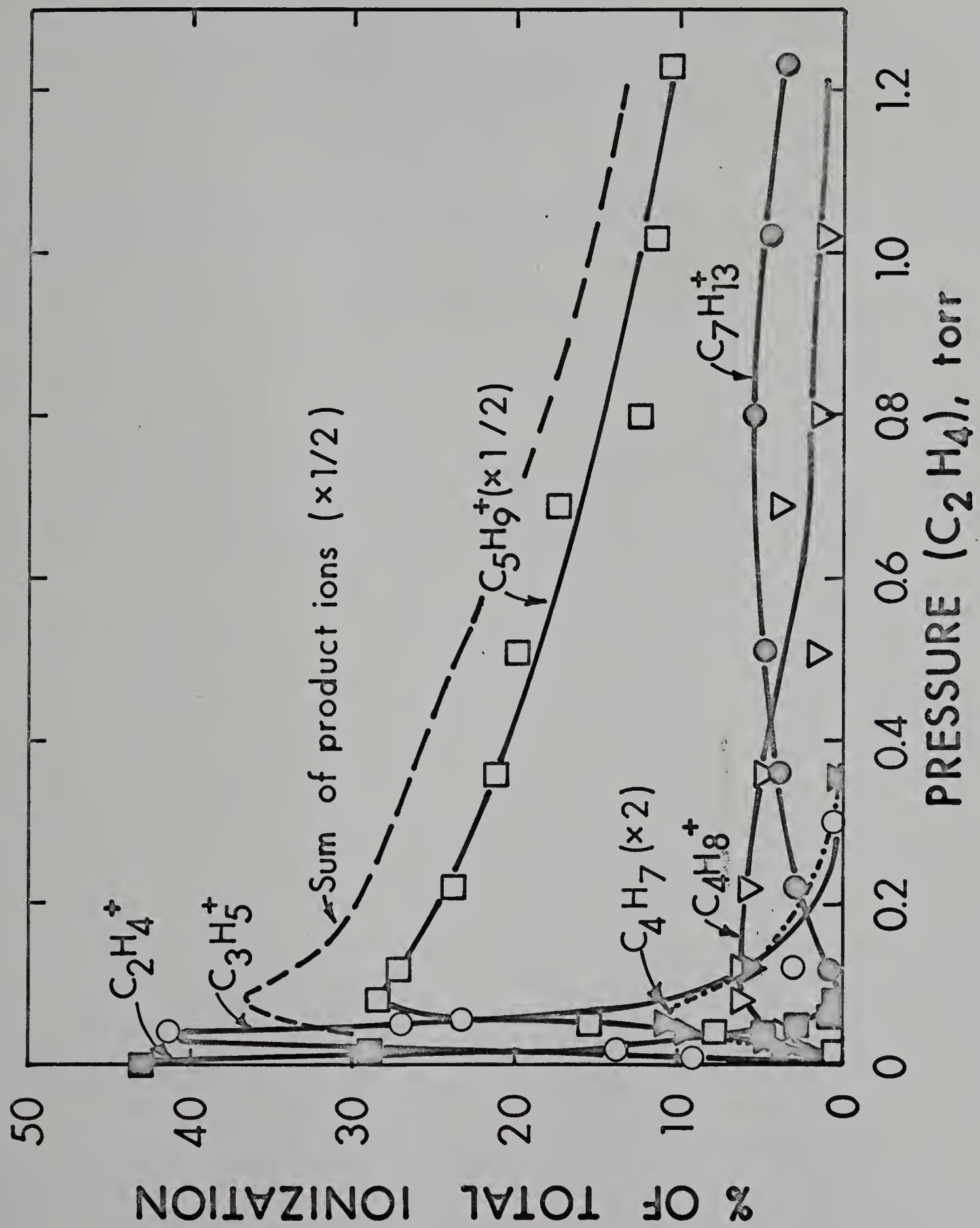


FIGURE 5.5

Variations with Pressure of Main Product Ions in Ethylene  
due to a  $\text{C}_2\text{H}_3^+$  Precursor

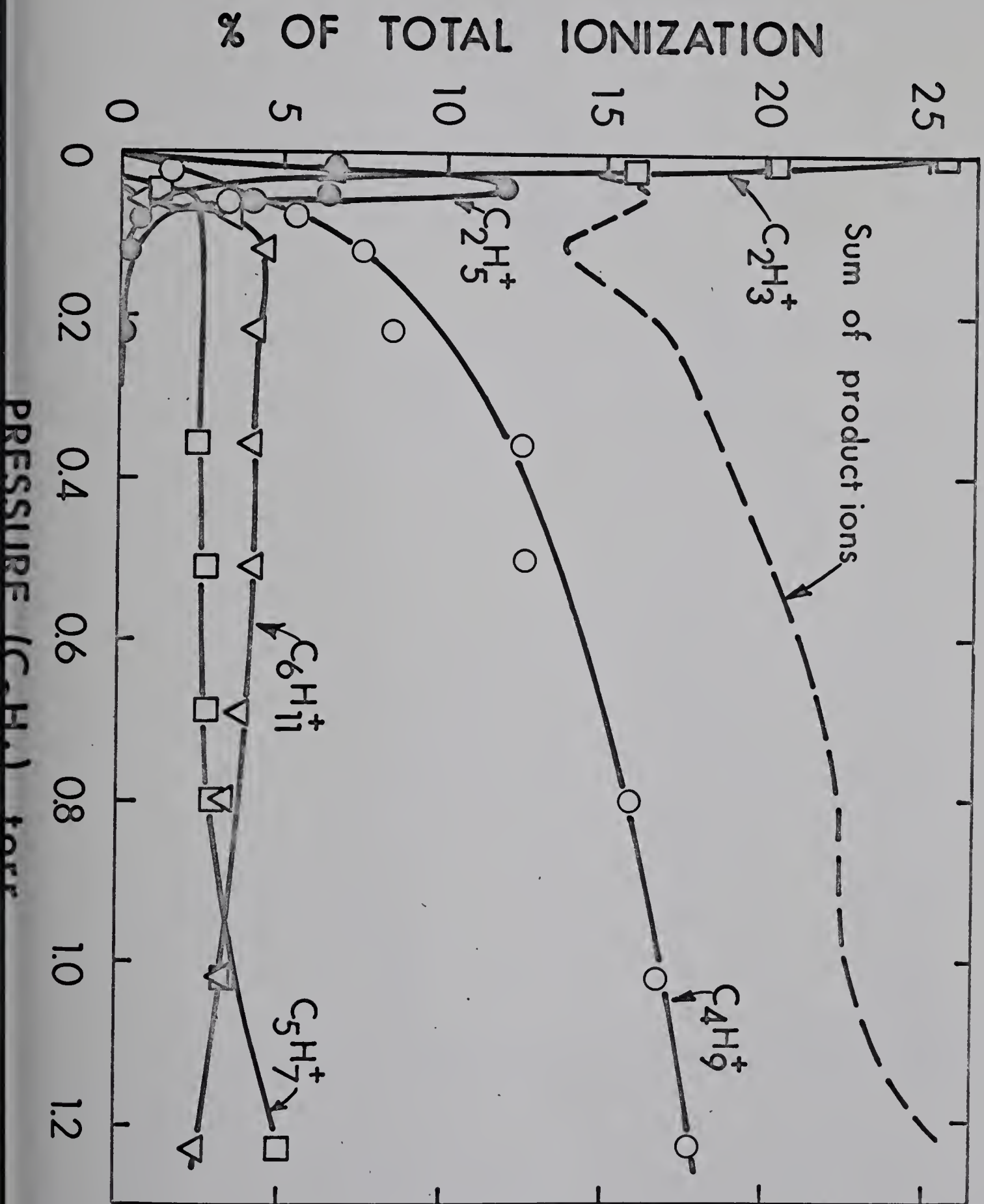
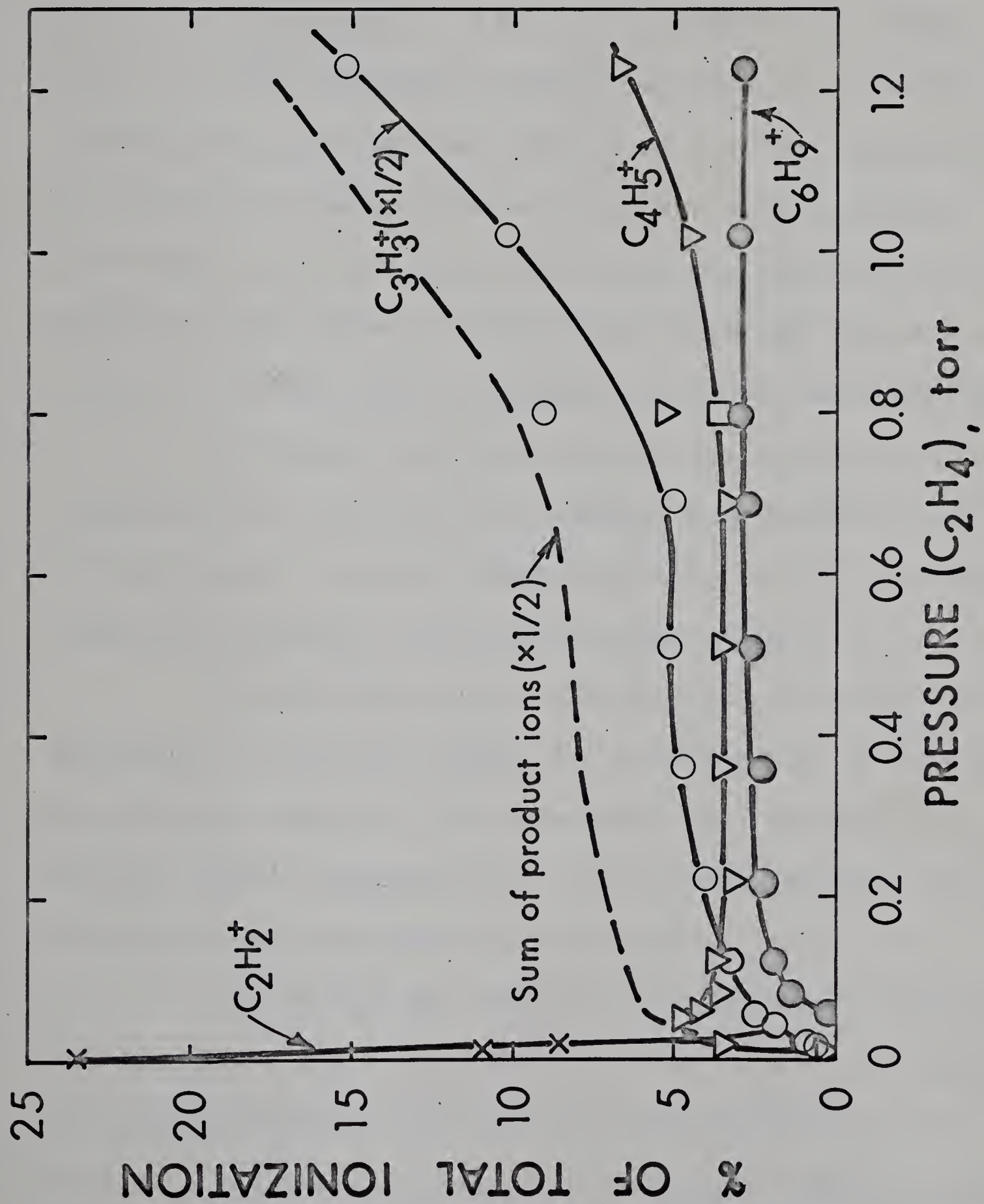


FIGURE 5.6

Variations with Pressure of Main Product Ions in Ethylene  
due to a  $\text{C}_2\text{H}_2^+$  Precursor







$C_kH_{2k-1}^+$  . The ions  $C_6H_{12}^+$ ,  $C_8H_{16}^+$  and  $C_{10}H_{20}^+$  which are higher homologues of  $C_4H_8^+$ , are observed (not plotted in Fig. 5.4) with increasing pressure but none of these ions individually are more than about 2% of the total ionization. At ion source pressures above 0.1 torr, the main product ions  $C_4H_8^+$ ,  $C_5H_9^+$  and  $C_7H_{13}^+$  all appear to react slowly with ethylene, since after reaching their respective maximum intensities on the plot, their respective R.A.'s all decrease slowly.

Of product ions due to vinyl ion reaction with ethylene (Fig. 5.5),  $C_4H_9^+$  is dominant at pressures above 0.1 torr and it is quite unreactive since its R.A. increases gradually throughout the pressure range studied.

All the main product ions thought to be due to the acetylene ion precursor appear to be nonreactive in ethylene. At pressures above 0.7 torr, the ions  $C_3H_3^+$  and  $C_4H_5^+$  exhibit sudden increases in R.A. with increasing pressure. This anomalous behaviour will be discussed later.

The sums of the product ion intensities indicated in Figs. 5.4-5.6 are also plotted in the respective figures. It will be noted that the sum of product ions due to  $C_2H_4^+$  precursor decrease gradually with increasing ethylene pressure while the totals of ions due to  $C_2H_3^+$  and  $C_2H_2^+$  respectively, increase with increasing pressure.

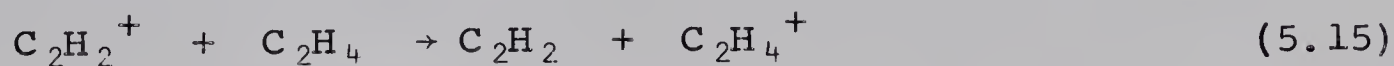




B. Agreement of totals of assigned product R.A.'s  
with the R.A. of their (initial) primary ion  
precursors.

The sums of all product ions assigned to the three  $C_2$  primary ion precursors are given at some different pressures in Table 5.2. The specific assignments have been given in subsection A. The low pressure ( $< 10^{-4}$  torr) primary ion intensities of  $C_2H_4^+$ ,  $C_2H_3^+$  and  $C_2H_2^+$  are also indicated for comparison. In general, the product ion total intensities due to  $C_2H_4^+$  are too high up to pressures of about 0.7 torr. The assignment of ions to  $C_2H_3^+$  is too low at lower pressures until 0.6 torr, whence reasonable agreement is obtained. The sum of ions due to  $C_2H_2^+$  ranges from too low values at low pressures to a dramatic increase at higher pressures.

Increases in R.A. of product ions due to reactions of  $C_2H_4^+$  with ethylene could be due to an increased intensity of  $C_2H_4^+$  formed by charge transfer. Field<sup>28</sup> and Wexler and Marshall<sup>68</sup> have found that the charge transfer reaction



is important for producing  $C_2H_4^+$  in excess of that due to the primary ionization. From a comparison of total reaction cross section of  $C_2H_2^+$  with the partial reaction cross sections for formation of  $C_3H_3^+$  and  $C_4H_5^+$ , Wexler and





TABLE 5.2

Ion Product Balance for Selected Ethylene Pressures

(Repeller = 11V/cm)

Pressure (torr) $\times 10^{-4}$	0.06	0.22	0.36	0.70	0.80	1.0	
Initial Precursor Ion	R.A.'s of Assigned Products						
$C_2H_4^+$	39%	70%	59%	56%	48%	36%	32%
$C_2H_3^+$	25	16	17	19	22	24	23
$C_2H_2^+$	<u>24</u>	<u>12</u>	<u>14</u>	<u>16</u>	<u>18</u>	<u>28</u>	<u>29</u>
Total R.A.	88	88	90	91	88	88	84



Marshall estimated that  $2/3$  of the  $C_2H_2^+$  initially formed, charge exchanges with  $C_2H_4$ . Similar conclusions can be made from Field's<sup>28</sup> study of ethylene. If we (arbitrarily) assume that  $1/2$  of  $C_2H_2^+$  charge exchanges with ethylene, then up to about 0.3 torr this would correct almost completely the product ion assignments. Thus at 0.22 torr the sum of ions due to  $C_2H_4^+$  would be corrected to 45% of the total ionization and those due to  $C_2H_2^+$  would be changed to 28%. In fact, above 0.24 torr Wexler and Marshall found that the effect of charge exchange decreased and ion-molecule reactions of  $C_2H_2^+$  with  $C_2H_4$  could compete more favorably.

That charge transfer should compete less favorably with ion-molecule reactions with increasing pressure can be explained by the fact that the average primary ion energy will decrease with increasing pressure (at constant repeller field strength). The charge transfer cross section for an exothermic reaction should change little at low ion velocities while the ion molecule cross section is proportional to  $v^{-x}$ , where  $v$  is the ionic velocity and  $1 \leq x \leq 2$ . This would predict that the ion molecule reactions would compete effectively with charge transfer as pressure is increased due to the decreasing ion energy.

According to the assumed product assignments, the values for  $C_2H_3^+$  are too low at pressures below 0.6 torr. Charge transfer of  $C_2H_3^+$  with ethylene to yield  $C_2H_4^+$







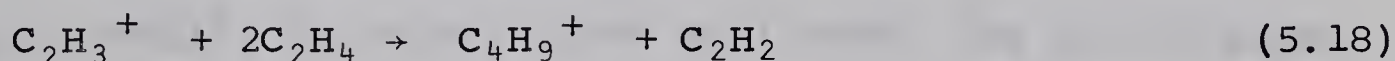
will probably not be important since the cross section for reaction (5.16) is only 1/12 of reaction (5.15) as measured by Szabo<sup>70</sup>. (The measurements by Szabo were done using primary 3 ev  $C_2H_2^+$  and 6 ev  $C_2H_3^+$  ions in a double mass spectrometer).

Another explanation for low product ion assignments of  $C_2H_3^+$  could be that the vinyl ion is reacting with ethylene<sup>to</sup> yield products partially ascribed to a  $C_2H_4^+$  precursor. One can write an exothermic termolecular reaction to yield  $C_5H_9^+$



$$\Delta H = -11 \text{ kcal/mole}^*$$

Now the major product ion ascribed to a  $C_2H_4^+$  reaction in this pressure range is  $C_5H_9^+$ . This reaction would have to compete with the reaction



$$\Delta H = -61 \text{ to } -85 \text{ kcal/mole}^\dagger$$

That reaction (5.18) is much more exothermal than reaction (5.17) may mean that higher pressures are required for  $C_4H_9^+$  to become stabilized and reaction (5.17) might be more efficient at somewhat lower pressures. There is however, no evidence from other sources for the occurrence of reaction (5.17).

---

\* Heats of formation of ions taken from the compilation in reference 48 unless otherwise noted.

† Depends on structure of  $C_4H_9^+$ .



C. Influence of external factors on the observed mass spectra.

External factors not related to the actual gaseous ionic reactions occurring in the ion source chamber might be effective. One possibility is that at higher pressures (where the puzzling increase of  $C_3H_3^+$ ,  $C_4H_5^+$  and  $C_5H_7^+$  occurs) the primary ionization spectra of ethylene is changing because of a change in proton beam energy. The stopping cross sections ( $\epsilon$ ) of ethylene to protons is almost constant at  $55 \times 10^{-15}$   $ev\text{-cm}^2/\text{molecule}$ <sup>71</sup> in the energy range 40 to 100 kev. From the equation

$$\epsilon \equiv \frac{dE}{dx} = n \frac{\Delta E}{\Delta x} \quad (5.19)$$

where  $n$  is molecules/cm<sup>3</sup>

$\frac{\Delta E}{\Delta x}$  is energy loss in ev/cm of path,

one can readily calculate that at 1 torr, the proton beam will be decreased in energy by about 7 kev, in the distance traversed from the ion source side of the beam entrance foil to the middle of the source exit slit (3.5 cm). From the previously measured primary 50 and 100 kev proton impact spectra and the spectra of Abbe\* extending to 20 kev, it can be noted that only small changes occur in the spectra from 100 to 20 kev. Since the measured primary ethylene spectra with the beam through foils is very similar to the previously measured proton spectra at 50 kev, (see Chapter 3) and from a consideration of energy loss through the first

\* J.-C Abbe, Private Communication





foil (Chapter 2, Sec. 2.6B), it is estimated that the primary ethylene ions formed at 1 torr could be due to 50 kev protons. Even if the beam energy was only 30 kev, no significant differences in the R.A.'s of primary ions formed initially would be expected.

Another effect to be considered is scattering and losses of ions in the analyzer tube due to increased pressures in that region. At about 0.7 torr in the ion source, pressure in the analyzer tube as measured by the ion gage is about  $5 \times 10^{-5}$  torr. There is no doubt that losses occur by charge transfer, collisional decomposition etc., but why the ions  $C_3H_3^+$ ,  $C_4H_5^+$ ,  $C_4H_9^+$  and  $C_5H_7^+$  would not be lost, while most of the others would be, seems strange and makes this idea untenable.

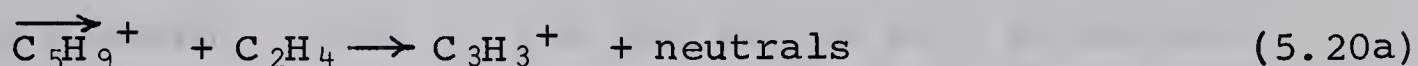
There is a possibility that part of the spectra observed are due to ion molecule reactions in the region between the ion source exit slit and the withdrawal slit. Since the distance between the bottom of the ion source and the withdrawal plate is only 1 mm, conduction of gas from this cylindrical volume of height 1 mm and diameter 3.2 cm would be very small. It is calculated, as shown in Appendix A, that one torr pressure in the ion source would correspond to 50 millitorr in the exit slit withdrawal slit region. Using





a collision cross section of  $75 \text{ \AA}^2/\text{molecule}$ , it is estimated that an ion will make at least one collision with a gas molecule in traversing this distance of 0.1 cm between exit slit and withdrawal slit.

The ion  $\text{C}_5\text{H}_9^+$  is one of the major ions that is decreasing due to further reaction, but for which no higher mass products are produced in appreciable amounts. Possibly it is reacting in a stripping type of mechanism as in reactions (5.20) to yield lower mass ions

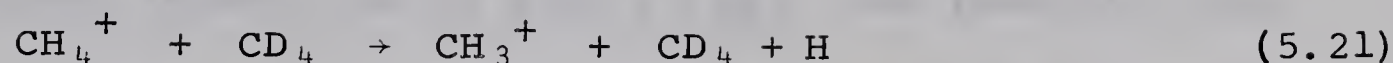


These reactions are quite endothermic but  $\text{C}_5\text{H}_9^+$  would experience large acceleration between the exit and withdrawal slits due to the negative (with respect to the ion chamber) drawout potential.

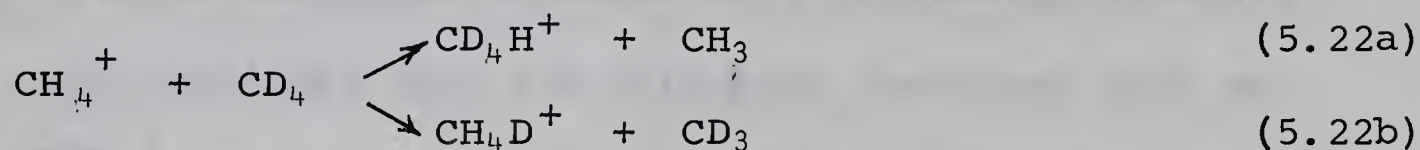
Futrell and Abramson have found<sup>72</sup> that endothermic reactions which did not occur at low energies could be made to occur by increasing the reactant ion energy to several ev. This demonstrates that translational energy can be converted into vibrational energy allowing the reaction to be essentially thermoneutral. These workers also found, using their double mass spectrometer, that collisionally induced decomposition of the impacting ion within the ion source becomes quite prominent as impacting ion energy is increased



They found that the reaction



which is absent at ion energy 0.5 ev, becomes much more prominent at 8 ev than the reactions



They suggest that such dissociation reactions could be quite general for polyatomic ions of several ev kinetic energy.

We think therefore, that reactions such as (5.20) could quite plausibly occur in the ion source exit withdrawal region due to the good probability for collision of these highly accelerated ions with molecules at the higher pressures (above 0.6 torr) studied. We can conclude that the sharp increase at pressures above 0.7 torr, of the intensities of especially  $\text{C}_3\text{H}_3^+$ , and probably also  $\text{C}_4\text{H}_5^+$  and  $\text{C}_5\text{H}_7^+$  are due to stripping type reactions such as reaction (5.20) occurring in the ion source exit withdrawal region of the mass spectrometer.

## 5.5 Conclusions

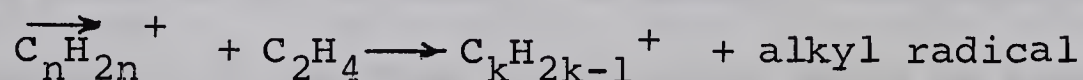
Comparison of our 1 torr mass spectra of ethylene with that of Kebarle and co-workers<sup>69</sup> at 2 torr measured with the alpha particle mass spectrometer show an apparent discrepancy between the results. Their results at a millisecond ion reaction time would indicate that our results at shorter (a microsecond) reaction times should show







prominent intensities of  $C_4H_8^+$ ,  $C_6H_{12}^+$  and possibly  $C_8H_{16}^+$ . These ions are of minor abundance in the proton beam mass spectra and in fact the sum of the total intensities of the  $C_nH_{2n}^+$  series decreases somewhat with increasing pressure. This could indicate that ion stripping reactions such as



occurring in the ion source exit withdrawal region break up the  $C_nH_{2n}^+$  ions.

Kebarle and co-workers did not observe the lower homologues such as  $C_4H_8^+$ ,  $C_6H_{12}^+$  and  $C_8H_{16}^+$  in pure ethylene at 2 torr. However using low concentrations (0.1%) of ethylene in 20 torr xenon these ions were observed, due to the collisional deactivation of the initially excited ionic species by the great excess of xenon. This could mean that the higher mass homologues such as  $C_{10}H_{20}^+$  in their pure ethylene spectra are not necessarily formed by a simple polymerization process starting with  $C_4H_8^+$ , but rather are formed by some other process.

The more prominent series of product ions in ethylene at pressures above 0.5 torr observed by Wexler<sup>62</sup> are very different than in the present results. At the moment there is no apparent explanation. The dissimilarity between the sets of results considered here, shows that caution must be taken in order that instrumental and other external factors do not obscure the true gaseous ionic chemistry occurring.



## 5.6 Suggestions for further research

A study to see if ion-molecule reactions of the stripping or collisional decomposition type are occurring in the region between ion source exit slit and withdrawal slit would seem to be in order. A design incorporating good conductance of gas from this region would be useful and studies to show the influence of the ion draw-out potential should be carried out. After these matters were resolved, studies at even higher pressures would be potentially interesting.





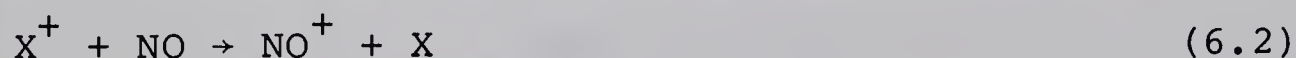
## 6. GASEOUS IONIC REACTIONS IN ETHYLENE-NITRIC OXIDE MIXTURES

### 6.1 Introduction

Nitric oxide is a well known free radical scavenger used originally in systems where free radicals were generated by pyrolysis or photolysis. More recently it has been used in radiolytic systems. It was thought that its presence would inhibit free radical attack on the substrate molecules and allow a distinction to be made between radical and ionic reactions. However, because of its low ionization potential, nitric oxide may also be involved in charge removal from the ionic species. That is, in addition to the radical scavenging reaction (6.1),



the charge transfer reaction



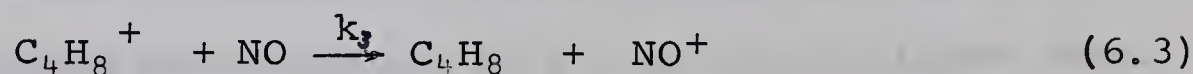
might also be occurring. The likelihood that free radical scavengers of low ionization potential (e.g. nitric oxide, iodine) may also get involved in the ionic mechanism was pointed out by several authors.<sup>30, 73, 74</sup> Studies of the ethylene-NO system with an intention of determining the effect of NO on the ionic mechanism were undertaken independently by Meisels<sup>74</sup> and Kebarle<sup>69</sup>. In studying the radiolytic neutral product yields, Meisels<sup>74</sup> observed that the addition of a few per cent of NO increased the yield of butenes. The increase levelled off at 10% NO where the products were in the ratio of 2-butene : 1-butene as 5:1. The G value\*

\*Molecules produced per 100 ev absorbed in ethylene.

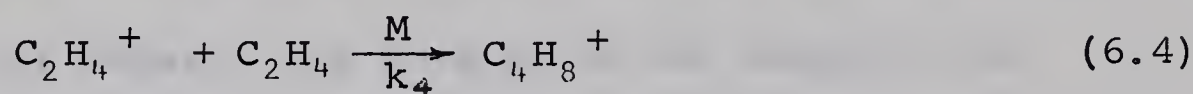




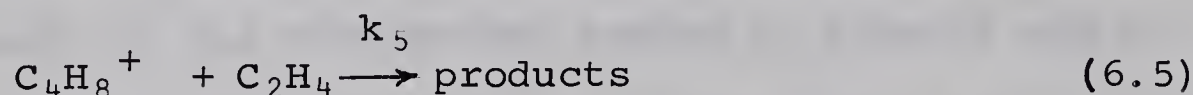
for the butene increase (at saturation) was found to be nearly equal to the G value for the formation of  $C_2H_4^+$  by the ionizing radiation. Meisels concluded that the butenes were formed by the charge exchange reaction (6.3), with



the  $C_4H_8^+$  being formed by addition of  $C_2H_4^+$  to ethylene (see Chapter 5):



$C_2H_4^+$  can also charge exchange with NO as has been shown by Field and Munson.<sup>75</sup> In order to explain why charge exchange occurred with  $C_4H_8^+$ , but not with  $C_2H_4^+$ , Meisels assumed that the rate constant  $k_4$  is very much larger than the rate constants  $k_5$  for the reaction of  $C_4H_8^+$  with ethylene reaction (6.5) :



Thus at 10% NO,  $C_2H_4^+$  disappears by a fast reaction with ethylene, but the NO is able to intercept all the  $C_4H_8^+$ , which is slow to react with ethylene. Kebarle and co-workers<sup>69</sup>, in their study of the ions in pure ethylene with the alpha particle mass spectrometer, determined that  $k_4 \approx 400 k_5$ , thus confirming the suggestion by Meisels.

In a separate study, Kebarle and Searles<sup>76</sup> using both the Cermak technique<sup>77</sup> and the internal ionization method, found that the charge exchange reaction of NO with  $C_2H_4^+$  and  $1-C_4H_8^+$  occurs with a rate constants of similar magnitude. Furthermore, these rate constants were close to the magnitude of  $k_4$ .





The 2-butene ions, however, were found not to charge exchange with NO. In fact  $\text{NO}^+$  was found to charge exchange with cis 2-butene. This latter charge transfer reaction is energetically permitted, whereas the opposite (from 2-  $\text{C}_4\text{H}_8^+$  to NO) is not, because the ionization potential (I.P.) of NO is higher than the I.P. of cis (or trans) 2-butene.\* Since the majority of the butene yields in Meisels' experiments were of 2-butenes, these results of Kebarle and Searles do not support the findings that the 2-butenes observed by Meisels were due to reaction (6.3). However the butene ions formed by reaction (6.4) are vibrationally excited. Some of this excitation might be retained until collisions with NO occur. Charge transfer under such conditions might occur also from 2- $\text{C}_4\text{H}_8^+$ .

A study of the ethylene-NO system by Kebarle and co-workers,<sup>69</sup> with the alpha particle mass spectrometer, showed that the addition of only trace amounts of NO (0.1%), to 20 torr ethylene, caused a large change in the observed ionic composition compared to that in pure ethylene. The results obtained by these authors are shown in Fig. 6.1. Comparing these results with those obtained under identical conditions but in the absence of NO, Kebarle et al. concluded that NO must be attaching to the unpaired electron of olefinic ions like  $\text{C}_4\text{H}_8^+$  and  $\text{C}_6\text{H}_{12}^+$  (and in general  $\text{C}_n\text{H}_{2n}^+$ ).

---

\* I.P. (NO) = 9.25 ev, I.P. (2-butene) = 9.13 ev as determined by K. Watanabe, T. Nakayama, J. Mottl, J. Quant. Spect. Radiative Transfer 2, 369 (1962).



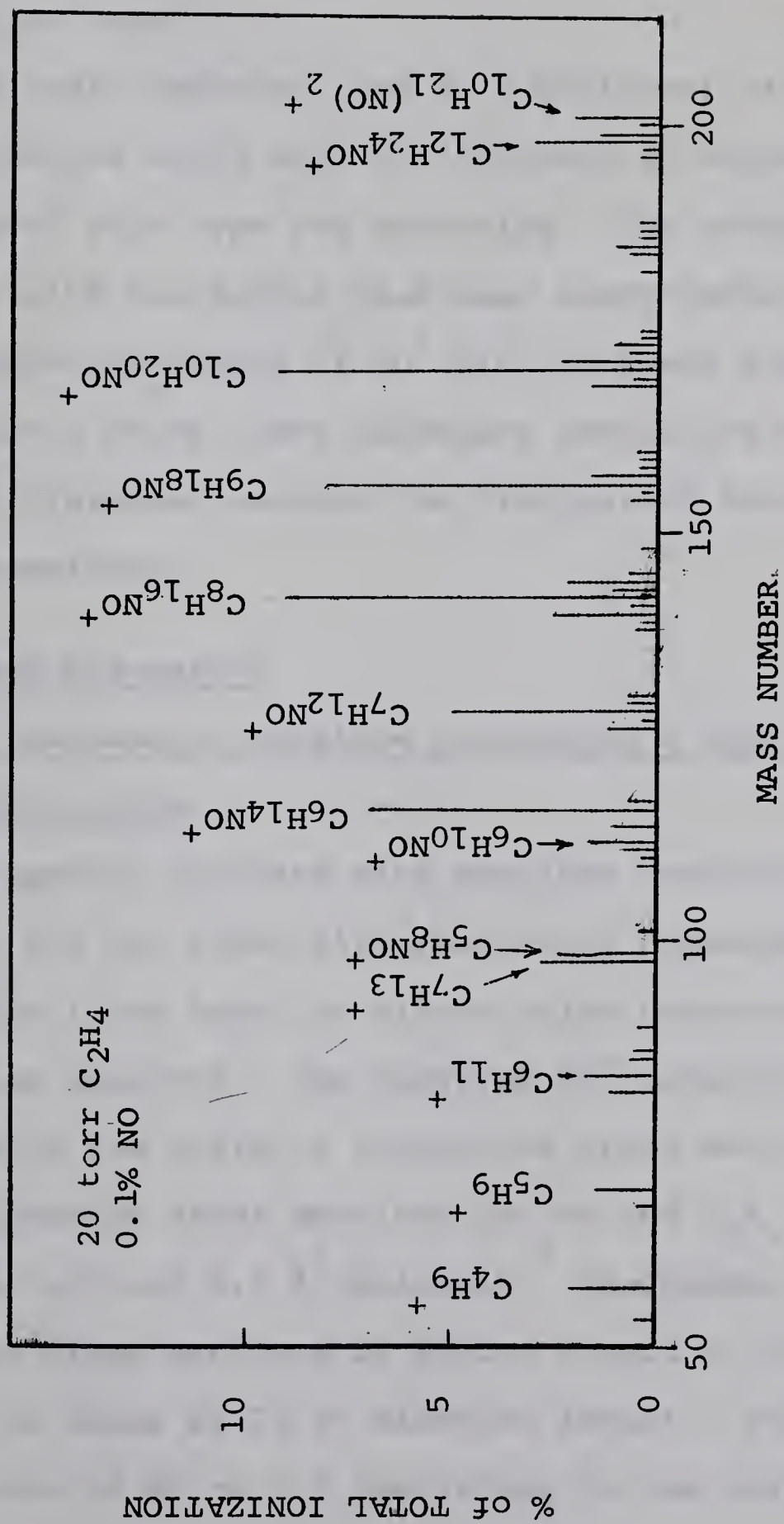


Increase of the concentration of NO to 10% did not change the spectra very significantly. The main effect was an increase of the  $C_4H_8NO^+$  ion to a relative intensity similar to that of the other major ions i.e.  $C_6H_{14}NO^+$ ,  $C_7H_{14}NO^+$ ,  $C_8H_{16}NO^+$ . The total ionization was found essentially unaffected by NO and no  $NO^+$  was observed.

FIGURE 6.1

Mass Spectrum of 20 torr Ethylene with 0.1% NO

Results of Kebarle and co-workers<sup>69</sup> obtained  
with the alpha particle mass spectrometer.





It is not impossible to reconcile these results with Meisels' observations. Thus at 10% NO, charge exchange of NO might be occurring from  $C_4H_8^+$  by reaction (6.3). The resulting  $NO^+$  might be rapidly reacting with ethylene to produce ions like  $C_2H_4NO^+$ ,  $C_6H_{12}NO^+$  etc.

The long ionic reaction time ( $\sim 1$  millisec) of the alpha particle ion source would make it difficult to establish whether  $NO^+$  reactions of this type are occurring. The purpose of the present study with the proton beam mass spectrometer was to establish whether reactions of  $NO^+$  with ethylene occur. It was also hoped that a study under different conditions might help explain the differences between the findings of Meisels and those of Kebarle and coworkers.

## 6.2 Results and Discussion

### A. Ionic reactions in ethylene containing a high concentration of nitric oxide.

The mass spectra obtained with ethylene containing 21% NO are shown in Fig. 6.2 for three different total pressures. At the lowest pressure (0.08 torr) no nitric oxide containing hydrocarbon ions are observed. The observed  $NO^+$  intensity is larger than expected on the basis of ionization cross sections. Thus the total ionization cross sections for NO and  $C_2H_4$  by 70 volt electrons are 3.05 and  $6.6 \times 10^{-18}$  Å<sup>2</sup>/molecule.<sup>78</sup> In Chapter 3, it was found that the cross sections by proton impact of 50-100 kev are proportional to those by 70 ev electron impact. Thus we may expect the ratio of NO to  $C_2H_4$  ionization in the present experi-

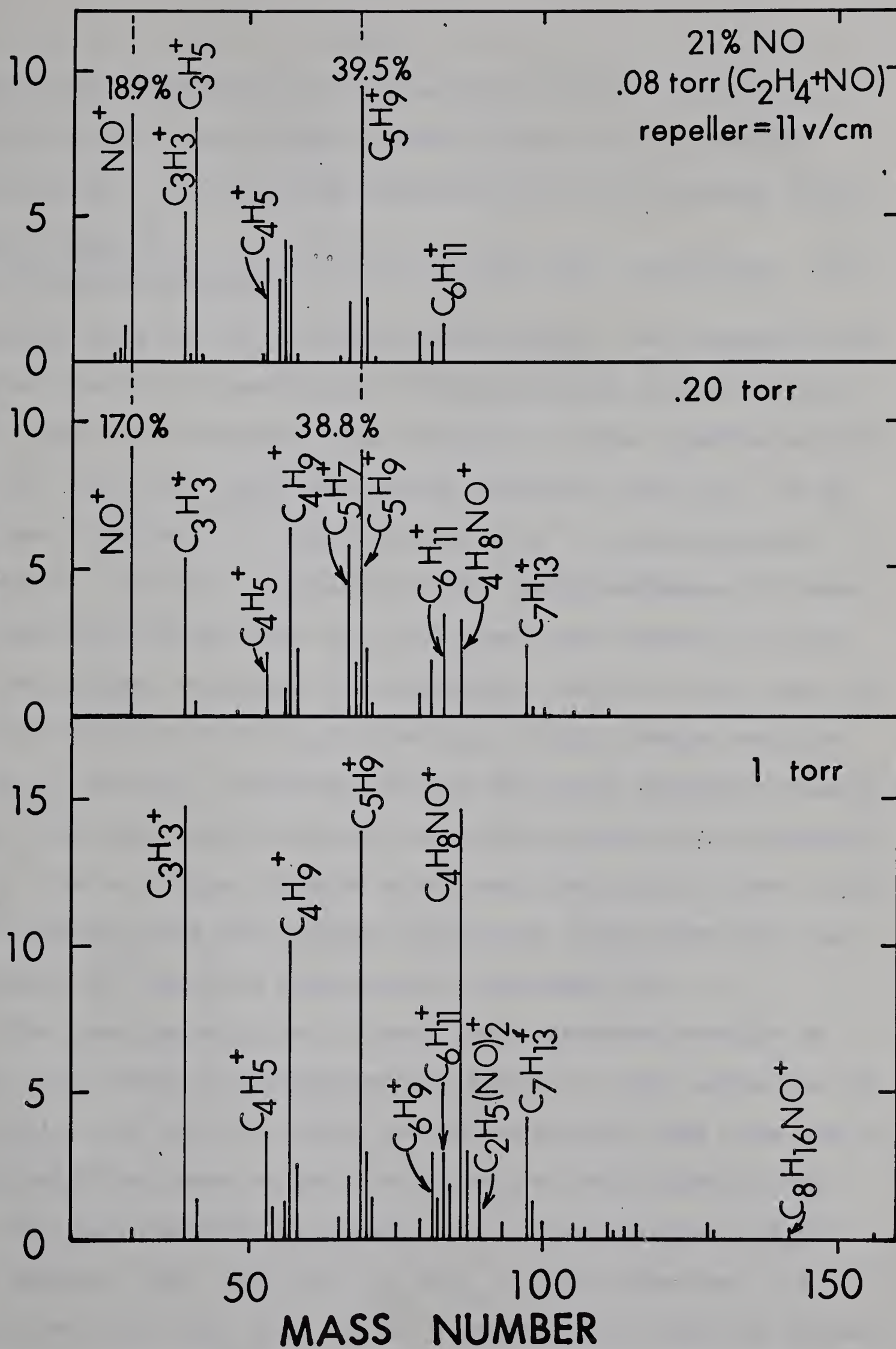


FIGURE 6.2

Mass Spectra of 21% NO - Ethylene Mixtures

Results obtained with the proton beam mass spectrometer.

# % OF TOTAL IONIZATION





ments to be proportional to the electron impact ionization cross sections and relative concentrations of ethylene and nitric oxide. For 21% NO we calculate the  $\text{NO}^+$  intensity to be

$$\frac{(100)(0.21)(3.05)}{(0.21)(3.05) + (0.79)(6.6)} = 10.9\% \text{ of the total ionization.}$$

The observed value of 19% is almost twice larger. We conclude that some of the  $\text{NO}^+$  is produced by charge exchange from ethylenic ions. The major ethylene ions involved in this reaction should be  $\text{C}_2\text{H}_4^+$  and  $\text{C}_2\text{H}_2^+$  since the charge transfer from  $\text{C}_2\text{H}_4^+$  to NO has been observed<sup>75, 76</sup> and that from  $\text{C}_2\text{H}_2^+$  is energetically favorable. If it is assumed that the charge exchange of these two ions with NO proceeds with the same rate constant as that for the further reactions with ethylene (see sec. 6.1), one calculates that 21% of the  $\text{C}_2\text{H}_4^+$  and  $\text{C}_2\text{H}_2^+$  would charge exchange. The  $\text{C}_2\text{H}_2^+$  and  $\text{C}_2\text{H}_4^+$  represent 64% of the total ethylene ionization. Thus, since the total ethylene ionization is 89%, the intensity of  $\text{NO}^+$  due to charge transfer would be:  $0.64 \times 0.21 \times 89\% = 12\%$ . This combined with the primary ionization of NO gives 23% for the total  $\text{NO}^+$  which is close to the observed 19%.

The mass spectrum at 0.2 torr total pressure and 21% NO (Fig. 6.2), shows the presence of  $\text{C}_4\text{H}_8\text{NO}^+$  at 33%, while the  $\text{NO}^+$  has fallen off to 17%. These two NO-containing ions thus add to 20.3% which is close to the 19% NO in the lower pressure run.

The mass spectrum at 1 torr total pressure shows  $\text{C}_4\text{H}_8\text{NO}^+$  as a dominant ion. The ion  $\text{C}_2\text{H}_5(\text{NO})_2^+$  is also observed. It should be noted that this was an intense ion (at high NO concentrations) also in the alpha particle mass spectra of Kebarle et al.<sup>69</sup>





The combined intensity of the NO containing ions is 18%, again in fair agreement with the NO intensities of the previous runs. The  $\text{NO}^+$  ion is almost absent (0.5%). Thus  $\text{NO}^+$  reacts with ethylene and the main final product of the reaction under the present conditions is  $\text{C}_4\text{H}_8\text{NO}^+$ .

The intensity decrease of the  $\text{NO}^+$  ion in these three pressure runs can be used for a rough estimate of the rate constant  $k$  and order  $n$  of the  $\text{NO}^+$  reaction with ethylene. The rate of disappearance of  $\text{NO}^+$  is given by

$$\frac{d[\text{NO}^+]}{dt} = -k[\text{C}_2\text{H}_4]^n[\text{NO}^+] \quad (6.6)$$

Upon integrating Eq. (6.6) and taking logarithms of the integrated equation we obtain

$$\log \frac{[\text{NO}^+]}{[\text{NO}^+]_0} = \log \frac{I_{\text{NO}^+}}{I_{\text{NO}^+}_0} = -k[\text{C}_2\text{H}_4]^n t \quad (6.7)$$

where  $I_{\text{NO}^+}$  is the observed  $\text{NO}^+$  intensity,  $[\text{C}_2\text{H}_4]$  is the ethylene concentration in molecules/cc, and  $t$  is the residence time (sec) of the  $\text{NO}^+$  in the ion source. A plot of  $\log I_{\text{NO}^+}$  versus the square of the ethylene pressure gave a good straight line, indicating a second-order dependence for the disappearance of  $\text{NO}^+$  by reaction with ethylene. The termolecular rate constant  $k$  can be evaluated from the slope of  $\log I_{\text{NO}^+}$  vs.  $[\text{C}_2\text{H}_4]^2$ , since slope =  $-kt$ . The residence time of  $\text{NO}^+$  in the ion source can be calculated from the standard expression

$$t = \left( \frac{2 \ell m_i}{e E_r} \right)^{1/2} \quad (6.8)$$



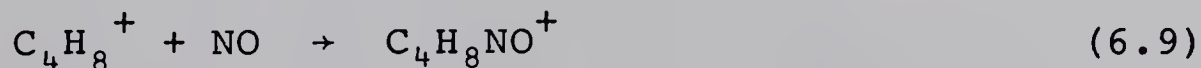
where  $\ell = 0.4$  cm,  $m_1$  is the mass of  $\text{NO}^+$ ,  $e$  is the charge of the electron and  $E_r$  is the repeller field strength.

The value of the termolecular rate constant obtained was  $k = 4 \times 10^{-27} \text{ cc}^2/\text{molecule}^2 \text{ -sec}$ , which agrees in magnitude with other termolecular rate constants found in ion-molecule reactions.<sup>28</sup>

The second order dependence found could be partly explained as follows. The addition of  $\text{NO}^+$  to  $\text{C}_2\text{H}_4$  to form  $[\text{C}_2\text{H}_4\text{NO}^+]$  is exothermic. The excess energy could be removed by a second collision with ethylene. The stabilized  $\text{C}_2\text{H}_4\text{NO}^+$  might then react with ethylene to form the observed product  $\text{C}_4\text{H}_8\text{NO}^+$ .

#### B. NO-ethylene mixtures at low (1% and 4%) NO concentration

The mass spectra of 1% and 4% NO in ethylene at about 1 torr ion source pressure are presented in Fig. 6.3. No  $\text{NO}^+$  is observed, but the NO containing ions (mainly  $\text{C}_4\text{H}_8\text{NO}^+$  and also  $\text{C}_2\text{H}_5(\text{NO})_2^+$ ) account for more than the primary  $\text{NO}^+$  ionization, even if  $\text{NO}^+$  is also initially produced by charge transfer from ethylene ions and all  $\text{NO}^+$  reacts completely with ethylene. This can be taken to mean that NO enters the charged state via ethylene ions, i.e. ions from ethylene react with NO to yield  $\text{C}_4\text{H}_8\text{NO}^+$  and the other NO-containing ions. If the NO is intercepted on the  $\text{C}_4\text{H}_8^+$  level as in reaction (6.9)



a high concentration of  $\text{C}_4\text{H}_8\text{NO}^+$  would probably not be expected to be observed at low NO concentration, unless the reaction of  $\text{C}_4\text{H}_8^+$  with ethylene [reaction (6.5)] is very much slower.

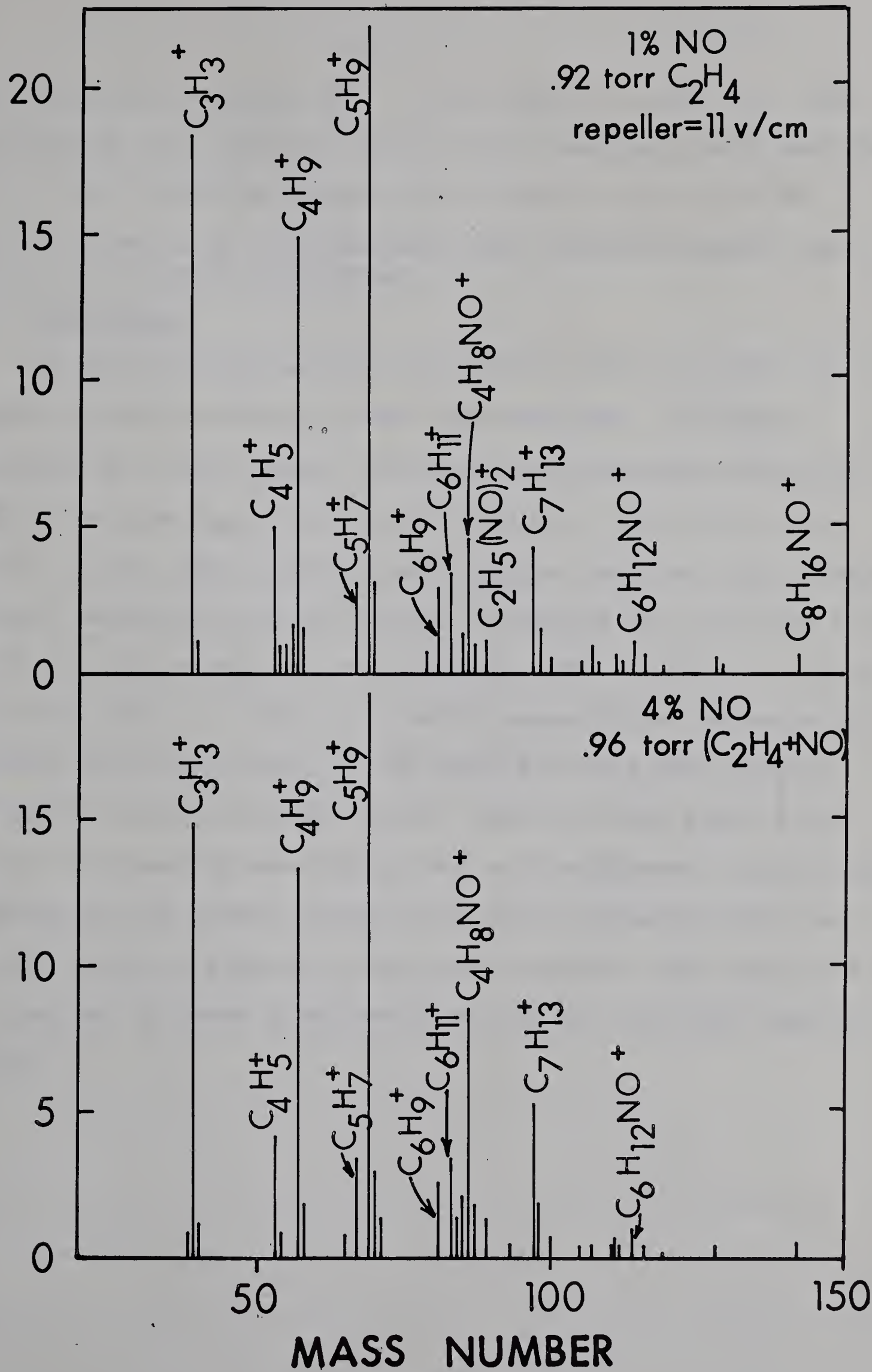
Another possibility is that the  $\text{C}_4\text{H}_8^+$  charge exchanges,

FIGURE 6.3

Mass Spectra of Ethylene - NO Mixtures at Low Concentration  
of Nitric Oxide



# % OF TOTAL IONIZATION







reaction (6.3), to yield  $\text{NO}^+$ . It was shown in Sec. 6.1 that the reaction (6.3) should compete very effectively with reaction (6.5). The  $\text{C}_4\text{H}_8\text{NO}^+$  we observe could then be due to the  $\text{NO}^+$  created by reaction (6.3) reacting with ethylene. However the nature of the  $\text{C}_4\text{H}_8^+$  is not known.

### (6.3) Conclusions

It can be concluded that ions of the type  $\text{C}_n\text{H}_{2n}\text{NO}^+$  are produced by the reactions of  $\text{NO}^+$  with ethylene. At higher pressures as in the results of Kebarle and coworkers ethylenic ions of the type  $\text{C}_n\text{H}_{2n}^+$  also react with NO. Both the complex results of the alpha particle mass spectra and the simple charge transfer mechanism used by Meisels to explain the increased butene yields are not necessarily at variance. The increase of  $\text{C}_4\text{H}_8\text{NO}^+$  intensity (which is absent at low NO concentration) observed with increasing NO concentration in the alpha particle mass spectra indicates, as shown by our results, that at least part of the  $\text{C}_4\text{H}_8\text{NO}^+$  is formed by reaction of  $\text{NO}^+$  with ethylene. By this type of mechanism the butene yields could still increase with the addition of NO to ethylene even though complex ionic reactions are observed in these experiments and the 20 torr mass spectral studies.



## 7. ION-SOLVENT MOLECULE INTERACTIONS IN THE GAS PHASE

### 7.0 General Introduction

#### A. Previous Work

The study of ion-solvent molecule interactions in solution dates back to the beginnings of physical chemistry, and is still an active field of chemical research. The mass spectrometric study of ion-solvent molecule interactions in the gas phase is only a few years old, and yet some significant results have already been obtained.<sup>79-81</sup>

Ionic reactions of polar (solvent) molecules in the gas phase contrast with those of hydrocarbons. With ethylene, for example, we have seen that a wide variety of complex ionic polymers are formed (Chapter 5). In water and ammonia it has been found that the ionic polymerization does not proceed by covalent bond formation, but, because of high dipole moment and high polarizability of the molecules involved, "physical polymerization" or clustering occurs. It might be reasonably expected that, at sufficiently high pressures, clustering would be a dominant mechanism for the gas phase ionic reactions of all polar molecules.

Historically, the ability of gas phase ions to form relatively stable clusters was recognized early.<sup>82, 83</sup> However, direct experimental evidence was very scanty and was based on anomalous ionic gas phase mobilities.<sup>84</sup> It is only recently that the direct evidence for formation of gas phase ion clusters have been given.<sup>85</sup>







Apart from clustering around an ion from the parent solvent molecule, solvation of various types of ions e.g. negative, organic and metal ions by polar solvent molecules has been shown recently to be amenable to study by mass spectrometric methods.<sup>81, 86</sup> Heats of monohydration of lithium, sodium and potassium ions have been recently evaluated in the mass spectrometry of flames.<sup>87</sup> Competitive inner- and outer-shell solvation of  $\text{NH}_4^+$  by water and ammonia molecules in the gas phase has been studied by Kebarle and co-workers<sup>81</sup> at pressures from 1 to 200 torr. They found that ammonia preferentially fills an inner shell of  $(\text{NH}_3)_4 \cdot \text{NH}_4^+$  whence water is then taken up in the outer shell.

Munson<sup>88, 89</sup> has shown that solvated protons ie. the neutral molecules clustered around a proton or protonated molecule ion, are the main products of ionic reactions in some gaseous Bronsted acids (water, methanol, formic acid, acetaldehyde and acetone) and in some amines. Munson's studies were done in a conventional electron impact mass spectrometer at pressures up to about 0.4 torr at 200°C.

## B. Present research

The first part of our study of gas phase ion-solvent molecule reactions was an examination of the hydration of  $\text{H}_3\text{O}^+$ .

The second part involves a study of competitive solvation in water-methanol mixtures.

## PART I THE SYSTEM $(\text{H}_2\text{O})_n \cdot \text{H}_3\text{O}^+$

### 7.1 Introduction

In water at higher pressures the only product ions formed are hydrates of  $\text{H}_3\text{O}^+$ . The hydronium ion, first observed<sup>90</sup> in 1940



in the mass spectrum of water vapor, is rapidly solvated by water molecules as the pressure of water vapor is increased. For example, Beckey<sup>91</sup> has observed hydrates of  $H_3O^+$  up to  $n=9$  in a field emission mass spectrometer. In discharges of water vapor at 0.4 torr Tickner and Knewstubb<sup>92</sup> observed hydrates of  $H_3O^+$  up to  $n=5$ . Using the high pressure alpha - particle mass spectrometer, Kebarle and co-workers<sup>79</sup> have observed hydrates up to  $n=8$  and higher, depending on the pressure studied.

Assuming equilibrium conditions, free energies of individual solvation or hydration steps can be measured. By varying the temperature, enthalpies and entropies of these individual steps can be obtained. The measurements have been done for the solvation of the hydronium ion by water<sup>86</sup> and for the solvation of the ammonium ion by ammonia<sup>81</sup>

Now, the central assumption of the treatment by Kebarle and co-workers was that equilibrium with regard to clustering is achieved in the ion source. The average reaction time in the alpha-particle mass spectrometer was about a millisecond. It was thought that if the same equilibrium constants could be calculated from the data obtained with the present (proton beam) instrument, whose reaction time is about a microsecond, strong support will be lent to the equilibrium assumption. Furthermore, if duplication of the data could be obtained with such different ionic reaction times, then it would be possible to show that an equilibrium is achieved rather quickly.





## 7.2 The Higher Pressure Mass Spectrum of Water Vapor

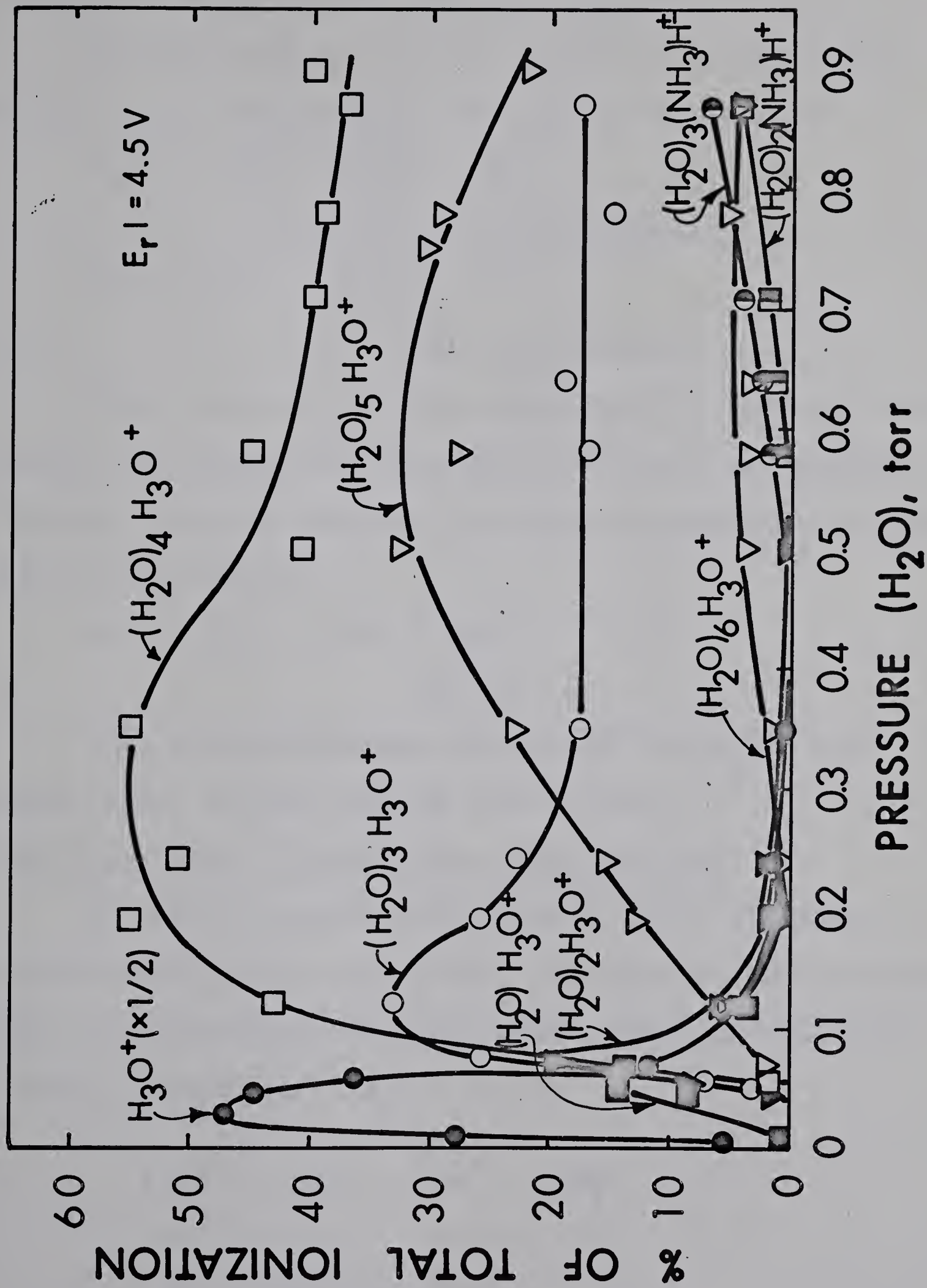
The higher pressure mass spectrum of water vapor was studied at pressures up to 1 torr. The results are presented in Fig. 7.1. At the highest pressures studied, up to seven water molecules hydrated around  $\text{H}_3\text{O}^+$  were found. As indicated by previous studies, essentially the only ionic products are hydrated protons or solvated hydronium ions of formula  $(\text{H}_2\text{O})_n \cdot \text{H}_3\text{O}^+$ . It can be readily seen that the various hydrates are formed by a series of consecutive reactions. Thus the  $\text{H}_2\text{O} \cdot \text{H}_3\text{O}^+$  and  $(\text{H}_2\text{O})_2 \text{H}_3\text{O}^+$  ions are not observed in high R.A. Probably they react rapidly to form higher hydrates. The hydrate  $(\text{H}_2\text{O})_3 \text{H}_3\text{O}^+$  shows a somewhat different behaviour than the other ions, since after reaching a maximum, its R.A. decreases only very slowly with increasing pressure. The hydrate  $(\text{H}_2\text{O})_3 \text{H}_3\text{O}^+$  is the dominant ion at all pressures above 0.1 torr.

The ions indicated as  $(\text{H}_2\text{O})_2 (\text{NH}_3) \text{H}^+$ ,  $m/e = 54$ , and  $(\text{H}_2\text{O})_3 (\text{NH}_3) \text{H}^+$ ,  $m/e = 72$ , were tentatively identified using  $\text{D}_2\text{O}$ . Now in the studies with  $\text{H}_2\text{O}$  at higher pressures small peaks at one mass lower than  $\text{H}_2\text{O} \cdot \text{H}_3\text{O}^+$ ,  $(\text{H}_2\text{O})_2 \text{H}_3\text{O}^+$ ,  $(\text{H}_2\text{O})_3 \text{H}_3\text{O}^+$  and  $(\text{H}_2\text{O})_4 \text{H}_3\text{O}^+$  were found. However using  $\text{D}_2\text{O}$ , these peaks (at one mass lower than the hydrates) had all disappeared. Since the deuterated ammonia hydrates,  $(\text{D}_2\text{O})_n (\text{ND}_3) \text{D}^+$ , have the same mass as  $(\text{D}_2\text{O})_n \cdot \text{D}_3\text{O}^+$ , it may be concluded that the identification of these impurity ions as hydrated ammonium ions is correct. In a study of hydration in "pure water" vapor<sup>93</sup> these ammoniated ions have been previously observed and were shown to be due to an ammonia impurity of very low concentration. The origin of the ammonia in our experiments is unknown. We will



FIGURE 7.1

Intensities of Hydrate Ions in Water Vapor at Pressures  
up to 1 Torr.





confine our discussion to the pure water hydrates.

### 7.3 Reactions of the Primary Ions, $\text{H}_2\text{O}^+$ and $\text{OH}^+$

The main primary ions ( $\text{H}_2\text{O}^+$  and  $\text{OH}^+$ ) can readily form hydronium ions by the exothermic reactions (7.1) and (7.2)



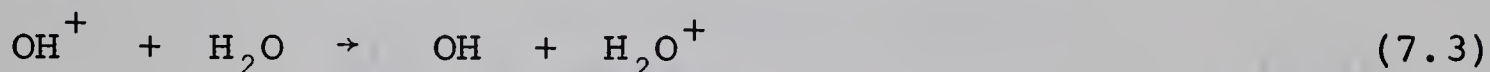
$$\Delta H = -12 \text{ kcal/mole}^{94}$$



$$\Delta H = -35 \text{ kcal/mole}^{94}$$

These reactions are well established<sup>90, 94, 95</sup> and are both found<sup>94</sup> to proceed with thermal rate constants  $k \approx 5 \times 10^{-10}$  cc/molecule - sec.

The hydroxyl ion could also react with water by exothermic charge transfer in the reaction

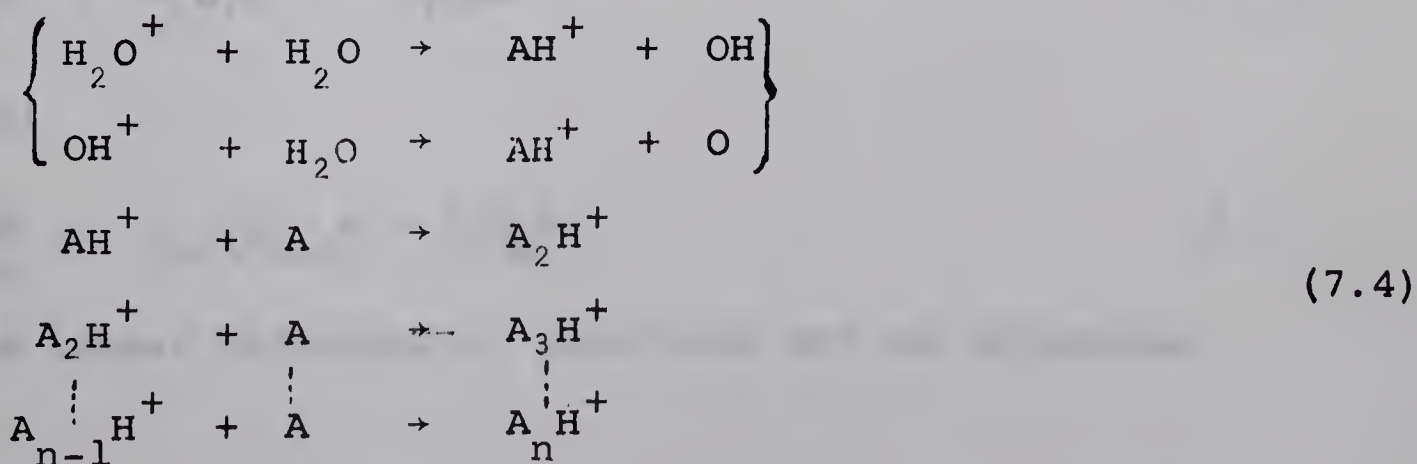


$$\Delta E = -0.2 \text{ ev}$$

Thus both primary ions of water ( $\text{OH}^+$  and  $\text{H}_2\text{O}^+$ ) will ultimately react to yield hydrated ions of water.

### 7.4 The "Beam Model" of Consecutive Hydration Steps

In order to discuss the results of Fig. 7.1 somewhat more quantitatively, we can assume that the hydration steps proceed initially by the following reaction scheme, where the notation A for a water molecule ( $\text{AH}^+ \equiv \text{H}_3\text{O}^+$ ) is used







It is assumed that the hydration proceeds by a consecutive bimolecular mechanism with cooling by third-body stabilization, and back reaction neglected. The ion intensities at the ion source exit slit are set equal to  $I_n$ .

The variations of the different ion intensities due to Reactions (7.4) at various pressures can be described by an extension of the "beam model" used by Wexler.<sup>29</sup> Primary ions formed in the plane of the ionizing beam will be attenuated by further reactions with molecules as the ions proceed toward the exit slit under the influence of the repeller field. The rate of loss of the primary ions,  $\text{OH}^+$  and  $\text{H}_2\text{O}^+$ , with respect to distance  $x(\text{cm})$  towards the ion source exit slit is

$$\frac{dI_1}{dx} = -Q_1 A I_1 \quad (7.5)$$

where  $Q_1$  is the phenomenological cross section for reaction of the primary ions with water molecules ( $\text{cm}^2/\text{molecule}$ ) and  $A$  is the concentration of water ( $\text{molecules/cc}$ ). The change of intensity of a product ion species at any position  $x$  between point of origin of its precursor and the exit is a balance between its formation and further reaction. For example, the change of intensity of  $I_2$  ( $\text{AH}^+$ ) with respect to  $x$  is given by

$$\frac{dI_2}{dx} = I_1 Q_1 A - I_2 Q_2 A \quad (7.6)$$

and in general

$$\frac{dI_n}{dx} = I_{n-1} Q_{n-1} A - I_n Q_n A \quad (7.7)$$

The linear differential equations may be integrated



between the limits  $x=0$  to  $x=\ell$ , ie. from the proton beam plane to the exit slit plane, to yield equations for the various (relative) ion intensities at the exit slit. The ion intensities at the exit slit will then be assumed proportional to those detected after mass analysis. The system of equations (Eq. 7.8) is given below

$$I_1 = I_1^0 e^{-Q_1 A \ell}$$

$$AH^+ \equiv I_2 = I_1^0 \frac{Q_1}{Q_2 - Q_1} \left( e^{-Q_1 A \ell} - e^{-Q_2 A \ell} \right)$$

$$A_2H^+ \equiv I_3 = I_1^0 Q_1 Q_2 \left[ \frac{e^{-Q_1 A \ell}}{(Q_2 - Q_1)(Q_3 - Q_1)} + \frac{e^{-Q_2 A \ell}}{(Q_1 - Q_2)(Q_3 - Q_2)} + \frac{e^{-Q_3 A \ell}}{(Q_1 - Q_3)(Q_2 - Q_3)} \right]$$

$$\vdots$$

$$A_{n-1}H^+ \equiv I_n = I_1^0 Q_1 Q_2 \dots Q_{n-1} \left[ \frac{e^{-Q_1 A \ell}}{(Q_2 - Q_1)(Q_3 - Q_1) \dots (Q_n - Q_1)} \right.$$

Eq. (7.8)

$$+ \frac{e^{-Q_2 A \ell}}{(Q_1 - Q_2)(Q_3 - Q_2) \dots (Q_n - Q_2)}.$$

$$+ \dots + \frac{e^{-Q_n A \ell}}{(Q_1 - Q_n)(Q_2 - Q_n) \dots (Q_{n-1} - Q_n)} \Bigg]$$

where  $I_1^0$  is the initial primary ion concentration in the plane of the proton beam.





The equations express the absolute intensities of the various ions but they can be normalized by setting  $I_1^0 = 1$  (ie. total primary ionization at the proton beam = 1) whence fractional intensities of the total ionization will be obtained.

The various I's can be calculated as a function of pressure using different trial cross section values so as to obtain a best fit with experimental results. Figure 7.2 shows calculated relative intensities as a function of water pressure. The cross sections used were:  $Q_1 = 100 \text{ Å}^2$ ,  $Q_2 = 10 \text{ Å}^2$ ,  $Q_3 = 50 \text{ Å}^2$ ,  $Q_4 = 35 \text{ Å}^2$ ,  $Q_5 = 15 \text{ Å}^2$  and  $Q_6 = 3 \text{ Å}^2$ , and  $\lambda = 0.4 \text{ cm}$ . The fit of the experimental results is reasonable up to 0.15 torr. We feel that even closer fits could be obtained with enough successive variations of the Q's involved. However the object of these calculations was not to obtain exact cross sections but rather to see if our assumed scheme of successive reactions fit the observed results. Up to about 0.15 torr the assumed reaction scheme is probably correct.

The values of the reaction cross sections used to calculate the plots are interesting, since they demonstrate more quantitatively what could be said qualitatively about the pressure dependences of the ions up to about 0.2 torr. The primary ions react very fast ( $Q_1 = 100 \text{ Å}^2$ ) to yield  $\text{H}_3\text{O}^+$  since they disappear very rapidly at very low pressures. The hydronium ion reacts more slowly ( $Q_2 = 10 \text{ Å}^2$ ) since at its maximum at 25 millitorr it is essentially the only ion in the spectrum. The ions  $\text{A}_2\text{H}^+$  and  $\text{A}_3\text{H}^+$  react rapidly ( $Q_3 = 50 \text{ Å}^2$  and  $Q_4 = 35 \text{ Å}^2$ ) relative to the rate at which they are formed, since their R.A.'s at the respective maxima on the pressure plot

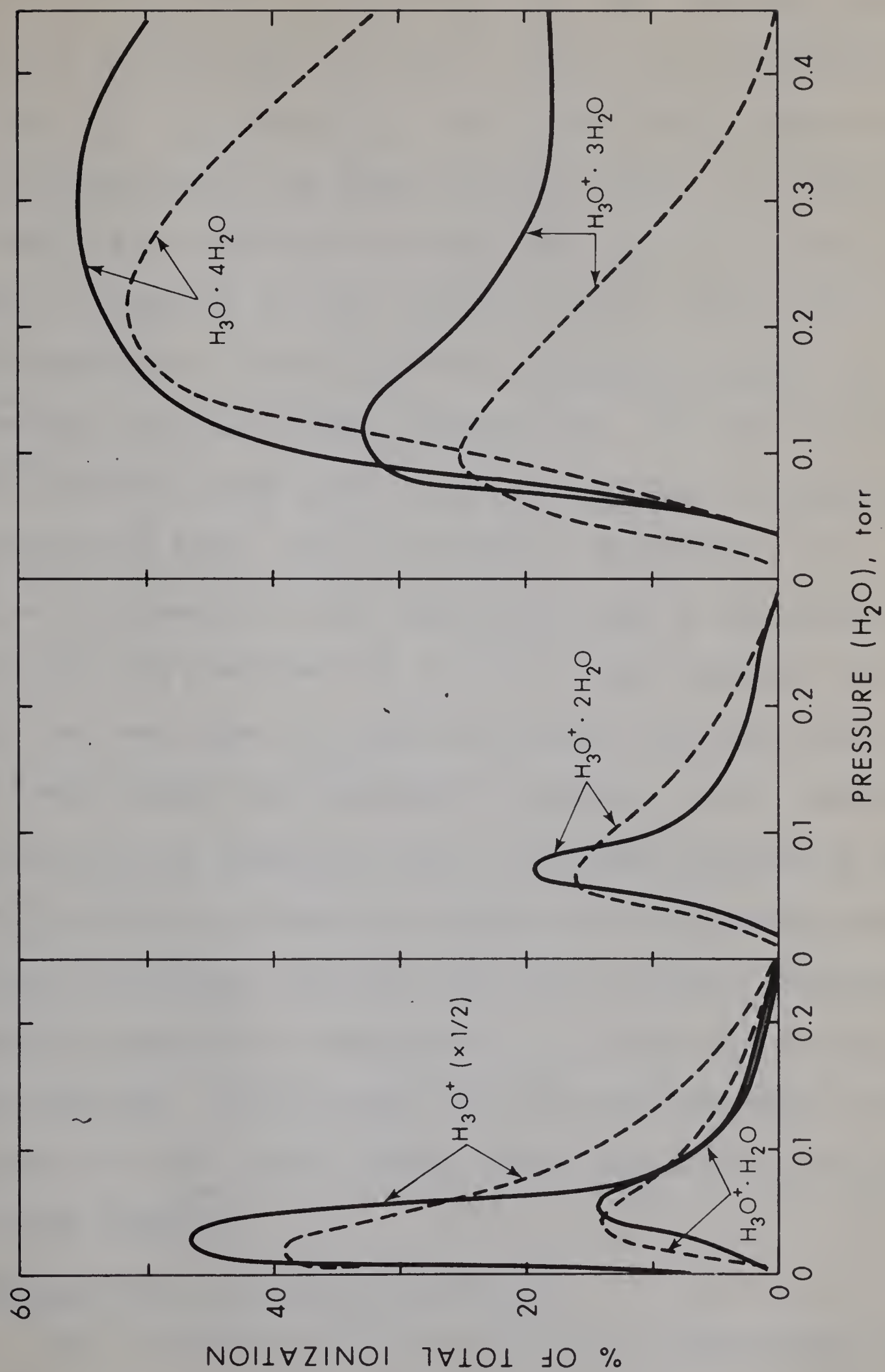
FIGURE 7.2

Fit of Experimental Water Vapor Mass Spectra to the  
Successive Reaction Scheme Calculated from Equations (7.8)

LEGEND:

dashed line: calculated from Equations (7.8)

solid line: experimental







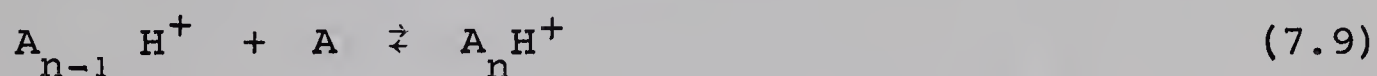
never account for more than 15 - 20% of the total ionization. The hydrates  $A_4H^+(Q_5 = 15\text{\AA}^2)$  and  $A_5H^+(Q_6 = 3\text{\AA}^2)$  react successively more slowly with further water molecules. However the intensities of these ions  $A_4H^+(I_5)$  and  $A_5H^+(I_6)$  and of the higher hydrates obviously cannot be described by the simple reaction scheme. No values of the cross sections for reactions of these ions inserted in the equations for their intensities can give the broad larger maxima and only gradual decreases of intensities with increasing pressure, as observed for these more highly hydrated ions. We could consider that cooling collisions might start to become important at pressures higher than 0.15 torr. If we introduced a dependence on the square of the pressure in the exponential terms of the derived equations for the predicted R.A.'s of the higher hydrates like  $A_4H^+$  and  $A_5H^+$ , an even worse fit would be obtained since the curves would drop off more sharply with increasing pressure. A more realistic possibility is that decompositions of the higher hydrates by loss of a water molecule is becoming important with increasing pressure. That is, the individual cross sections for the reverse reactions are becoming comparable in magnitude to the cross sections for further reactions. Thus the very low cross sections used to obtain a semblance of a fit for the higher hydrate ion intensities probably reflect back reaction.

#### 7.5 Equilibrium in the Hydration of $H_3O^+$

The introduction of back reactions in the reaction scheme might be technically feasible but leads to a greatly increased



complexity of the treatment. Therefore instead of introducing back reactions into the reaction scheme we will approach the system now from the standpoint of equilibrium. It is possible to calculate an equilibrium mass spectrum for hydration reactions in water vapor at pressures from 0.2 to 1.0 torr. This can be done by making use of equilibrium constants for the various hydration steps, calculated from the equilibrium room temperature mass spectrum of water vapor at 1 torr measured, using the alpha - particle mass spectrometer of these laboratories.<sup>86</sup> Considering the general hydration reaction



we can write the equilibrium constant  $K_{n-1, n}$  for this hydration step. It is

$$K_{n-1, n} = \frac{pA_n H^+}{pA_{n-1} H^+ \cdot p H_2 O} \equiv \frac{I_n}{I_{n-1} \cdot p H_2 O} \quad (7.10)$$

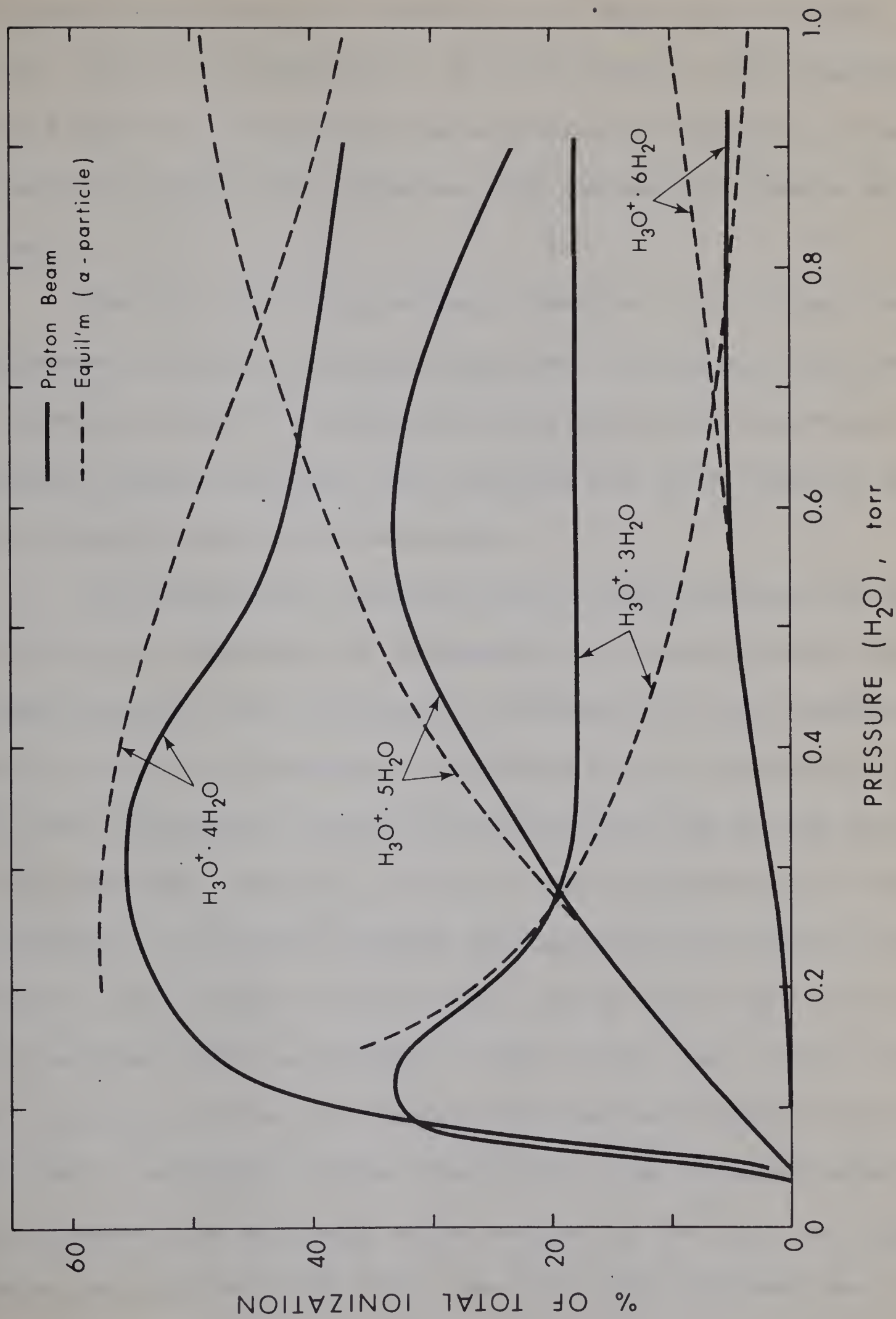
where the measured ionic intensities  $I_n$  are proportional to the equilibrium concentrations of the ions in the ion source and  $p H_2 O$  is the water pressure. Since all the K's are known at one pressure the ionic concentrations at other pressures can be very readily obtained and these are plotted in Fig. 7.3 as per cent of the total ionization. We see that the calculated equilibrium ionic concentrations give an approximate fit of the experimental results, which becomes particularly good at about 0.2 to 0.4 torr, while at higher pressures the agreement is, in general, not too good. Thus the equilibrium mass spectrum predicts that the R.A. of  $A_n H^+$  should

FIGURE 7.3

Fit of Experimental Water Vapor Mass Spectra to the  
Equilibrium Mass Spectra

Legend: \_\_\_\_\_ present results  
----- calculated equilibrium mass  
spectra from equilibrium  
constants measured at 1 torr  
water pressure<sup>86</sup>







decrease with increasing pressures above 0.3 torr while the experimental plot stays at a constant R.A. above this pressure.

The R.A. of  $A_6H^+$  is predicted to increase steadily with pressure from 0.4 torr to 1.0 torr, while experimentally a maximum is reached and the R.A. of  $A_6H^+$  then decreases with increasing pressure above 0.6 torr.

The fit with the experimental data at 0.2 torr and the disagreement at higher pressures might be a coincidence since we are comparing results of widely differing experimental systems. On general grounds one might have expected the fit to improve at higher pressures and not become worse.

We propose that the deviations at high pressure can be explained by the influence of instrumental artifacts rather than non-equilibrium in the ion source. In Chapter 5, it was estimated that because of the low conductance (calculated to be 1 liter/sec) of the small flat cylindrical volume between the bottom of the ion source and the withdrawal electrode, at an ion source pressure of 1 torr the pressure in the region between the ion source exit slit and the withdrawal slit is about 50 millitorr. Since ions traversing this region receive a high acceleration ( $\sim 100$  volts) over a short distance (1mm) collisions of the ion cluster with the water vapour molecules might lead to stripping of the clusters ie. loss of water molecules. Using a hard-sphere collision cross section of  $75\text{\AA}^2$  for the larger hydrates, we calculate that these ions will make at least one collision with water molecules in the region between the ion source





exit slit and the withdrawal electrode. To test whether decompositions are occurring in this region, experiments with redesigned ion source geometry giving better pumping at this region and a study of the effect of variation of the withdrawal potential would be in order.

Unfortunately this did not become obvious while experiments were being done and only became apparent upon a closer examination of the data.

However, in order to examine the effect of acceleration by electric fields in the ion source proper on the composition of the hydrates, we studied the cluster intensities as a function of repeller field strength at a constant pressure of 0.36 torr water vapor. The results obtained are shown in Fig. 7.4. Here  $E_r^{\ell}$  is the acceleration energy that an ion formed in the proton beam acquires if it reaches the ion source exit slit without suffering collisions. Figure 7.3 shows that with increasing ion energy the hydrated clusters become stripped of water so that at  $E_r^{\ell} = 35$  eV and higher, the hydronium ion,  $H_3O^+$ , becomes the most prominent in the spectrum. The prominent ion  $(H_2O)_4 H_3O^+$  at  $E_r^{\ell} = 0$  to 15 eV probably decomposes to  $(H_2O)_3 H_3O^+$  at higher ion energies. The general trend is that more highly hydrated species become less abundant as the ion energy is increased.

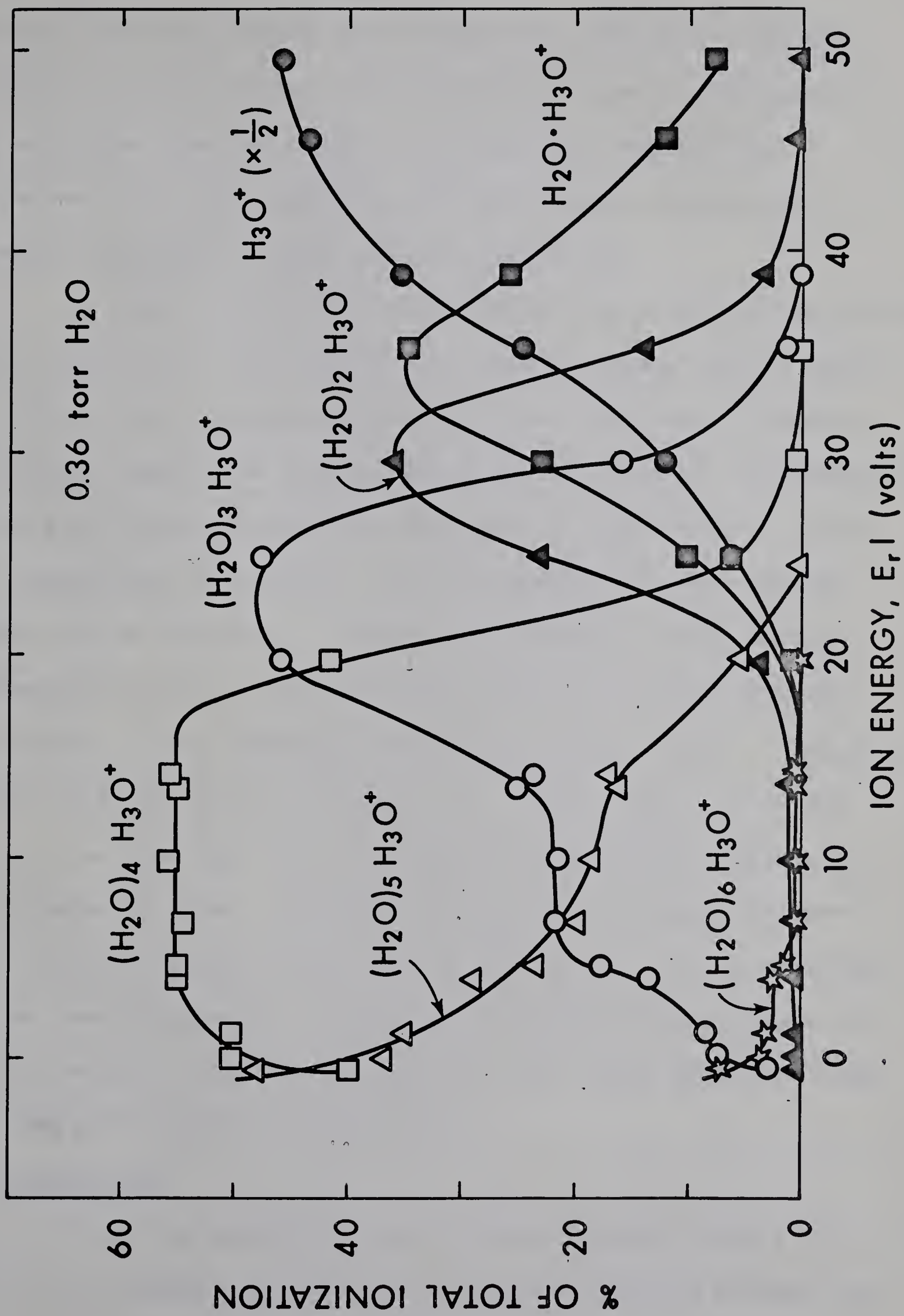
The decrease of cluster size with increasing ion energy may be due to a number of effects. Firstly, the cross sections for the clustering reactions:  $A_n H^+ + A \rightarrow A_{n+1} H^+$  will probably decrease with increase of ion velocity (ie. velocity dependence of the Langevin-Gioumousis - Stevenson<sup>23</sup> type). In the second place, the quenching collisions required for the removal of the excess energy (released in the

FIGURE 7.4

Effect of Increasing Ion Exit Energy in the Mass Spectrum  
of Water Vapor at 0.36 torr

$E_r$  is repeller field strength

$\ell$  is the distance from plane of primary  
ionization to the ion source exit slit.







clustering reaction) should also become less effective. Thirdly, collisions at high relative velocities should lead to stripping of water molecules from the cluster. The last two effects are interrelated since the quenching collisions become heating and stripping collisions at high relative velocities.

In order to utilize the results of Fig. 7.4 so as to establish whether reduction of the cluster size occurs between the ion source exit slit and the withdrawal electrode, one would have to examine the relative importance of the effects mentioned above. Unfortunately the state of knowledge about the phenomena involved does not allow safe predictions to be made. Only the effects of cross section decrease may be estimated. Assuming the Stevenson cross section dependence, the ratio of the two cross sections  $Q_1$  and  $Q_2$  for the same reaction at two different ion energies  $(E_{r\ell})_1$  and  $(E_{r\ell})_2$ , is given by  $Q_1/Q_2 = \left[ (E_{r\ell})_2 / (E_{r\ell})_1 \right]^{1/2}$ . Taking  $(E_{r\ell})_1 = 5$  ev and  $(E_{r\ell})_2 = 50$  ev (see Fig. 7.4) we predict a cross section change by only a factor of three. Considering the drastic changes observed in the cluster composition for such a change in  $E_{r\ell}$ , it is concluded that the overriding effect is not that of cross section change but that of energetic ("hot" ion) collisions with water molecules leading to reduction of the cluster size.

## 7.6 Conclusions

It may be concluded that the high pressure results of Fig. 7.1 are probably adulterated by cluster stripping between the

...the ... of the ...  
 ...the ... of the ...  
 ...the ... of the ...  
 ...the ... of the ...

...the ... of the ...  
 ...the ... of the ...  
 ...the ... of the ...  
 ...the ... of the ...

...the ... of the ...  
 ...the ... of the ...  
 ...the ... of the ...  
 ...the ... of the ...

...the ... of the ...  
 ...the ... of the ...  
 ...the ... of the ...  
 ...the ... of the ...

...the ... of the ...  
 ...the ... of the ...  
 ...the ... of the ...  
 ...the ... of the ...

ion exit slit and withdrawal electrode. For example the observed constancy of the  $(\text{H}_2\text{O})_3\text{H}_3\text{O}^+$  ion from 0.35 to 0.9 torr is probably due to the generation of this ion from larger clusters which are stripped outside the ion source. Thus it might be concluded that this ion actually decreases in intensity with pressure. This expected decrease of intensity brings the results in closer agreement with the intensity changes predicted by the equilibrium treatment. In the absence of the instrumental defect the results would have probably agreed with those of the equilibrium curves obtained from the alpha particle mass spectrometer. Since the ionic residence times in the alpha particle mass spectrometer are of the order of milliseconds, while those in the proton beam mass spectrometer are in the microsecond range, the tentative agreement of the two sets of data suggests that at pressures above 0.4 torr, clustering equilibrium is established very rapidly.

Figure 7.1 could be considered to have three pressure ranges: (1) from 0 to .2 torr a range of dynamic consecutive reactions (which can be fitted by the reaction scheme given before), (2) an intermediate range from 0.2 to 0.4 torr, and (3) a range above 0.4 torr where equilibrium conditions are probably established.

#### 7.7 Suggestions for Further Experiments

It is felt that further experiments on the present system with a redesigned geometry between the ion source exit slit and withdrawal electrode to increase the gas conductance of this region would be helpful. Use of a transparent mesh grid in place of the withdrawal slit would be one way of achieving this. The effect of







varying the drawout potential should also be examined. Experiments performed at higher pressures and with temperature variations would be pertinent. In fact, experiments at higher pressures of water by using ultra - fast or "infinite" pumping speed cryogenic pumping are being planned now.

Studies of clustering and solvated ions of other polar molecules such as alcohols, ethers and amines would be very interesting. Experiments at pressures where an equilibrium exists could show if any of these molecules exhibit solvated "inner" and "outer" shell structures. Solvation studies with a different ion around which hydration could take place would be enlightening. Possibilities of experiments using metal ions such as the alkali metals and varying the solvent molecule (eg. water, methanol, ammonia, etc) seem promising. Solvation of negative ions such as the halides (eg.  $\text{Cl}^-$ ) would be of interest. An example of competitive solvation (between methanol and water) is discussed in Part II of this Chapter.

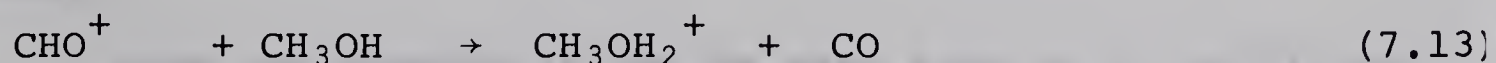
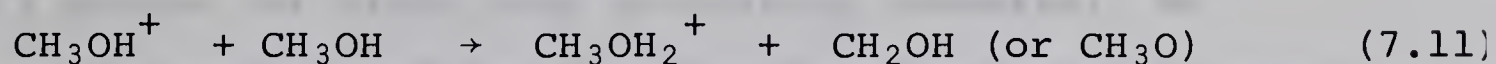


## PART II. COMPETITIVE SOLVATION IN THE GAS PHASE

### THE SYSTEM WATER-METHANOL

#### 7.8 Introduction

In both water and methanol, protonated molecule ions are formed readily by ion-molecule reactions in the gas phase. The hydronium ion,  $\text{H}_3\text{O}^+$ , is formed by Reactions (7.1) and (7.2) given previously. Since the primary proton impact mass spectra of various molecules for 50 to 100 kev protons were shown to be similar to ordinary electron impact mass spectra (see Chapter 3, Part II), the main primary methanol ions (accounting for 95% of the total ionization) are  $\text{CH}_3\text{OH}^+$ ,  $\text{CH}_2\text{OH}^+$  and  $\text{CHO}^+$ . The following proton transfer reactions of these ions with methanol have been observed or postulated:<sup>88, 91, 96-99</sup>



In addition Munson<sup>88</sup> has observed the disolvated ion  $(\text{CH}_3\text{OH})_2\text{H}^+$  which is probably formed by the reaction of  $\text{CH}_3\text{OH}_2^+$  with methanol.

In a short preliminary study, the major series of ions  $(\text{CH}_3\text{OH})_n \cdot \text{CH}_3\text{OH}_2^+$  were observed in pure methanol at 0.36 torr (at room temperature). In fact these clusters accounted for ca. 99% of the total ionization. The presence of this major series suggested the possibility of studying competitive solvation of  $\text{CH}_3\text{OH}_2^+$  by methanol and water molecules.





The study would be based on observing the R.A.'s of mixed clusters such as  $H^+ \cdot xCH_3OH \cdot y H_2O$ . No additional reactions are expected to occur, since it was shown in Part I of this chapter that water solvates completely as  $H^+ \cdot yH_2O$  in the gas phase.

## 7.9 Results

Ionic reactions in mixtures of methanol and water vapour were studied at a constant (.36 torr) water vapor pressure. The methanol concentration was varied from one to about 40 millitorr. The mass spectrum of pure methanol and pure water was also measured at .36 torr. Some representative spectra are presented in Figs. 7.5 - 7.7. Essentially the only product ions observed are clusters involving water or methanol molecules. Since the central ion about which the molecules cluster could be  $CH_3OH_2^+$  or  $H_3O^+$  at low methanol concentrations, this ion will be assumed to be a proton for simplicity in writing formulas. We will use the notation M for a methanol molecule and A (aqua) for water.

From the spectra it can be seen that at 2.4 millitorr methanol, corresponding to 0.66% of the water concentration, clusters containing one or two methanol molecules are quite prominent. With 8.4 millitorr  $CH_3OH$ , or a concentration of about 2% that of the water, the pure water clusters  $A_n H^+$  are almost entirely suppressed and pure methanol clusters e.g.  $M_3 H^+$  and  $M_4 H^+$ , become visible. At the highest methanol concentration (11.3%) of 41 millitorr, the pure methanol cluster  $M_4 H^+$  is the dominant one in the spectrum, and the next peaks of higher R.A.,  $M_3 A H^+$

FIGURE 7.5

Mass Spectra of Water and Water-Methanol Mixture

Top: Mass spectrum of pure water vapor at 0.36 torr  
ion source pressure.

Bottom: Mass spectrum of 2.4 millitorr methanol and  
0.36 torr water mixture.

% OF TOTAL IONIZATION

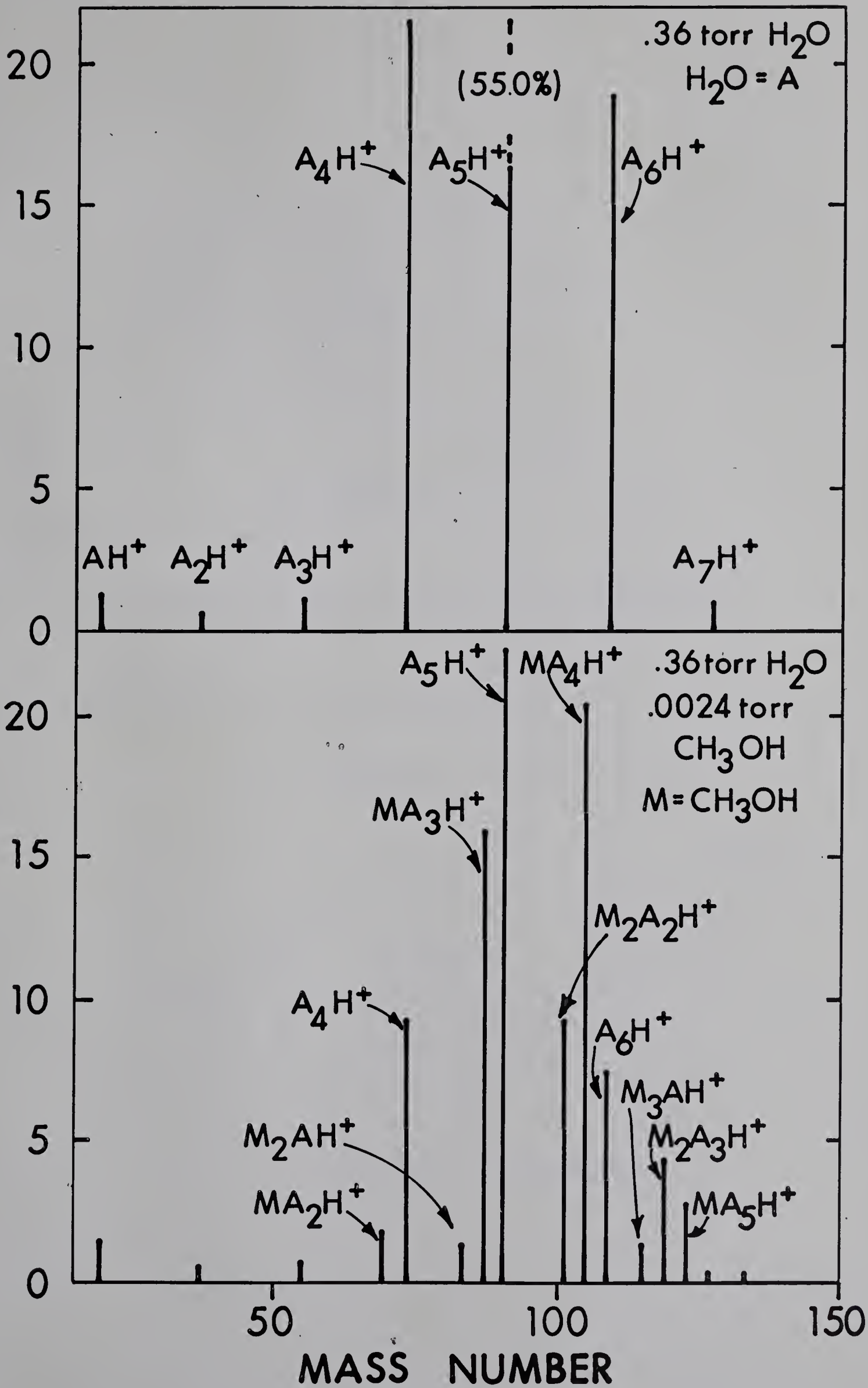


FIGURE 7.6

Mass Spectrum of Methanol-Water Mixture

Ion source pressure of water vapor is 0.36 torr  
and of methanol is 8.4 millitorr.



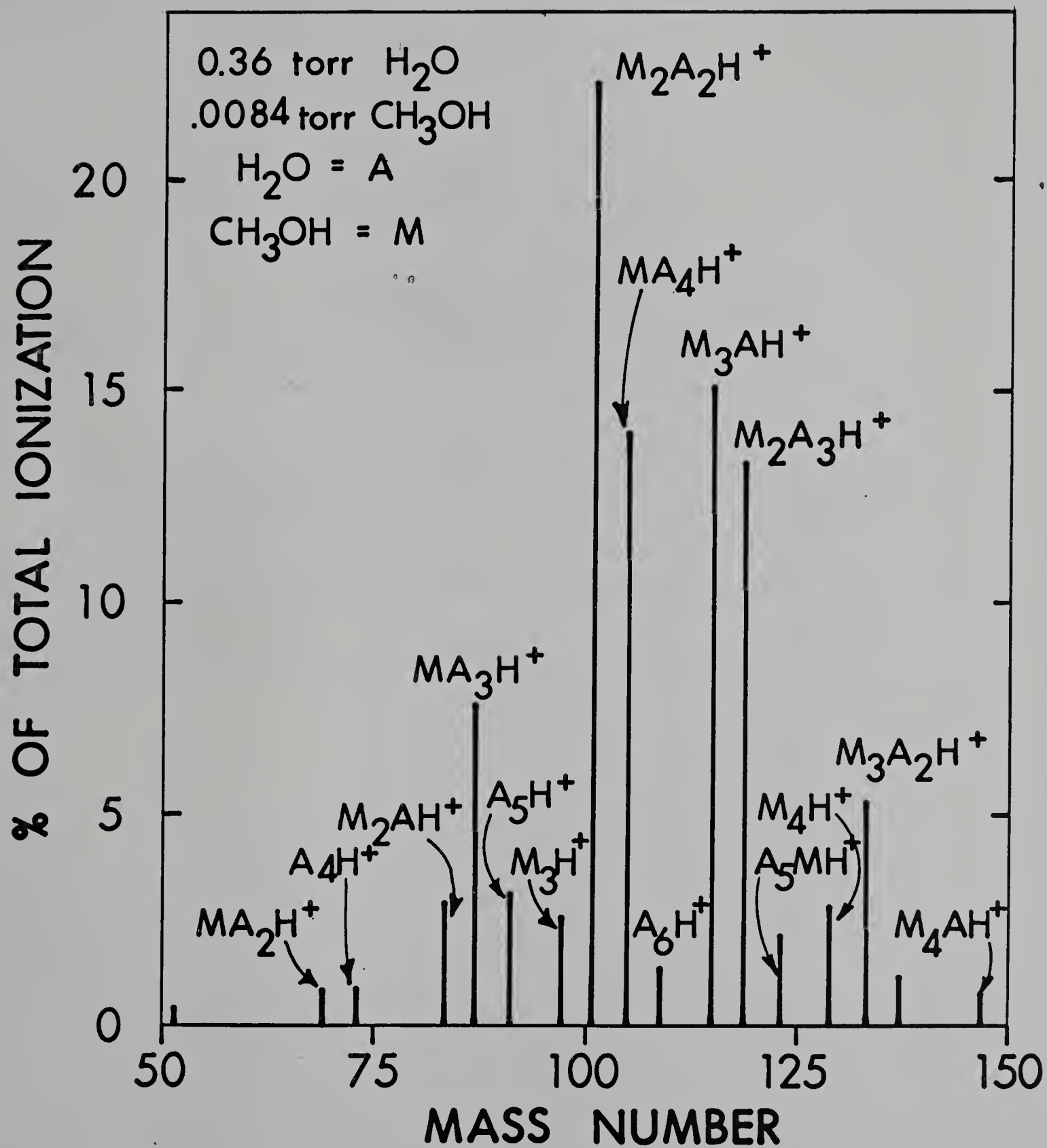


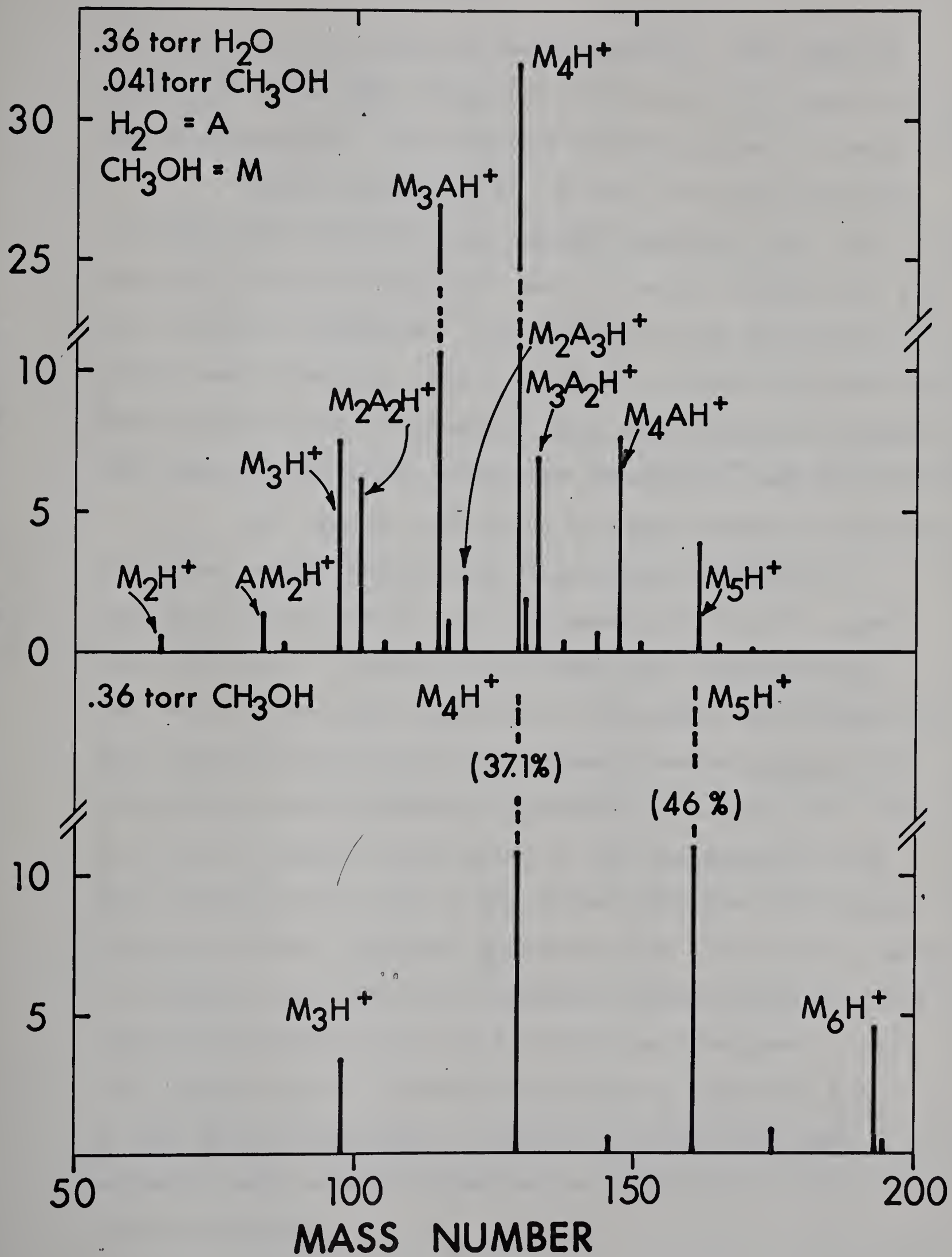
FIGURE 7.7

Mass Spectra of Water-Methanol Mixture and Pure Methanol

Top: Mass spectrum of 0.36 torr water with  
41 milli torr methanol

Bottom: Mass spectrum of pure methanol at  
0.36 torr ion source pressure.

% OF TOTAL IONIZATION







and  $M_4AH^+$  contain only one water molecule. Mass spectra were also taken (not shown) for .33, 1.32, 5.17, and 8.1 per cent methanol. The combined data are shown in Table 7.1.

In pure methanol at .36 torr, the pure methanol clusters are about the only species observed, with the dominant clusters being  $M_4H^+$  and  $M_5H^+$  which account for 85% of the total ionization. Two different ions of low R.A.'s (0.7%) were observed. These could be written as  $M_3(CH_3OCH_3)H^+$  and  $M_4(CH_3OCH_3)H^+$  in agreement with the findings of Munson<sup>100</sup> who reported the lower homologues  $(CH_3OCH_3)H^+$  and  $M(CH_3OCH_3)H^+$ .

The sums of each group of equal number of molecules clustered around a proton are also shown in Table 7.1. The ions represented by  $L_3H^+$  for example are  $A_3H^+$ ,  $A_2MH^+$ ,  $AM_2H^+$  and  $M_3H^+$ . The R.A.'s of these ions (expressed as per cent of the total ionization) are summed and called  $\Sigma L_3H^+$ . The intensities of the various summed cluster groups  $\Sigma L_nH^+$  are plotted versus methanol concentration in Fig. 7.8. The one and two ligand clusters are of low concentration but some trends can be seen in the higher clusters. The three molecule cluster gradually increases from 1.2% in pure water to a maximum of 13.9% for a methanol concentration of 5.17% and then decreases again to 3.5% with pure methanol. The four cluster  $\Sigma L_4H^+$  gradually increases to a maximum R.A. of 66% for 8.1% methanol. The R.A. of  $\Sigma L_4H^+$  for 100% methanol seems somewhat anomalous at only 37.1% of the total ionization.



TABLE 7.1

Mass Spectra of Water-Methanol Mixtures at 0.36 torr  
Water and Varying Methanol Concentrations

%	Methanol*	(pure water)	.33%	.66%	1.32%	2.33%	5.17%	8.1%	11.3%	(pure methanol)
m/e	ion	Relative Abundances (% of total ionization)								
19	AH <sup>+</sup>	1.4	1.4	1.5	0.8	0.8	0.6	0.3	0.2	
33	MH <sup>+</sup>			0.1	0.2	0.4	0.5	0.5	0.4	0.1
	ΣLH <sup>+</sup>	1.4	1.4	1.6	1.0	1.2	1.1	0.8	0.6	0.1
37	A <sub>2</sub> H <sup>+</sup>	0.6	0.6	0.6	0.4	0.2	0.1			
51	AMH <sup>+</sup>			0.2	0.2	0.4	0.4	0.2	0.1	
65	M <sub>2</sub> H <sup>+</sup>									0.2
	ΣL <sub>2</sub> H <sup>+</sup>	0.6	0.6	0.8	0.6	0.6	0.5	0.2	0.2	0.2
55	A <sub>3</sub> H <sup>+</sup>	1.2	0.7	0.7	0.4	0.2				
69	A <sub>2</sub> MH <sup>+</sup>		0.8	1.8	1.5	0.4	0.7	0.2	0.1	
83	AM <sub>2</sub> H <sup>+</sup>		0.3	1.4	2.3	3.0	4.5	2.4	1.4	
97	M <sub>3</sub> H <sup>+</sup>			0.1	0.9	2.7	8.7	8.2	7.5	3.5
	ΣL <sub>3</sub> H <sup>+</sup>	1.2	1.8	4.0	5.1	6.8	13.9	10.8	9.0	3.5
73	A <sub>4</sub> H <sup>+</sup>	21.6	11.4	9.3	3.9	0.9	0.2			
87	A <sub>3</sub> MH <sup>+</sup>		7.5	14.9	12.8	7.7	3.3	0.9	0.3	
101	A <sub>2</sub> M <sub>2</sub> H <sup>+</sup>		2.0	9.3	17.5	22.5	19.7	11.0	6.1	
115	AM <sub>3</sub> H <sup>+</sup>		0.14	1.4	5.8	15.2	29.3	30.7	27.0	0.1
129	M <sub>4</sub> H <sup>+</sup>				0.5	2.9	12.2	23.6	32.1	37.0
	ΣL <sub>4</sub> H <sup>+</sup>	21.6	20.9	34.9	40.5	49.2	64.7	66.2	65.5	37.1
91	A <sub>5</sub> H <sup>+</sup>	55.0	37.1	22.3	10.7	3.2	0.4			
105	A <sub>4</sub> MH <sup>+</sup>		15.4	20.3	21.5	14.2	3.0	1.0	0.3	
119	A <sub>3</sub> M <sub>2</sub> H <sup>+</sup>		1.4	4.3	10.1	13.4	6.2	4.0	2.5	
133	A <sub>2</sub> M <sub>3</sub> H <sup>+</sup>			0.4	1.9	5.3	5.9	7.2	6.9	
147	AM <sub>4</sub> H <sup>+</sup>				0.2	0.8	2.1	4.8	7.5	0.2
161	M <sub>5</sub> H <sup>+</sup>						0.4	1.6	3.9	46.0
	ΣL <sub>5</sub> H <sup>+</sup>	55.0	53.9	47.3	44.4	36.9	18.0	18.6	21.1	46

CONT.





TABLE 7.1 continued

%	Methanol	(pure water)	.33%	.66%	1.32%	2.33%	5.17%	8.1%	11.3%	(pure methanol)
109	A <sub>6</sub> H <sup>+</sup>	19.0	16.6	7.4	3.9	1.48	0.11			
123	MA <sub>5</sub> H <sup>+</sup>		2.7	2.8	3.3	2.24	0.31		0.11	
137	M <sub>2</sub> A <sub>4</sub> H <sup>+</sup>			0.32	0.84	1.24	0.37	0.29	0.21	
151	M <sub>3</sub> A <sub>3</sub> H <sup>+</sup>				0.08	0.28	0.18	0.27	0.30	
165	M <sub>4</sub> A <sub>2</sub> H <sup>+</sup>							0.13	0.25	
179	M <sub>5</sub> AH <sup>+</sup>								0.09	
193	M <sub>6</sub> H <sup>+</sup>									4.5
	Σ L <sub>6</sub> H <sup>+</sup>	19.0	19.3	10.50	8.12	5.24	0.97	0.84	0.96	4.5

\* % methanol =  $\frac{\text{PRESSURE METHANOL}}{\text{PRESSURE WATER}} \times 100$

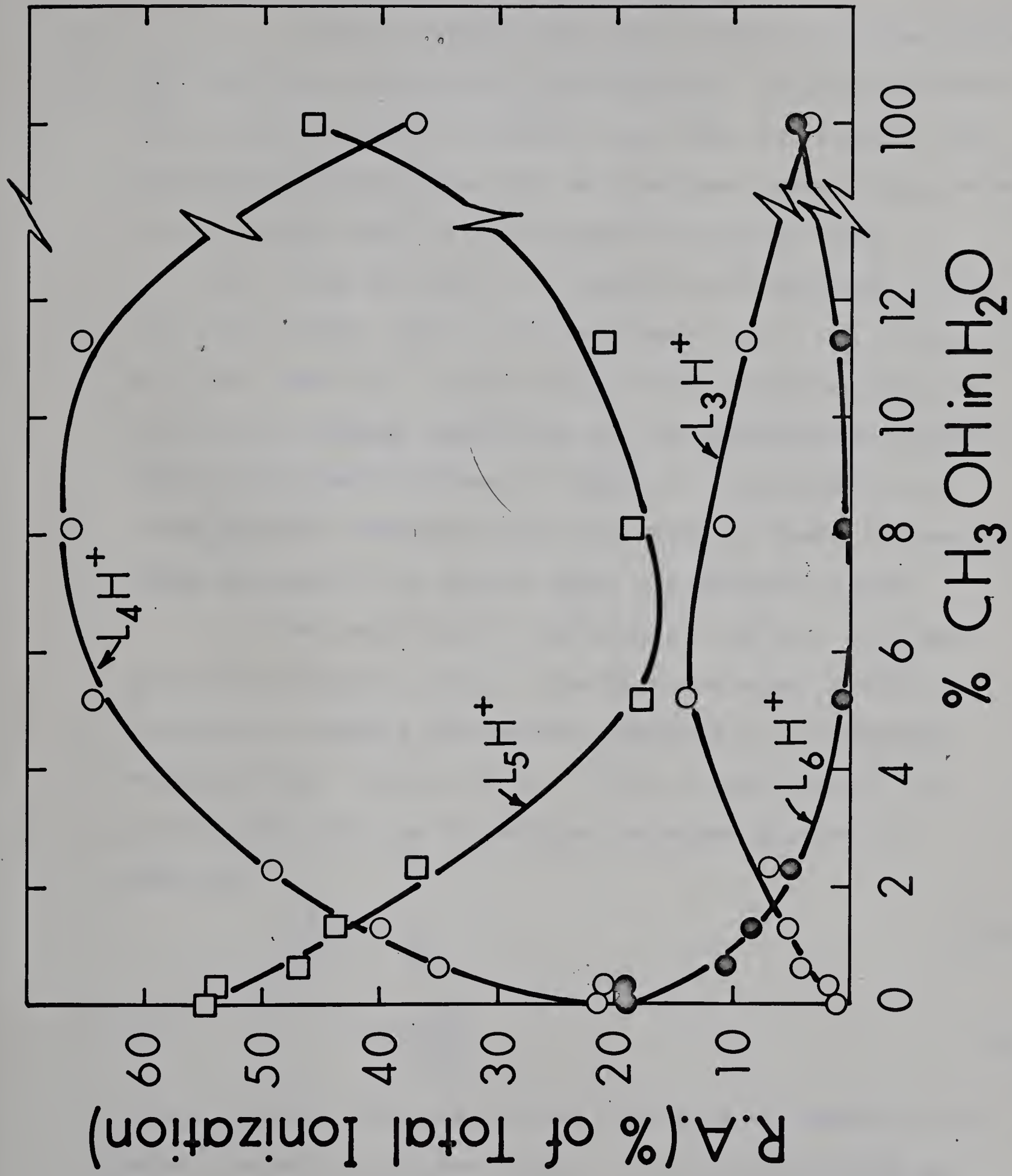
FIGURE 7.8

Variations of Summed Cluster Groups of  $L_nH^+$ , in Methanol-  
Water Mixtures

Water pressure in ion source is constant at 0.36 torr

% methanol is  $\frac{\text{pressure of methanol}}{\text{pressure of water}} \times 100$

The  $L_nH^+$  represent the total R.A. of all clusters  
with n solvated molecules.







7.10 Calculation of the Preferential Take Up of Methanol into the Water - Methanol Clusters.

It can be shown that composition of a given cluster  $L_nH^+$  follows a probability distribution. Calling the probability for methanol inclusion  $m$  and that for water  $a$ , the calculated probabilities for an  $n$  solvate containing  $n$  molecules will be equal to the binomial expansion terms of  $(a + m)^n$ . Thus for the  $n = 3$  group the intensities of the ions  $A_3H^+$ ,  $A_2MH$ ,  $AM_2H^+$ , and  $M_3H^+$  should be in the ratios of  $a^3: 3a^2m: 3am^2: m^3$ . Values for  $a$  and  $m$  could be obtained by fitting binomial expansions to the experimental results. The fit obtained is shown in Table 7.2. Agreement for other methanol concentrations not shown in Table 7.2 was at least as good as, or better than, the examples given.

For convenience, the sums of the R.A.'s of each group of the same  $n$  ( $\sum L_nH^+$ ) has been set equal to 100. In order to compare the results obtained with different methanol-water ratios, in Eq. (7.14) a coefficient ( $\gamma$ ) of preferential take up of methanol into the cluster is defined:

$$\gamma \cdot \frac{P_M}{P_A} = \frac{m}{a} \quad (7.14a)$$

or

$$\gamma = \frac{m/P_m}{a/P_A} \quad (7.14b)$$

where  $P_M$  and  $P_A$  are the partial pressures of methanol and water present in the ion source. The  $\gamma$ 's calculated are constant within 10% over the concentration range studied within a given series,  $L_nH^+$ , of  $n$  ligands for  $n = 3$  to 6. The average  $\gamma$ 's (called  $\gamma_{H^+}$ ) as calculated from all the



TABLE 7.2

Mass spectra of Methanol-water mixtures showing competitive solvation of the proton by methanol and water molecules.

% methanol*		1.32%		5.17%			11.3%		
Ion	Expl. <sup>†</sup>	Calc. <sup>§</sup>	$\gamma^{\parallel}$	Expl. <sup>†</sup>	Calc. <sup>§</sup>	$\gamma^{\parallel}$	Expl. <sup>†</sup>	Calc. <sup>§</sup>	$\gamma^{\parallel}$
	R.A.	R.A.		R.A.	R.A.		R.A.		
A <sub>3</sub> H <sup>+</sup>	8	6.4	113	-	.27	119	-	0.2	141
A <sub>2</sub> MH <sup>+</sup>	29	28.8		5	5.06		1.2	1.02	
AM <sub>2</sub> H <sup>+</sup>	45	43.2		32	31.1		15.6	15.9	
M <sub>3</sub> H <sup>+</sup>	18	21.6		63	63.6		83.2	83.1	
A <sub>4</sub> H <sup>+</sup>	9.6	9.2	61	0.3	1.3	37.5	-	.07	47
A <sub>3</sub> MH <sup>+</sup>	30.0			5.1	10.5		0.5	1.4	
A <sub>2</sub> M <sub>2</sub> H <sup>+</sup>	43.2	36.8		30.6	30.2		9.3	10.8	
AM <sub>3</sub> H <sup>+</sup>	14.3	20.1		45.5	39.1		41.2	37.9	
M <sub>4</sub> H <sup>+</sup>	1.3	4.1		18.9	19.0		49.0	49.8	
A <sub>5</sub> H <sup>+</sup>	24.1	25.4	23.8	2.1	4.6	16.5	-	.24	21
A <sub>4</sub> MH <sup>+</sup>	48.5	40.3		16.7	19.5		1.4	2.8	
A <sub>3</sub> M <sub>2</sub> H <sup>+</sup>	22.8	25.3		34.4	33.1		11.9	13.2	
A <sub>2</sub> M <sub>3</sub> H <sup>+</sup>	4.3	8.0		32.8	28.4		32.7	30.9	
A M <sub>4</sub> H <sup>+</sup>	.45	1.26		11.7	12.1		35.5	36.0	
M <sub>5</sub> H <sup>+</sup>	-	.08		2.0	2.1		18.5	16.8	
A <sub>6</sub> H <sup>+</sup>	47	46.4	10.3	11	11.8	9.2	-	2.2	8.0
A <sub>5</sub> MH <sup>+</sup>	40.6	38.0		31	30.3		11.5	11.8	
A <sub>4</sub> M <sub>2</sub> H <sup>+</sup>	10.3	12.9		37	32.5		22	26.1	
A <sub>3</sub> M <sub>3</sub> H <sup>+</sup>	1.1	2.3		18	18.5		31	30.9	
A <sub>2</sub> M <sub>4</sub> H <sup>+</sup>					5.9		26	20.5	
AM <sub>5</sub> H <sup>+</sup>							9.5	7.3	
M <sub>6</sub> H <sup>+</sup>								1.1	

\* %Methanol =  $\frac{\text{pressure methanol}}{\text{pressure water}} \times 100$ . <sup>†</sup> Abundances renormalized to 100 for each group. <sup>§</sup> Abundances calculated from the binomial expansion. <sup>||</sup> Factor of preferential methanol to water solvation.





spectra measured at various methanol concentrations, are presented in Table 7.3, column 2.

At methanol concentrations higher than 2%, almost no pure water clusters are present and one could consider that molecules solvate around a protonated methanol ( $\text{MH}^+$ ) core. The proton was assigned to the methanol oxygen ion since the proton affinity of methanol is about 10 to 20 kcal/mole<sup>100</sup> higher than that of water. This assignment seems consistent since even for the 5% methanol mixture, where the water concentration is overwhelming, pure water hydrates  $\text{A}_n\text{H}^+$  are approximately zero (e.g. R.A. of  $\text{A}_3\text{H}^+ = 0\%$ , R.A. of  $\text{A}_4\text{H}^+ = 0.2\%$ ) whereas pure methanol clusters  $\text{M}_n\text{H}^+$  are observed in noticeable intensity (eg. R.A. of  $\text{M}_4\text{H}^+ = 12.2\%$ ) Above methanol mixture concentrations of 2%, the clusters contain, on the average, considerably more methanol than water. Methanol is, therefore the stronger solvent in the observed clusters, i.e. clusters containing up to five solvent molecules.

Using data from the three highest concentrations of methanol, we can calculate a  $\gamma_{\text{MH}^+}$  in exactly the same manner as for  $\gamma_{\text{H}^+}$ . These  $\gamma_{\text{MH}^+}$ 's are also constant for a given number of solvating molecules i.e. for clusters of the same n. These values are also presented in Table 7.3 column 3. Both the  $\gamma_{\text{H}^+}$  and  $\gamma_{\text{MH}^+}$  show gradual decreases as n is increased. Thus for solvation of  $\text{MH}^+$ , methanol is preferentially taken up by a factor of 80, 31, 14 and 6 for clusters containing 2, 3, 4 and 5 solvent molecules.



TABLE 7.3

Coefficients of preferential methanol take up ( $\gamma$ ) in the  
water-methanol clusters

$n^*$	$\gamma_{H^+}^{\dagger}$	$\gamma_{MH^+}^{\S}$
2		$80 \pm 10\%$
3	$120 \pm 10\%$	31
4	45	14
5	22	5.5
6	9.1	

\* number of solvating molecules

† molecules are considered to solvate  $H^+$  (calculated from Table 7.2) i.e.  $L_n H^+$

§ molecules are considered to solvate an  $MH^+$  core i.e.  $L_n MH^+$





### 7.11 Equilibrium in the Solvation of $MH^+$ by Water and Methanol

So far in this discussion we have omitted any reference to the question of cluster equilibrium. It can be estimated that an ion will make 20 - 40 collisions with neutral gas molecules at 0.36 torr pressure before exiting the ion source if a collision cross section of 50 to 100 Å<sup>2</sup> is assumed.\* This estimate is probably conservative considering the large size of the clusters. However using these estimates, at 1% methanol concentration an ion will only have about one chance in two or three to collide with a methanol molecule. At 5% methanol concentration, every ion can collide with at least one or two methanol molecules in traversing the ion source. At methanol concentrations below 5% where pure water clusters,  $A_nH^+$ , are still observed, it is considered that no equilibrium would exist. In the remainder of this discussion only competitive solvation of  $MH^+$  by methanol and water at mixture concentrations of 5% methanol and higher will be considered. Here pseudo-equilibrium conditions are expected to apply for reasons to be given below.

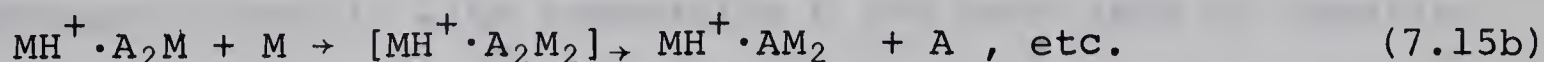
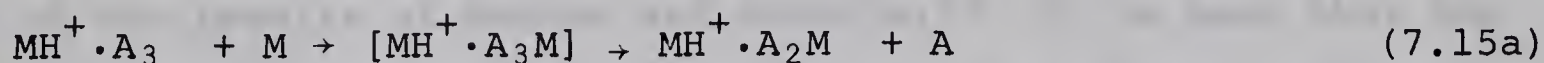
---

\* To a good approximation, the number of collisions an ion makes with molecules in travelling the distance  $\ell$  (from plane of ionization to ion source exit slit) is given by  $\ell / \lambda$  as discussed in the Introduction, Chapter 1, Sec. 1.7. The mean free path of an ion  $\lambda$  is given by  $\lambda \approx (\sigma n)^{-1}$ , where  $\sigma$  is the collision cross section for an ion colliding with a gas molecule and  $n$  is gas concentration in molecules/cc.



### A. Qualitative model

A qualitative physical model may be used to demonstrate why a pseudo-equilibrium might be assumed. Considering first the very high water concentration experiments, the initial ion formed by ion-molecule reaction will be  $\text{H}_3\text{O}^+$ , which on collisions with water<sup>molecules</sup> will form  $\text{H}_3\text{O}^+ \cdot n\text{H}_2\text{O}$ . Upon the first collision with a methanol molecule, a complex  $\text{H}^+ \cdot \text{M} \cdot (n+1)\text{H}_2\text{O}$  will be formed. Since every addition or solvation of the cluster by another molecule is exothermic, excess energy must be removed in order that the cluster not decompose. This energy can be removed by a third body (most likely water) or one or even two water molecules might be "boiled off". Because of the difference in proton affinities of methanol and water ( $> 13 \text{ kcal/mole}$ )<sup>100</sup> more energy must be removed upon addition of a methanol molecule to the cluster than for a water molecule addition. The cluster could be envisaged as becoming enriched in methanol and depleted in water as in the following example:



### B. Comparison with other equilibrium results

Additional support for the argument that the present results represent at least a pseudo-equilibrium picture of competitive solvation of methanol and water about  $\text{MH}^+$ , has come from some very recent results on a study of the same system by Kebarle and co-workers<sup>86</sup> using the alpha particle mass spectrometer of these laboratories. Studies were done at 2 and 5 torr total pressure with varied methanol and water concentrations at







50° C. The R.A.'s of the clusters  $\text{MH}^+ \cdot n\text{L}$  are very similar to that observed in the present research. Using the high pressure alpha particle mass spectrometer a better approach of the system to equilibrium can be assumed because of the higher pressures and the much longer ionic reaction times present (about a millisecond compared to a microsecond in the proton beam mass spectrometer). These workers found  $\gamma_{\text{MH}^+}$  's of 55, 25 and 8 for solvation of 3, 4 and 5 ligands respectively. The values for our results (Table 7.3) are 31, 14, 5.5. In both sets of data,  $\gamma$ 's were constant within a group of equal  $n$  ligands. Both these sets of  $\gamma$ 's exhibit similar trends and considering the agreement (within a factor of two) our results must reflect a near-equilibrium formation of solvated  $\text{MH}^+$  clusters at methanol concentrations above 5%.

#### 7.12 Further Discussion of the Solvation of $\text{MH}^+$ by Methanol and Water

##### A. Variation of $\gamma$ with increasing $n$

In Fig. 7.9 we have plotted  $\log \gamma_{\text{MH}^+}$  versus  $n$ , the number of solvating molecules in the cluster. Also included are some of the results of Haynes and Kebarle.<sup>86</sup> It is seen that  $\log \gamma$  decreases linearly with increasing  $n$  for both sets of results. If one extrapolates the  $\log \gamma_{\text{MH}^+}$  line to zero the abscissa is crossed by both sets of data  $n = 7$ , indicating that for seven ligands solvating, the probability for water or methanol inclusion is equal. For  $n > 7$ ,  $\gamma$  becomes less than unity, i.e. water begins to take precedence.

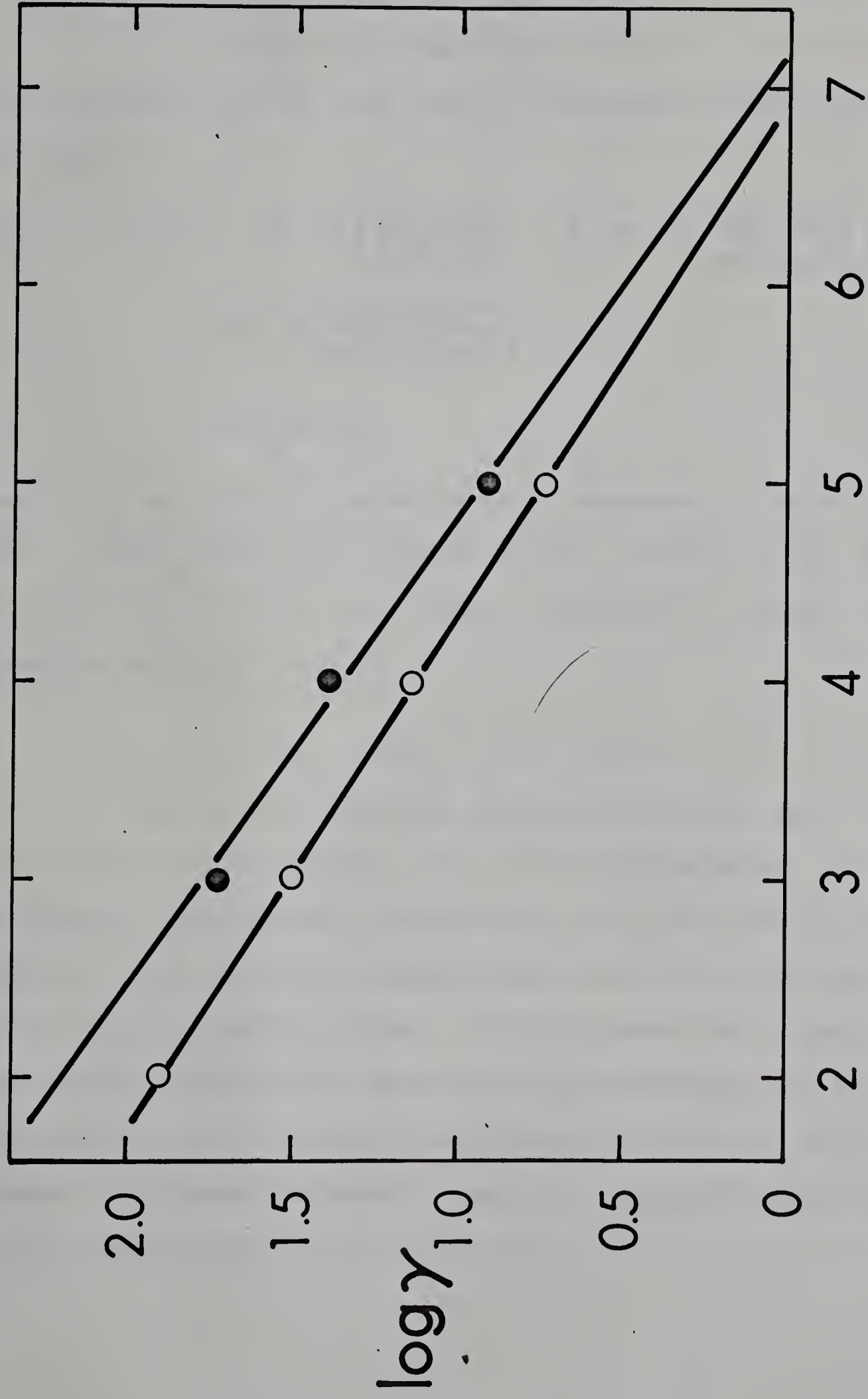
Whether the linearity of  $\log \gamma$  with  $n$  is significant is not immediately obvious. One can calculate (approximately) the difference in stability between solvation of  $\text{MH}^+$  by water

FIGURE 7.9

Variation of  $\log \gamma$  versus Number of Solvated Molecules (n)

$\gamma$  is coefficient of preferential methanol take-up in the clusters  $MH^+ \cdot nL$ , where n is the number of solvating ligands (water or methanol) clustering around  $MH^+$ .

—●—	Data of Kebarle <sup>86</sup> measured in the alpha particle mass spectrometer at 2 and 5 torr.
—○—	Present results







only and by methanol only. Considering equations (7.16) and (7.17)



we can write for the free energy difference between water and methanol

$$\begin{aligned} \Delta F_A^\circ - \Delta F_M^\circ &= -RT \ln \left( \frac{\text{MH}^+ \cdot n\text{A}}{\text{MH}^+ [\text{A}]^n} \right) - \left[ -RT \ln \left( \frac{\text{MH}^+ \cdot n\text{M}}{\text{MH}^+ [\text{M}]^n} \right) \right] \\ &= RT \ln \left( \frac{\text{MH}^+ \cdot n\text{M} [\text{A}]^n}{\text{MH}^+ \cdot n\text{A} [\text{M}]^n} \right) \\ &= RT \ln \gamma_n^n \end{aligned} \quad (7.18)$$

where [A] and [M] indicates partial pressure of water and methanol and  $\gamma_n$  is  $\gamma_{\text{MH}^+}$  for the cluster  $\text{MH}^+ \cdot n\text{L}$ . Using values read directly from Fig. 7.9, the free energy difference is easily calculated from the working equation

$$\Delta F_A^\circ - \Delta F_M^\circ = 1.38 n \log \gamma_n \quad (7.19)$$

For  $n = 2$ , the free energy difference is 5.2 kcal/mole, for  $n = 3$ , 6.2 kcal/mole,  $n = 4$ , 6.3 kcal/mole and  $n = 5$ , 5.2 kcal/mole. The values indicate that the free energy differences between water only and methanol only solvating are constant for 2 to 5 ligands solvating  $\text{MH}^+$ . If considered per ligand, the free energy differences are gradually decreasing so that methanol is becoming less strongly bound compared to water as the total number of ligands increase. This, of course, is also demonstrated by the decreasing  $\gamma$  with increasing  $n$ .



B. Use of the "electrostatic theory" in the interpretation of competitive solvation

In the interpretation of the present results considerable help can be obtained from the "electrostatic theory" for metal-ion coordination complexes.<sup>101</sup> This theory, using simple electrostatic concepts, allows the calculation of the binding energies of metal complexes in the gas phase. The results of such calculations have been in many cases very successful. In general, the potential energy of a complex ion is built up of four terms. These are due to the attraction between the ion and the permanent and induced dipole of the ligands, the mutual repulsion of the dipoles, the energy required to form the induced dipoles and the van der Waals repulsions between the ligands and the central ion. Comparing the potential energies of an ion having water or methanol molecules as ligands, it is found that the first term is the decisive one. The first term contains the sum of the permanent dipole and the polarizability. The dipole moments of water and methanol are 1.85 and 1.69 D while the polarizabilities are 1.48 and 3.23 Å<sup>3</sup>. The potential energy of an ion dipole interaction varies inversely with the square of the distance while the polarizability interaction depends on the fourth power. It follows that the methanol molecules with their slightly lower dipole moment but considerably higher polarizability will be more strongly solvating than water at close range to the ion. The experimentally observed preference for methanol is thus to be understood as resulting from the higher methanol polarizability.







C. Evidence for shell structure in competitive solvation of  $MH^+$  by methanol and water

In a study of the competitive solvation of  $NH_4^+$  by water and ammonia, Kebarle and co-workers<sup>81</sup> found that ammonia preferentially fills an inner shell of  $NH_4^+ \cdot 4NH_3$  whereupon water is then taken up into the outer shell. Some of the evidence for this conclusion was the fact that for 5 ligands solvating  $NH_4^+$ , no probability distribution could fit the experimental results. However, if the additional ligands were considered to solvate around an inner shell of  $NH_4 \cdot 4NH_3$ , then the results were found to fit a probability distribution from the binomial expansion and outer shell  $\gamma$ 's could be calculated. These outer shell  $\gamma$ 's were found to be about a factor of 1000 lower than the inner shell  $\gamma$ 's. Since the present results for competitive solvation of methanol and water about  $MH^+$  fit probability distributions for 2 to 5 ligands, it may be concluded that these clusters do not contain molecules which occupy a distinct outer shell. Therefore the inner shell would contain at least five solvent molecules.

7.13 Conclusions

The ability to fit a cluster of constant  $n$  ( $n$  = number of solvating molecules) with a probability distribution is somewhat unexpected, even if all molecules belong to the same solvation shell. A probability distribution means, for example, that in the four cluster,  $MH^+ \cdot 4L$ , the preference for methanol over water is the same whether the remaining four ligands are water or methanol or a mixture of the two. It would be thought that this is not strictly true. Thus the data from these experiments must



indicate that, in the first approximation, the nature of the other occupants is not important in regard to further solvation of the cluster by either a water or methanol molecule.

Because of the good agreement between these results (obtained where the ionic reaction time is about a microsecond) and the results of Kebarle and co-workers (obtained where the ionic reaction time is about a millisecond) it may be concluded the clustering equilibrium is established very rapidly; furthermore the present results approach equilibrium conditions.

As was noted, while  $\gamma$  remains constant for a cluster distribution with  $n$  constant, it was observed that  $\gamma$  decreases as  $n$  increases. This can be understood if it is assumed that whenever  $n$  is increased by one molecule, the effective radius of the (inner) shell increases. This causes the polarizability to become less important and leads to a decrease of the preference for methanol. An increase of the effective radius might be expected because of the mutual repulsion due to dipole and van der Waal's forces between the ligands.

#### 7.14 Suggestions for Further Research

The author thinks that many exciting possibilities exist for further studies in solvation of polar molecules about various ions and in competitive solvation of the type studied here. The present study of the system methanol-water could be expanded greatly with variation of total pressure and temperature, just to mention two variables. Competitive solvation of other alcohols and other polar solvents with water would be of much interest.





BIBLIOGRAPHY

1. J. B. Hasted, Adv. Elec. Electron Phys. 13, 31 (1960).
2. N. V. Fedorenko, Soviet Phys. - Uspekki 2, 526 (1959).
3. E. W. McDaniel, Collision Phenomena in Ionized Gases, John Wiley and Sons, N.Y., 1964, Chapter 6.
4. J. B. Hasted, Physics of Atomic Collisions, Butterworths, London, 1964, Chapters 11 and 12.
5. J. J. Thomson and G. P. Thomson, Conduction of Electricity Through Gases, Second Edition, Vol. II, Cambridge University Press, Cambridge, 1933.
6. N. F. Mott and H. S. W. Massey, The Theory of Atomic Collisions, Second Edition, Oxford University Press, Oxford, 1952.
7. V. L. Tal'roze, Pure and App. Chem. 2, 455 (1962).
8. W. A. Chupka and E. Lindholm, Arkiv Fysik 25, 349 (1963) and references therein.
9. J. B. Homer, R. S. Lehrle, J. C. Robb and D. W. Thomas, Trans. Far. Soc. 62, 619 (1966).
10. H. Bethe, Ann. Phys. 5, 325 (1930).
11. H. S. W. Massey and E. H. S. Burhop, Electronic and Ionic Impact Phenomena, Oxford University Press, Oxford, 1952.
12. J. A. Takacs and G. R. Freeman, Nature 208, 996 (1965).
13. J. W. Hooper, D. S. Harmer, D. W. Martin and E. W. McDaniel, Phys. Rev. 121, 1123 (1961); ibid., 125, 2000 (1962).
14. P. Kebarle and E. W. Godbole, J. Chem. Phys. 36, 302 (1962).
15. S. Wexler, J. Chem. Phys. 41, 2781 (1964).
16. R. N. Schuler and F. A. Stuber, J. Chem. Phys. 40, 2035 (1964); ibid 41, 901 (1964).
17. J. C. Abbé and J. P. Adloff, Phys. Letters 11, 28 (1964).
18. P. S. Rudolph and C. E. Melton, J. Chem. Phys. 45, 2227 (1966).
19. R. H. Huddleston and S. L. Leonard (eds.), Plasma Diagnostic Techniques, Academic Press, N.Y., U. S. A., 1965, Chapter 12.



20. J. Desesquelles, G. Do Cao and M. Dufay, C. R. Acad. Sc. Paris 262B, 1329 (1966).
21. V. L. Tal'roze and A. K. Lyubimova, Dokl. Akad. Nauk U.S.S.R. 86, 909 (1952).
22. D. P. Stevenson and D. O. Schissler, J. Chem. Phys. 23, 1353 (1955).
23. G. Gioumousis and D. P. Stevenson, J. Chem. Phys. 29, 294 (1958).
24. P. Langevin, Ann. Chim. Phys. 5, 245 (1905); translated into English in Appendix II of ref. 3 by E. W. McDaniel.
25. D. P. Stevenson and D. O. Schissler, in "Actions chimiques et biologiques des Radiations", V sér., Paris-Londres, (1961), pp. 169-270.
26. M. Saporoschenko, Phys. Rev. 111, 1550 (1958).
27. C. E. Melton, J. Chem. Phys. 33, 647 (1960).
28. F. H. Field, J. Am. Chem. Soc. 83, 1523 (1961).
29. S. Wexler and N. Jesse, J. Am. Chem. Soc. 84, 3425 (1962).
30. P. Kebarle and A. M. Hogg, J. Chem. Phys. 42, 668 (1965).
31. F. W. Lampe, J. L. Franklin, and F. H. Field, in "Progress in Reaction Kinetics" 1, 69 (1961).
32. V. L. Tal'roze, Adv. Mass. Spec. 3, 211 (1966).
33. C. F. Giese, Adv. Chem. Phys. 10, 247 (1966).
34. F. N. Farllee, H. M. Rosenstock and J. T. Herron, "A Bibliography of Ion Molecule Reactions", NBS Tech. Note 291, National Bureau of Standards, Washington, D.C. (1966).
35. J. D. Cockcroft and E. T. S. Walton, Proc. Roy. Soc. A136, 619 (1932).
36. C. D. Moak, H. Reese, W. M. Good, Nucleonics 9, No. 3, 18 (1951).
37. See for example Mass Spectrometry (ed.) by C. A. McDowell, McGraw Hill Book Co., Inc., New York (1963).
38. S. D. Warshaw, Phys. Rev. 76, 1759 (1949).
39. J. H. Beynon, Mass Spectrometry and its Application to Organic Chemistry, Elsevier Publishing Co., Amsterdam (1960), p. 200.







40. E. S. Solov'ev, R. N. Il'in, V. A. Oparin and N. V. Fedorenko, Soviet Phys. JETP 15, 459 (1962); N. V. Fedorenko, V. V. Afrosimov, R. N. Il'in, and E. S. Solov'ev. Proceedings of the Fourth International Conference on Ionization Phenomena in Gases, (ed.) N. R. Nilsson, North Holland Publishing Co., Amsterdam, Vol. I, (1960), p. 47.
41. H. H. Podgurski and F. N. Davis, Vacuum 10, 377 (1963).
42. B. L. Schram, F. J. de Heer, M. J. Van der Wiel, and J. Kistemaker, Physica 31, 94 (1965).
43. N. G. Utterback and T. Griffith, Rev. Sci. Instr. 37, 866 (1966).
44. J. W. Otvos and D. P. Stevenson, J. Am. Chem. Soc. 78, 546 (1956).
45. F. W. Lampe, J. L. Franklin, and F. H. Field, J. Am. Chem. Soc. 79, 6129 (1957).
46. A. G. Harrison, E. G. Jones, S. K. Gupta and G. P. Nagy, Can. J. Chem. 44, 1967 (1966).
47. Landolt-Bornstein, "Zahlenwerte und Funktionen", 6 Auflage, "Atom und Molecularphysik", 3 Teil, (Springer-Verlag, Berlin, (1950), pp. 510-517.
48. F. H. Field and J. L. Franklin, Electron Impact Phenomena, Academic Press, New York, 1957.
49. R. Taubert, Adv. Mass Spec. 1, 489 (1959).
50. J. Bracher, H. Ehrhardt, R. Fuchs, O. Osberghaus and R. Taubert, Adv. Mass Spec. 2, 285 (1962).
51. J. C. Abbé and J. P. Adloff, C. R. Acad. Sci. Paris, 258, 3003 (1964).
52. U. Fano and W. Lichten, Phys. Rev. Letters 14, 627 (1965); see also V. V. Afrosimov, Uy. S. Gordeev, M. N. Panov, and N. V. Fedorenko, Soviet Phys.-Tech. Phys. 9, 1248, 1256 and 1265 (1965).
53. H. von Koch, Arkiv Fysik 28, 529 (1965).
54. G. C. Eltenton: Monthly Reports of Shell Development Co., Emeryville, California. April, 1940. Referred to by D. P. Stevenson in Chapter 13 of ref. 37.
55. D. O. Schissler and D. P. Stevenson, J. Chem. Phys. 24, 926 (1956).
56. F. H. Field, J. L. Franklin and F. W. Lampe, J. Am. Chem. Soc. 79, 2419 (1957).



57. V. L. Tal'roze and E. L. Frankevich, Russ. J. Phys. Chem. 34, 1275 (1960).
58. R. Fuchs, Z. Naturforsch. 16a, 1026 (1961).
59. F. H. Field, J. L. Franklin, and M. S. B. Munson, J. Am. Chem. Soc. 85, 3575 (1963).
60. F. A. W. Derwish, A. Galli, A. Giardini-Guidoni, and G. G. Volpi, J. Chem. Phys. 40, 5 (1964).
61. F. H. Field and M. S. B. Munson, J. Am. Chem. Soc. 87, 3289 (1965).
62. S. Wexler, A. Lifshitz, and A. Quattrochi, Adv. in Chem. 58, 193 (1966).
63. F. P. Abramson and J. H. Futrell, J. Chem. Phys. 45, 1925 (1966).
64. R. M. Haynes and P. Kebarle, J. Chem. Phys. (1967), in press.
65. M. S. B. Munson and F. H. Field, J. Am. Chem. Soc. 87, 3294 (1965).
66. S. K. Searles, private communication.
67. C. E. Melton and P. E. Rudolph, J. Chem. Phys. 24, 1128 (1960).
68. S. Wexler and R. Marshall, J. Am. Chem. Soc. 86, 781 (1964).
69. P. Kebarle, R. M. Haynes, and S. Searles, Advances in Chem., 58, 210 (1966).
70. I. Szabo, Arkiv Fysik 31, 287 (1966).
71. J. T. Park and E. J. Zimmerman, Phys. Rev. 131, 1611 (1966).
72. J. H. Futrell and F. P. Abramson, Advances in Chem. 58, 107 (1966).
73. P. Ausloos, S. G. Lias and R. Gorden, J. Chem. Phys. 39, 3341 (1963).
74. G. G. Meisels, J. Chem. Phys. 42, 3237 (1965); Advances in Chem. 58, 243 (1966).
75. M. S. B. Munson and F. H. Field, J. Am. Chem. Soc. 87, 4242 (1965).
76. P. Kebarle, S. K. Searles, Unpublished results.







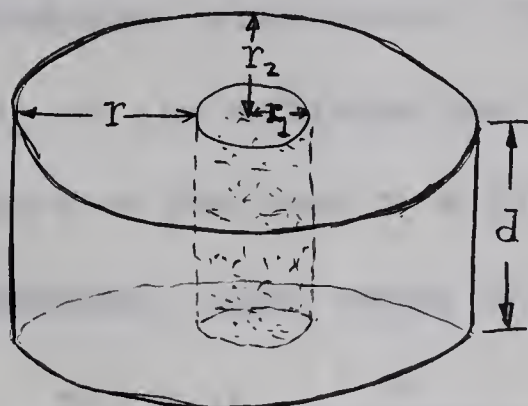
77. V. Cermak and Z. Herman, *Nucleonics* 19, 106 (1961).
78. R. Reed, Ion Production by Electron Impact, Academic Press, London, (1962), p. 63.
79. P. Kebarle and A. M. Hogg *J. Chem. Phys.*, 42, 798 (1965).
80. A. M. Hogg and P. Kebarle, *J. Chem. Phys.* 43, 449 (1965).
81. A. M. Hogg, R. M. Haynes and P. Kebarle, *J. Am. Chem. Soc.* 88, 28 (1966).
82. P. Langevin, *Ann. Chim. Phys.* 28, 289 (1903).
83. J. J. Thomson, *Phil. Mag.* 47, 337-378 (1924).
84. E. W. McDaniel, Ref. 3 Chapter 9.
85. P. Kebarle and E. W. Godbole, *J. Chem. Phys.*, 39, 1131 (1963).
86. P. Kebarle, "Applications of Mass Spectrometry to Inorganic Chemistry", *Advances in Chem.* (1967).
87. A. N. Hayhurst and T. M. Sugden, *Proc. Roy. Soc.* A293, 36 (1966).
88. M. S. B. Munson, *J. Am. Chem. Soc.* 87, 5313 (1965).
89. M. S. B. Munson, *J. Phys. Chem.* 70, 2034 (1966).
90. M. M. Mann, A. Hustrulid & J. T. Tate, *Phys. Rev.* 58, 340 (1940).
91. H. D. Beckey, *Z. Naturforsch.* 15a, 822 (1960).
92. P. F. Knewstubb and A. W. Tickner, *J. Chem. Phys.* 38, 464 (1963).
93. P. Kebarle and A. M. Hogg, Unpublished results.
94. J. C. J. Thynne and A. G. Harrison, *Trans. Far. Soc.* 62, 2468 (1966).
95. F. W. Lampe, F. H. Field, and J. L. Franklin, *J. Am. Chem. Soc.* 79, 6132 (1957).
96. P. Wilmenius and E. Lindholm, *Arkiv Fysik*, 21, 97 (1962).
97. E. Lindholm and P. Wilmenius, *Arkiv Kemi*, 20, 255 (1963).
98. K. R. Ryan, L. W. Sieck, & J. H. Futrell, *J. Chem. Phys.* 41, 111 (1964).
99. J. C. J. Thynne, F. K. Amenu-Kpodo, and A. G. Harrison, *Can. J. Chem.* 44, 1655 (1966).
100. M. S. B. Munson, *J. Am. Chem. Soc.*, 87, 2332 (1965).
101. F. Basolo and R. G. Pearson, Mechanisms of Inorganic Reactions, John Wiley and Sons, New York, 1958, p. 46 ff.



# APPENDIX

## Calculation of Conductance of Region between Ion Source

### Exit Slit and Withdrawal Plate



The region between the bottom of the ion source and the withdrawal electrode is a squat cylinder of height  $d=0.1$  cm and a radius  $r_2=1.8$  cm.

The gas is considered to bleed out of the ion source in a smaller cylindrical region of radius 0.2 cm and height  $d = 0.1$  cm. The gas then flows outwards between the two electrodes (top and bottom of cylinder) to the low pressure region.

A general equation for the flow conductance  $F$  of a tube is given by\*

$$F = \frac{4}{3} \frac{v}{\int_0^l (H/A^2) dl} \quad (1)$$

where  $v$  is average molecular velocity in cm/sec

$H$  is circumference of cross section in cm

$A$  is area of cross section in  $\text{cm}^2$

$l$  is length in cm

---

\* S. Dushman, Scientific Foundations of Vacuum Technology, Second Edition, John Wiley and Sons, Inc., New York, 1962 p. 88







In this case the length considered is along the radius of the cross section of the cylindrical region, i.e. the distance  $r$ , since the gas flow is considered to take place from the region between the source and withdrawal slits but not through the slit in the withdrawal electrode. The area considered is the outside of the cylinder but not including the ends. Therefore  $A = 2\pi r d$  and  $H = (2) (2\pi r) + 2d = 4\pi r$ , since  $2\pi r \gg d$ . Inserting these terms in Eq. (1) we obtain

$$F = \frac{4}{3} v \frac{1}{\int_{r_1}^{r_2} \frac{4\pi r dr}{4\pi^2 r^2 d^2}} = \frac{4}{3} v d^2 \pi \frac{1}{\int_{r_1}^{r_2} \frac{dr}{r}}$$

$$F = \frac{4}{3} \frac{v \pi d^2}{\ln(r_2/r_1)} \quad (2)$$

Upon inserting numerical values we obtain  $F=950$  cc/sec  $\approx$  1 liter/sec.

Now the rate of gas flow to the ion source, at an ion source pressure of one torr is  $Q=50$  torr-cc/sec, as measured by the pressure drop with time, of gas bleeding from the sample reservoir bulb through the molecular leak to the ion source. The pressure  $p$  in the source exit withdrawal region is readily determined from the conductance  $F$  of this region [from Eq. (2)] and  $Q$  since

$$Q = Fp \quad (3)$$



where it is assumed that the pressure of the vacuum envelope is much smaller than  $p$ . This pressure  $p$  is calculated to be 50 millitorr, upon inserting the values of  $F = 1$  liter/sec and  $Q = 50$  torr-cc/sec = 50 millitorr-liter/sec. in Eq. (3).

Therefore, for a 1 torr ion source pressure, the pressure in the region between ion source exit and withdrawal slit is 50 millitorr.







**B29867**